WRDC-TR-89-3063

ROBUST CONTROL DESIGN FOR FLIGHT CONTROL

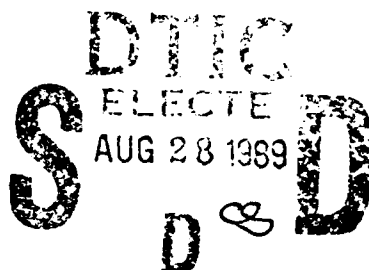William H. Bennett

Harold G. Kwatny

Keith Glover

Techno-Sciences, Inc.

7833 Walker Drive, Suite 620

Greenbelt MD 20770

DTIC FILE

DTIC
ELECTE
AUG 2 8 1989
S   D
D

July 1989

Final Report for the Period July 1988 to March 1989
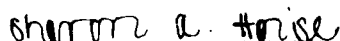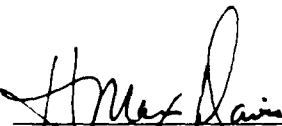
89 8 25 018

NOTICE

When Government drawings, specifications, or other data are used for any purpose other than in connection with a definitely Government-related procurement operation, the United States Government thereby incurs no responsibility nor any obligation whatsoever; and the fact that the Government may have formulated, furnished, or in any way supplied the said drawings, specifications, or other data, is not to be regarded by implication or otherwise as in any manner licensing the holder or any other person or corporation, or as conveying any rights or permission to manufacture, use, or sell any patented invention that may in any way be related thereto.

This technical report has been reviewed and is approved for publication.

SHARON A. HEISE , 1st Lt, USAF
Project Engineer
Control Dynamics Branch
Flight Control Division

DAVID K. BOWSER, Chief
Control Dynamics Branch
Flight Control Division

FOR THE COMMANDER

H. MAX DAVIS, Assistant for
Research and Technology
Flight Control Division
Flight Dynamics Laboratory

REPORT DOCUMENTATION PAGE	Form Approved OMB No. 0704-0188

1a REPORT SECURITY CLASSIFICATION UNCLASSIFIED	1b RESTRICTIVE MARKINGS

2a SECURITY CLASSIFICATION AUTHORITY	3 DISTRIBUTION/AVAILABILITY OF REPORT APPROVED FOR PUBLIC RELEASE;
2b DECLASSIFICATION/DOWNGRADING SCHEDULE	DISTRIBUTION IS UNLIMITED

4 PERFORMING ORGANIZATION REPORT NUMBER(S) TSI-89-04-06-WB	5. MONITORING ORGANIZATION REPORT NUMBER(S) WRDC-TR-89-3063

6a. NAME OF PERFORMING ORGANIZATION TECHNO-SCIENCES, INC	6b. OFFICE SYMBOL (If applicable)	7a. NAME OF MONITORING ORGANIZATION WRIGHT RESEARCH AND DEVELOPMENT CENTER FLIGHT DYNAMICS LABORATORY (WRDC/FIGCA)

6c. ADDRESS (City, State, and ZIP Code) 7833 WALKER DRIVE, SUITE 620 GREENBELT MD 20770	7b. ADDRESS (City, State, and ZIP Code) WRDC/FIGCA WRIGHT-PATTERSON AFB OH 45433-6553

8a. NAME OF FUNDING/SPONSORING ORGANIZATION	8b OFFICE SYMBOL (If applicable)	9. PROCUREMENT INSTRUMENT IDENTIFICATION NUMBER F33615-88-C-3606

8c. ADDRESS (City, State, and ZIP Code)	10. SOURCE OF FUNDING NUMBERS			
	PROGRAM ELEMENT NO. 65502F	PROJECT NO. 3005	TASK NO 40	WORK UNIT ACCESSION NO 28

11. TITLE (Include Security Classification)

ROBUST CONTROL DESIGN FOR FLIGHT CONTROL

12. PERSONAL AUTHOR(S)
BENNETT, WILLIAM H.; KWATNY, HAROLD G.; GLOVER, KEITH

13a. TYPE OF REPORT FINAL	13b. TIME COVERED FROM 88JUL29 TO 89MAR31	14. DATE OF REPORT (Year, Month, Day) JULY 1989	15. PAGE COUNT 90

16. SUPPLEMENTARY NOTATION

17.	COSATI CODES		18. SUBJECT TERMS (Continue on reverse if necessary and identify by block number)
FIELD	GROUP	SUB-GROUP	FLIGHT CONTROL, ROBUST CONTROL THEORY, OPTIMAL CONTROL
01	04		THEORY, RELAXED STABILITY AIRCRAFT, AIRCRAFT LONGITUDINAL DYNAMICS

19. ABSTRACT (Continue on reverse if necessary and identify by block number)

This project studies the application of new and advanced methods of control law synthesis for robust stabilization with respect to a combination of both unstructured model uncertainty (arising from neglected parasitic dynamics) and structured model uncertainty (arising from parametric variations which occur as flight conditions change). Efforts have focused on the characterization of a class of nonlinear models for longitudinal dynamics of aircraft in level flight subject to changes in static stability. Such "relaxed stability" aircraft configurations are currently at issue in a wide variety of advanced designs including commercial transport and high performance aircraft.

The control design approach employs H-infinity synthesis methods for optimal robust stabilization for the unstructured model uncertainty, and the requirement of worst case (i.e., robust) design for parametric uncertainty is included using a minimax optimization criteria.

(CONTINUED ON REVERSE)

20 DISTRIBUTION/AVAILABILITY OF ABSTRACT [X] UNCLASSIFIED/UNLIMITED ☐ SAME AS RPT ☐ DTIC USERS	21. ABSTRACT SECURITY CLASSIFICATION UNCLASSIFIED	
22a NAME OF RESPONSIBLE INDIVIDUAL SHARON A. HEISE, 1LT, USAF	22b TELEPHONE (Include Area Code) (513) 255-8683	22c OFFICE SYMBOL WRDC/FIGCA

DD Form 1473, JUN 86 — Previous editions are obsolete. — SECURITY CLASSIFICATION OF THIS PAGE

BLOCK 19.   (CONTINUED)

This study has focused on a class of flight control models with physically based parametric
uncertainty. For these models, the solution of the minimax or worst case design is
achieved by a straightforward procedure which can be readily combined with the requirements
for robustness to parasitic dynamics using the closed form solution of the optimal robust
stabilization method.

Project Summary

Modern requirements for high performance aircraft require advanced control configured flight vehicles where an increasing reliance is placed on computer control systems for flight performance. Such aircraft will be equipped with multiple sensors and actuators and employ centralized control implemented by a high speed digital computer. For such systems, requirements for reliable multiloop control laws which are robust to a variety of changes in flight dynamics are prerequisite for successful flight operation. Typical methods for the synthesis of high performance feedback control is based on a nominal dynamic model for the aircraft flight dynamics. Such models are subject to various limitations including the effect of changes in flight conditions affecting trim or equilibrium and consequent changes in the linear perturbation dynamics. Typical control design methods are based on the linear dynamics which will be subject to various sources of model uncertainty in flight control applications.

In this project we have initiated studies of the application of new and advanced methods for control law synthesis for robust stabilization with respect to a combination of both *unstructured model uncertainty* (arising from neglected or parasitic dynamics) and *structured model uncertainty* (arising from parametric variations which occur as flight conditions change.) Our efforts have focused on the characterization of a class of nonlinear models for longitudinal dynamics of aircraft in level flight subject to changes in static stability. Such "relaxed stability" aircraft configurations are currently at issue in a wide variety of advanced designs including commercial transport and high performance aircraft.

Our approach for control design is to employ H^∞ synthesis methods for optimal robust stabilization for the unstructured model uncertainty using a computationally tractable approach of Glover and McFarlane. The requirement for worst case (i.e. robust) design to parametric uncertainty is included using a minimax optimization criteria. Our studies have focused on a class of flight control models with physically based parametric uncertainty. For these models we have the solution of the minimax or worst case design by a straightforward procedure which can be readily combined with the requirements for robustness to parasitic dynamics using the closed form solution of the optimal robust stabilization method developed by Glover and McFarlane.

Robust design for stability can be combined with requirements for robust performance using frequency dependent constraints on the system gains. In this study we highlight the extension of the optimization-based methods for robust design with respect to performance and stability. Examples are included to illustrate the methods.

Significantly, these methods allow frequency dependent weighting (i.e., "loop shaping") to be performed without specific regard to phase and can be applied with equal ease to both single and multi-loop design problems.

In our modeling studies we have also focused on the relation between the basic statement of the control design problem and the nonlinear aircraft model subject to physically based parametric uncertainty. We have identified a relationship between the choice of actuation and sensing (i.e., inputs and outputs), the nonlinear aircraft dynamics, and the linear perturbation models used for control synthesis which highlights the limitations of robust control synthesis. In particular, we identify a relationship between conditions for the existence of static bifurcations of the equilibria and the location of transmission zeros for the linear perturbation model. Among many questions which this analysis can help to address we identify—under realistic scalings of a generic relaxed stability aircraft—the limits of linear control synthesis for parametric uncertainty.

We also demonstrate the computational simplicity of the proposed method for combined structured/unstructured uncertainty synthesis for the relaxed static stability aircraft model. Comparisons are given with several recently developed methods for robust control design for linear system models subject to various combinations of parasitic and parametric model uncertainty.

TABLE OF CONTENTS

1. Introduction and Background

Future aerospace vehicles will be expected to perform under circumstances in which the dynamics of these vehicles are not expected to be well known. Moreover, because they will be required to function close to, or even beyond, open loop stability limits, it is essential that their flight control systems will be able to cope with modeling uncertainty.

The important considerations are typically of two types, variation of modeled system parameters and unmodeled parasitic dynamics. Some examples of the former may be found in the pitch axis dynamics of the AFTI/F-16 [52], the longitudinal dynamics of an advanced subsonic transport airplane [1], and the vertical dynamics of a helicopter [2]. Examples of the latter include elastic structural deformations of the airframe [3] as well as sensor and actuator dynamics [4]. Parametric variations are *structured uncertainties*, whereas unmodeled dynamics are *unstructured* and typically associated with time scale separation or high frequency effects.

Of special concern are those situations in which the aircraft is intentionally designed to be open loop unstable or to have markedly reduced stability margins. In such cases parameter variations dramatically affect the dynamics of the vehicle and its flyability. It is necessary to equip such aircraft with stability augmenting feedback controllers which shape the handling qualities and reduce the sensitivity to parameter variations. McRuer et al [4] provide a thoughtful assessment of the current status and deficiencies in such systems. They note the following points:

> (i) Controllers tend to be of wide bandwidth, resulting in sensitivity to vehicle structural flexure, actuator dynamics and other high frequency effects; viz. unstructured model uncertainty.
>
> (ii) While the feedback controller may be designed to produce desired responses to pilot commands, responses to external (atmospheric) disturbances may be unusual and deleterious.
>
> (iii) The effective handling qualities introduced by augmented feedback control systems have not been thoroughly investigated and opportunities for "task tailored dynamics" should be exploited.
>
> (iv) Flying qualities may deteriorate substantially near the limits of control effectiveness.

The fact that such compensators for control configured aircraft are of high bandwidth is repeatedly noted in the flight control literature [3]. It is also observed that many approaches to design of stabilizing controllers, robust with respect to structured uncertainty, often lead to high gain controllers. However, Schmitendorf [5] illustrates by example that high gain is not a necessary element of robust control. It is clear that methods are needed which simultaneously address design for both structured and unstructured model uncertainty.

Certain nonlinear issues are central to the design of controllers for relaxed static stability aircraft. As already noted, augmented aircraft performance may radically diminish near limits of control authority. Methods of control system design are needed which explicity account for control saturation. Relaxed stability aircraft operate near equilibria with small domains of attraction and, consequently, the ability to recover from disturbances may be dramatically improved with nonlinear feedback laws. An example is given by Garrard and Jordan [6] in which the ability to recover from stall is significantly improved for a fighter aircraft, operating at a high angle of attack, by the use of a nonlinear controller. Gain scheduling in terms of measurable parameters has been found necessary [1] to achieve desired performance over the full flight envelope when linear feedback is employed. Exact linearization methods [48] provide means for designing nonlinear feedback laws which satisfy these requirements. However, exact linearization is not always compatible with control authority constraints and very little is known about the suitability of these methods under conditions of incipient instability. Efficient methods are required for the design of nonlinear controllers which articulate the tradeoff between performance and control restraints.

In recent years, numerous investigators have considered a variety of approaches to the quantification of aircraft handling qualitites in a way which would be useful in analytical control system design [7]. Such efforts take on special significance for the design of augmented flight control systems. Some general discussion is given by McRuer et al [4] and additional insights may be found in Wilhelm and Schafranek [8]. Nevertheless, many basic questions need to be answered if the notion of systematically 'designing in' desired flying qualities via feedback augmentation is to become a reality. For example, common control architectures suggested for stabilizing open loop unstable aircraft result in nonminimum phase zeros in the dynamics as seen by the pilot. This issue has not been previously addressed although the control of nonminimum phase plants is notoriously difficult.

In this report, we present preliminary results concerning the design of linear controllers for flight control applications which are robust with respect to both structured and unstructured uncertainties. Our approach centers around two elemental themes. First, we are concerned with the origins of

2

parametric (structured) uncertainty in aircraft and in the development of an understanding of when any such parametric variations are critical and cannot be imbedded in the unstructured uncertainty without unacceptable conservatism. Second, we propose a method of worst case design for dealing with combined structured and unstructured model uncertainty based on a formulation of the H^∞ optimization problem due to McFarlane and Glover [33].

In Section 2 we review control design methods for unstructured model uncertainty, thereby developing the required foundational background for Section 3. Section 3 provides a review of alternative approaches to extending these methods to accommodate structured model uncertainties in combination with unstructured model uncertainties and also introduces our view of addressing structured uncertainties as a minimax optimal control problem. Section 4 consists of a benchmark design problem: robust control system design for the longitudinal dynamics of a relaxed static stability aircraft. We introduce in a rudimentary way our ideas about the use of bifurcation analysis as a means of articulating the fundamental limits imposed by parametric variations in the aircraft's inherently nonlinear dynamics. In this example the minimax approach is shown to be an method of control system design. In Section 5 we summarize our conclusions and outline promising directions for future research.

2. Robust Control Design for Unstructured Model Uncertainty

Analysis of control system stability plays a fundamental role in design tradeoffs for feedback compensation. Classical design methods focus on a frequency domain description of SISO systems to articulate the tradeoff between performance (e.g. sensitivity reduction) and stability margins. The use of gain/phase margins provide a standard quantifiable description of these tradeoffs directly in terms of frequency response data. From experience with classical design methods it has become apparent that phase contributions and particularly phase errors due to unmodeled dynamics play a significant role in the achievable performance and stability margins. In particular, phase errors can ultimately limit implementable gains and thus control bandwidth with its intrinsic relation to system performance. For MIMO system design problems there is no simple stability margin concept which can separately address the change in stability due to phase errors in the model.

Recently, practical design for MIMO systems has focused on the natural extensions of gain margin concepts to the multiloop case using the spectral matrix norm. Model uncertainty for a nominal plant model $G(s)$ may be described in an unstructured way by reference to an absolute error (or additive perturbation, $G(s) \rightarrow G(s) + \Delta_a(s)$) or a relative error (or multiplicative perturbation

3

$G(s) \rightarrow [I + \Delta_m(s)]G(s))$. The model error is described by a bounding function of an appropriate form as:

$$\left\| \Delta_a(j\omega) \right\|_2 \leq l_a(\omega)$$

$$\left\| \cdot_m(\omega) \right\|_2 \leq l_m(\omega)$$

Such measures of model error are gross in the sense that they bound the model uncertainty in terms of a conservative measure of the multiloop system *gain* as given by the choice of norm.

For application to design and analysis of closed loop stability with uncertain models as above we are concerned with conditions under which the feedback will stabilize any one of all possible plant models satisfying the above bounds. Consider the following design paradigm for unstructured model uncertainty [15]. Assume that a nominal plant model G(s) is used to obtain a stabilizing controller K(s) so that the resulting closed loop transfer function, $H(s) = G(s)(I + GK(s))^{-1}$, is stable. The design is said to be robust with respect to stability if we can show that the fixed K(s) will also stabilize $\left[I + \Delta_m(s) \right] G(s)$ for any perturbation subject to the frequency dependent bound. Early developments in methods for robust control design as in [15] focus on requirements for frequency dependent shaping of the MIMO loop transmission KG(s) in terms of the above notion of system gain; i.e., sufficient conditions for robust stability are:

(i) $\Delta_m(s)$ is a stable transfer function and

(ii) $\left\| KG(j\omega) \right\|_2 \leq \dfrac{1}{l_m(\omega)}$, for $0 \leq \omega < \infty$ in the region where $l_m \gg 1$.

The interpretation of the above conditions is intuitively appealing in that it generalizes typical engineering practice of loop shaping to multiloop designs. In application it may be constraining for several reasons:

1) The characterization of system gain may result in a very conservative description of model uncertainty.

2) The restriction (i) may invalidate results in certain important applications.

Initial attempts to generalize the notion of system gain and thus permit analysis and design for more realistic problems were based on generalization of conic sector bounds for transfer functions [57]. In this line of thinking the system perturbation was assumed to have the form

$$\Delta(s) = L^{-1}(s)\Phi(s)R(s) \, ,$$

4

where L,R are stable transfer functions chosen to represent the frequency dependent model uncertainty in a somewhat more structured way and Φ is a stable unknown transfer function subject to the frequency response bound

$$\left\|\Phi(j\omega)\right\|_2 \le 1 \quad,$$

for all ω. Application of the small gain theorem [18] will justify various sufficient conditions for robust closed loop stability depending on where we choose to represent the model uncertainty within the closed loop model. Typical model uncertainty assumptions and corresponding frequency dependent sufficient conditions are summarized in Table 1.

Table 1: Conditions for robust stability

Model Uncertainty	Frequency dependent conditions for robust stability
1-neglected sensor dynamics $G \rightarrow (I + \Delta)G$	$\left\|\left[RGK(I + GK)^{-1}L^{-1}\right](j\omega)\right\|_2 < 1, \quad \forall\, \omega$
2-neglected actuator dynamics $G \rightarrow G(I + \Delta)$	$\left\|\left[RKG(I + KG)^{-1}L^{-1}\right](j\omega)\right\|_2 < 1, \quad \forall\, \omega$
3-neglected plant modes $G \rightarrow G + \Delta$	$\left\|\left[RK(I + GK)^{-1}L^{-1}\right](j\omega)\right\|_2 < 1, \quad \forall\, \omega$

In practical design problems, the engineer may be forced to consider a variety of model error sources in combination, and in many cases, certain forms of model errors may be more significant in certain loops. This form of structured uncertainty was considered by Doyle et al [16]. He suggested that plant model uncertainty could be represented in a general way by isolating the model uncertainty in an additional external feedback loop as shown in Figure 1. Thus the model uncertainty is viewed as a parasitic feedback from certain error outputs e to certain disturbance inputs w. In this case if we take the transfer function model P, representing the known dynamics, in the form,

$$\begin{bmatrix} e \\ y \end{bmatrix} = \begin{bmatrix} P_{ew} & P_{eu} \\ P_{yw} & P_{yu} \end{bmatrix} \begin{bmatrix} w \\ u \end{bmatrix}$$

the assumed form of the uncertain plant is that of a Linear Fractional Transformation (LFT);

$$G(\Delta) = P_{yu} + P_{yw}\Delta(I - P_{ew}\Delta)^{-1}P_{eu}.$$

In this form sufficient conditions for robust stability can be obtained by direct application of the small gain theorem (using possible frequency dependent weighting functions L,R) in terms of an LFT of P and K in the form;

$$\left\| R\left[P_{ew} + P_{eu}K(I - P_{yu}\Delta)^{-1}P_{yw} \right]L^{-1} \right\|_2 < 1$$

for all real frequencies.
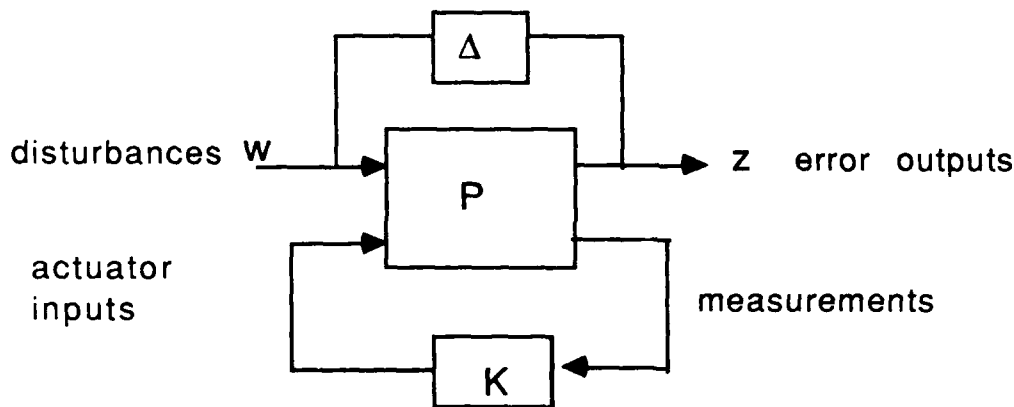
Figure 1: The general structure of the robust control problem.

Then a natural characterization of the significance of loop dependent modeling errors is to consider the parasitic dynamic model to be structured in the sense that the transfer function has the form $\Delta = \mathrm{diag}(\Delta_1,...,\Delta_m)$.

The association be ... ween the spectral matrix norm (understood as a matrix norm subordinate to the Euclidean vector norm ' nite dimensions) and the maximum singular value makes contact with the spectral properties of singular value decomposition [18]. Following this line of reasoning, Doyle postulated the existence of a *structured singular value* (SSV), defined with respect to particular block diagonal structure of the loop parasitics. The definition of the SSV proposed by

6

Doyle was chosen to emulate the spectral properties of singular values. In particular, the fact that the maximum (resp. minimum) singular values are related to the spectral matrix norm as;

$$\sigma_{max}\{A\} = \|A\|_2, \quad \sigma_{min}\{A\} = \|A^{-1}\|_2^{-1}$$

for A a nonsingular matrix. Thus, the minimum and maximum singular values are useful in bounding the spectrum of matrices under perturbations. Considerable effort has been expended in the search for computationally feasible algorithms for estimating the SSV [58], however, as of this writing only fairly simple structures can be computed with any accuracy.

An important feature for robust control design methods is the incorporation of frequency shaping requirements given by any of the various frequency dependent conditions for robust stability described above. Such considerations have been implicit in design methods dating back to early 1970's [28]. One popular method provides an extension to the state space constructions of Linear Quadratic Gaussian (LQG) optimal control problem by the incorporation of Loop Transfer Recovery (LTR) [19]. We remark that the limitations described above all apply to LQG/LTR type methods. The popularity of this method derives from the generality of approach to MIMO design and the computational support available from various standard numerical algorithms available for its implementation.

In the Phase I study we have investigated application of several new results in analysis and design of robust control systems which address the above limitations. First, we employ a new type of stability margin for multiloop feedback which quantifies closed loop internal stability in a perfectly general way and embraces possibly unstable model uncertainty. The stability margin can be alternately described from a geometric viewpoint or as the supremum over frequency of the gain of a transfer function specially constructed from normalized coprime factorizations for the plant and the compensator. Furthermore, recent results of Glover and McFarlane provide a synthesis procedure for obtaining a controller which achieves (if possible) a prespecified stability margin of this type. Their methods provide a simple computational scheme for determining the maximum possible stability margin attainable for a given plant model. To illustrate the application of these results we have focused on a physically motivated flight control design example which is discussed in the next section.

2.1. Geometric Stability Margin and Normalized Coprime Factorization
The geometric view of feedback considers the general MIMO feedback equations with G(s) a p×m plant transfer function and K(s) m×p;

$$y(s) = G(s)u(s)$$
$$u(s) = -K(s)y(s) \tag{2.1}$$

in the form

$$\begin{bmatrix} I_m & K(s) \\ G(s) & -I_p \end{bmatrix} \begin{pmatrix} u(s) \\ y(s) \end{pmatrix} = 0. \tag{2.1a}$$

In this form we focus attention on the relative orientation of two abstract objects; $G_s=ker[G(s),I_p]$, $K_s=ker[I_m,K(s)]$, which can be viewed for any complex s as a pair of subspaces in a p+m dimensional complex vector space of values of inputs and outputs. Moreover, a number s for which these subspaces intersect nontrivially; i.e. $dim(G_s \cap K_s)>0$ is a closed loop pole. Following this line of thinking Brockett and Byrnes [21] describe a Nyquist stability criterion for the general $p \neq m$ case based on frequency response data. Their result---which is somewhat abstract---provides an encirclement condition on an abstract space called the Grassman manifold. Despite the abstract nature of the resulting stability test it does retain several essential features of the popular single loop test developed by Nyquist. In particular, it identifies a Nyquist contour Γ_G for the plant as the image of the imaginary axis $s=j\omega$ under the map $ker[G(s),-I_p]$ and a separate object, Γ_K, obtained from the imaginary frequency response of $ker[I_m,K(s)]$.

In [22] Bennett and Baras describe a geometric stability margin based on an angle measure of the distance between the intersection of the respective Nyquist contours, Γ_G and Γ_K. Their measure is described in geometric terms but is meant to extend to the general MIMO feedback case the natural practical notion of stability margin for the SISO case as;

$$\min_{s=j\omega} \left| g(s) + \frac{1}{f(s)} \right|.$$

The simplest way to motivate the definition of the geometric stability margin is to recall the definition of the canonical or principal angles between a pair of subspaces.

Definition [24]: The *principal angles* $\theta_k \in [0,\frac{\pi}{2}]$ between a pair of complex subspaces, X, Y, under the assumptions, **dim X** =p, **dim Y**=m and $p \leq m$, are given recursively for k=1,2,...,p as,

$$\cos\theta_k = \max_{\substack{u \in X \\ \|u\|_2=1}} \max_{\substack{v \in Y \\ \|v\|_2=1}} u^* v = u_k^* v_k$$

subject to the constraints

8

$$u_j^* u = 0, \quad v_j^* v = 0$$

for j=1,...,k-1. Then the *principal vectors* for the pair of subspaces are $\{u_1,...,u_p,v_1,...,v_m\}$.

Canonical angle analysis has found application in a number of areas including the computation of statistical correlations. Numerical algorithms for the computation of canonical angles are largely based on singular value decompostion [24]. In [24] Bjorck and Golub show that the computations can be implemented by obtaining a pair of matrices Q_X, Q_Y of dimension nXp, nXm, respectively such that $Q_X^* Q_X = I_p$, $Q_Y^* Q_Y = I_m$ and Q_X, Q_Y are a basis for X (resp. Y)--- using, for example, Gram-Schmidt procedure. Then the SVD of the product;

$$Q_X^* Q_Y = Y_X \Sigma Y_Y^*$$

has singular values as

$$\Sigma = \text{diag}\{\sigma_1, ..., \sigma_p\} = \cos \Theta$$

which if ordered as $\sigma_1 \geq ... \geq \sigma_p$ then the principal angles are obtained from

$$\Theta = \text{diag}\{\theta_1,...,\theta_p\}$$

with $\theta_1 \leq ... \leq \theta_p$.

Finally, in [22] Bennett and Baras show that via an alternate form of the above principal angle computation one can associate a certain minimum singular value with a measure of how nearly two subspaces intersect in a nontrivial way. In this case we obtain an nX(n-p) matrix $Q_X^\perp$ with orthonormal columns whose span is the orthogonal complement of X. Then the SVD of the product,

$$Q_X^{\perp *} Q_Y = \Psi_X \Lambda Y_Y$$

has singular values related to the canonical angles as

$$\Lambda = \sin \Theta.$$

Thus the minimum singular value $0 \leq \lambda_1 \leq 1$ is nonnegative, real number which indicates how nearly the pair of subspaces intersect. Let $\gamma = \lambda_1(X, Y)$, which we refer to as the minimum gap.

Definition: The geometric stability margin for the closed loop system is given as

$$\theta_{sm} = \min_{s=j\omega} \gamma(G_s, E_s). \tag{2.2}$$

In [23] we show that the computational problem of orthonormalization can be replaced by the introduction of a pair of normalized coprime factors for G(s) and K(s).

Definition: A p×m transfer function G(s) has a stable normalized right (resp. left) coprime factorization $G=N M^{-1}$ (resp. $G=\tilde{M}^{-1}\tilde{N}$) if N,M (resp. $\tilde{M},\tilde{N}$) are stable transfer functions which satisfy,

$$N*M+M*M=I_m \qquad (\text{resp.} \quad \tilde{N}*\tilde{N}+\tilde{M}*\tilde{M}=I_p). \tag{2.3}$$

Moreover, it is shown in [25] that every p×m transfer function has a Normalized Right (resp. Left) Coprime Factorization (NRCF or NLCF) which is unique up to a unitary change of basis in input space $\mathbf{C}^m$ (resp. output space $\mathbf{C}^p$).

We can then show [23] that the geometric stability margin for the general MIMO case can be computed as follows. Obtain the NLCF of the plant $G=\tilde{M}^{-1}\tilde{N}$ and the NRCF of the compensator $K = PQ^{-1}$. Then the geometric stability margin can be given as

$$\theta_{sm} = \min_{s=j\omega} \sigma_{min}\{\Phi(s)\} \tag{2.4}$$

where

$$\Phi = \tilde{N}P + \tilde{M}Q \tag{2.5}$$

To see the significance of this construction consider that the normalization processes obtains a frequency dependent change of basis in the p-dimensional space of outputs such that the matrices

$$\begin{bmatrix} K \\ I_p \end{bmatrix} = \begin{bmatrix} P \\ Q \end{bmatrix} Q^{-1}$$

has orthnormal columns and

$$[G,I_p] = \tilde{M}^{-1}[\tilde{N},\tilde{M}]$$

has orthonormal rows.

An alternative expression for plant uncertainty advocated by Vidyasagar [25-27] in terms of additive stable perturbations to the factors in a coprime factorization of the plant has certain advantages in analysis of feedback systems. In recent work Glover and McFarlane [31] also considered this class of unstructured perturbations and obtained a surprisingly explicit and intuitively appealing solution to the corresponding robust stabilization problem when the coprime factorization is normalized. In particular, they considered the problem of stabilization of a nominal plant transfer function G(s) and a family of transfer functions given in terms of its NLCP

$$G = \tilde{M}^{-1}\tilde{N}$$

given as

$$G_\varepsilon = \{(\tilde{M}+\Delta_M)^{-1}(\tilde{N}+\Delta_N): \|[\tilde{M}\tilde{N}]\|_\infty < \varepsilon\} \tag{2.6}$$

where $\|.\|_\infty$ is the H^∞ norm of the transfer function given as

$$\|G(s)\|_\infty = \sup_{s=j\omega} \sigma_{max}\{G(s)\}$$

and Δ_M, Δ_N are stable unknown, transfer functions which represent the uncertainty in the nominal plant model. It was demonstrated by Vidyasagar [25-27] that this description of plant uncertainty has advantages over additive or multiplicative unstructured uncertainty models. For example, the number of unstable poles may change as the plant is perturbed. Figure 2 illustrates the class of systems described by perturbations of normalized coprime factors.

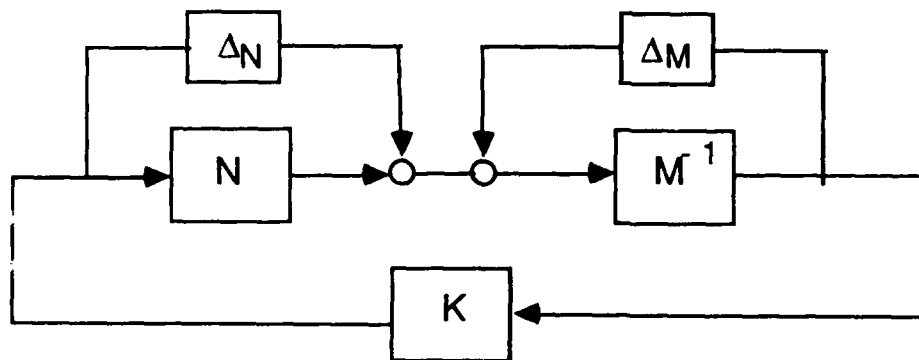Figure 2: Perturbation of NCPF

It is now apparent the role of coprime factorization originally conceived in the work of Youla, Rosenbrock, and others was somewhat constraining. The goal of much of this reaserch was to extend the obvious constructions for rational scalar transfer functions of factorization in terms of numerator and denominator polynomials to the required matrix constructions for multiloop

11

systems. More recently, connections with state space constructions have become evident by introducing an alternate viewpoint [25]. Instead, we think of coprime factorization over an alternate algebraic ring of rational tranfer functions whose poles are contained in some arbitrary left half plane within C. Since in most cases we are concerned with asymptotic stability, it suffices to consider coprime factorizations over $\mathfrak{R}\mathbf{H}_\infty$, the space of all rational functions of the Laplace variable s analytic for Re s>0. Then a state--space construction for the normalized left (resp. right) coprime factorizations over $\mathfrak{R}\mathbf{H}_\infty$ can be obtained in terms of the solution to the Control (resp. Filter) Algebraic Riccati Equation:

$$A^T X + XA - XBB^T X + C^T C = 0 \qquad\qquad \text{(CARE)}$$
$$AY + YA^T - YC^T CY + BB^T = 0 \qquad\qquad \text{(FARE)}$$

Specifically, let G(s) be realized by a linear state space system;

$$\dot\xi(t) = A\xi(t) + Bu(t)$$
$$z(t) = C\xi(t)$$

so that $G(s) = C[sI - A]^{-1}B$ with (A,B,C) a minimal realization. Then the respective left normalized coprime factors can be shown to be realized as

$$\tilde N(s) = C[sI-A_0]^{-1}B \qquad\qquad (2.7a)$$
$$\tilde M(s) = I - C[sI-A_0]^{-1}H \qquad\qquad (2.7b)$$

where

$$H = -YC^T, \quad A_0 = A + HC. \qquad\qquad (2.8)$$

The geometric stability margin provides a numerically attractive measure of closed loop stability which includes the class of perturbations just described. It will recognize possible pole/zero cancellations which might occur in the formation of any variation of the return difference matrices and it provides a characterization of plant neighborhoods for robust analysis as above in terms of metric specifically designed for the stability margin for multiloop stability directly in terms of the generalized Nyquist criterion [21].

2.2. Design Methods for Optimal MIMO Stability Margins

The primary reason for the introduction of coprime factorization by Youla et al [28] was to facilitate analytic optimization for the resolution of engineering tradeoffs in design. The coprime factorization permits optimization to be carried out without regard for stability of the closed loop system. This fact follows from the following well known lemma.

12

<u>Lemma</u>: For each real rational G(s) there exists left and right coprime factorizations; $G=NM^{-1}= \tilde{M}^{-1}\tilde{N}$, each contained in $\Re H_{\infty}$, and functions $V,U,\tilde{V},\tilde{U} \in \Re H_{\infty}$ such that

$$\begin{bmatrix} \tilde{V} & -\tilde{U} \\ -\tilde{N} & \tilde{M} \end{bmatrix} \begin{bmatrix} M & U \\ N & V \end{bmatrix} = \begin{bmatrix} I & 0 \\ 0 & I \end{bmatrix} \tag{2.9}$$

With the above notation the Youla parametrization provides a complete parametric description of all stabilizing compensators for a given plant transfer function G(s).

<u>Lemma</u>: Any compensator transfer function K(s) which stabilizes the plant G(s) in closed loop can be factored as

$$K = (U+MQ)(V+NQ)^{-1} = (\tilde{V}+\tilde{N}Q)^{-1}(\tilde{U}+\tilde{M}Q) \tag{2.10}$$

for some $Q \in \Re H_{\infty}$.

This has been called the Q-parametrization by Desoer et al [60]. It is significant to recognize that this parametrization guarantees that the closed loop system (see Figure 2) is *internally stable*; i.e., the composite transfer function satisfies,

$$\begin{bmatrix} (I_p - GK)^{-1} & K(I_p - GK)^{-1} \\ (I_m - KG)^{-1}G & (I_m - KG)^{-1} \end{bmatrix} \in \Re H_{\infty}$$

The focus of the current phase 1 project is to investigate the application of some recent results of K. Glover and D. McFarlane [31-33] on robust stabilization. In the next few paragraphs we summarize the basis for their results.

<u>Defintion</u>: A feedback system consisting of plant transfer function G(s) and compensator K(s) is *robustly stable with respect to the margin* ε (or ε-robustly stable) if and only if the feedback system of (2.1) K, G_{ε} is internally stable for any $G_{\varepsilon} \in G_{\varepsilon}$ (as given in (2.6)).

The symbol ε represents a *stability margin* for the system in the sense that it indicates the `size' of tolerable perturbations internal to the plant (in terms of the coprime factorization). (As we will demonstrate shortly, this stability margin is identical to the geometric stability margin described above.) The robust design problem is to stabilize not only the nominal plant, G, but the family of

perturbed plants defined in (2.6) using a single feedback controller K(s) (see Figure). Their first result provides necessary and sufficient conditions for robust stabilization of a given plant.

Lemma: The feedback system with plant $G=\tilde{M}^{-1}\tilde{N}$ is ε-robustly stabilizable by some compensator K if and only if

$$\inf_{K(s)\in\Re H_{\infty}} \left\| \begin{bmatrix} K(I-GK)^{-1}\tilde{M}^{-1} \\ (I-GK)^{-1}\tilde{M}^{-1} \end{bmatrix} \right\|_{\infty} \leq \frac{1}{\varepsilon} \qquad (2.11)$$

This is stated in the form of an H^{∞} optimization problem which could be solved by the standard iterative procedures outlined in Francis [20]. To follow this approach one could first proceed by recasting the optimization problem as a "standard problem". This is illustrated in Figure 3.

Figure 3: Robust Stabilization Problem in Standard Form
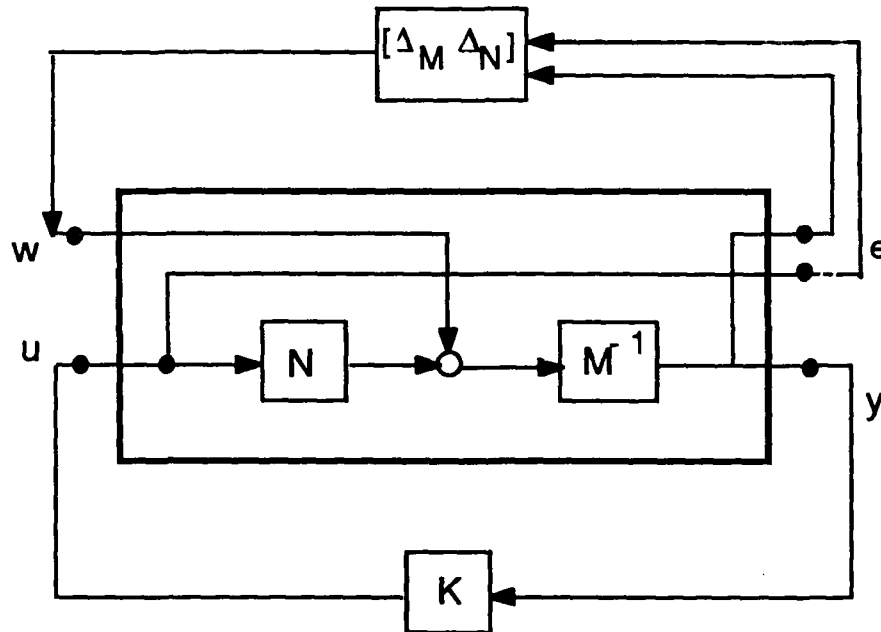
This can be seen by comparing the standard problem of Figure 1 where in this case we take

$$P = \begin{bmatrix} \begin{bmatrix} 0 \\ M^{-1} \end{bmatrix} & \begin{bmatrix} I \\ M^{-1}N \end{bmatrix} \\ M^{-1} & M^{-1}N \end{bmatrix} \qquad (2.12)$$

Then the standard H^{∞} problem is to minimize the H^{∞} norm of the transfer function from w to e;

14

$$P_{11} + P_{12}K(I - P_{22}K)^{-1}P_{21} = \begin{bmatrix} K(I - GK)^{-1}M^{-1} \\ (I - GK)^{-1}M^{-1} \end{bmatrix},$$

(2.13)

which demonstrates the interpretation displayed in Figure 3.

However, by using normalized coprime factorizations, Glover and McFarlane show that the iterative procedures can be avoided altogether, and an exact solution can be obtained very simply. The key idea is to combine the Youla parameterization of stabilizing controllers described above together with interpolation results of Nehari and Glover for the computation of the Hankel norm. In particular, they show that the plant G is ε-robustly stabilizable if and only if

$$\varepsilon^2 \leq 1 - \| [\tilde{M}, \tilde{N}] \|_H^2$$

(2.14)

where the Hankel norm of a stable, proper system $G(s) = C[sI-A]^{-1}B$ is given as

$$\|G(s)\|_H = \sigma_{max}\{\Gamma_G\} = \sqrt{\lambda_{max}(PQ)};$$

(2.15)

i.e., the maximum singular value of the associated Hankel operator,

$$(\Gamma_G)(t) = \int_0^\infty Ce^{A(t+\tau)}Bv(\tau)d\tau$$

(2.16)

It is also shown in [30] that the Hankel norm can be obtained from the state space realization of the stable system via the solutions of the pair of associated Lyapunov equations;

$$AP + PA^t + BB^t = 0$$
$$A^tQ + QA + C^tC = 0,$$

(2.17)

as shown above.

Using these constructions Glover and McFarlane show that the optimal stability margin for $G(s) = C[sI-A]^{-1}B$ given by the minimum achievable ε_0 in (2.11) can be directly obtained from X, Z>0, the positive definite solutions of the pair of Riccati equations (CARE) and (FARE) as

$$\varepsilon_0 = \frac{1}{\sqrt{1 + \lambda_{max}(ZX)}}.$$

(2.18)

Significantly, Glover and McFarlane also provide formulae for the characterization of all controllers which achieve ε-robust stabilization and from the previous discussion such level is achievable only if $\varepsilon \leq \varepsilon_0$, with ε_0 the optimal stability margin obtained from (2.14). Formulae for

the desired ε-robust compensators are given directly in terms of state space realizations which facilitates computer based computation. Details are given in [32]. It is also potentially important to recognize the flexibility available in this characterization which permits consideration for various additional design tradeoffs. In this study we have focused on the simplest form for realizing an ε-robust compensator. This is summarized as follows.

Theorem: A compensator $K(s)$ which achieves the specified stability margin ε, $0 \leq \varepsilon \leq \varepsilon_0$, is obtained in the form

$$K(s) = C_k [sI - A_k]^{-1} B_k,$$ (2.19)

where the state space realization is given by the matrices

$$A_k = A_c + \gamma^2 (W^t)^{-1} Z C^t C,$$

$$B_k = \gamma^2 (W^t)^{-1} Z C^t,$$

$$C_k = B^t X,$$ (2.20)

and where the matrix terms are

$$A_c = A + BF,$$

$$F = -B^t X,$$

$$W = XZ - \zeta I,$$ (2.21)

and the scalar terms are

$$\gamma = \tfrac{1}{\varepsilon}, \qquad \zeta = \sqrt{\gamma^2 - 1}.$$ (2.22)

The following demonstrates the connection between the geometric stability margin and the ε stability margin used above.

Claim: The geometric stability margin is identical with the ε stability margin introduced by Glover and McFarlane in the context of the robust stabilization problem.

Proof: To see this consider a plant transfer function together with NLCP factorization $G = M^{-1} N$ over $\mathfrak{R} H^\infty$. Then for some $K(s)$ which stabilizes $G(s)$ the achieved stability margin ε is defined in terms of the H^∞ norm as,

$$\gamma = \frac{1}{\varepsilon} = \left\| \begin{bmatrix} K \\ I_p \end{bmatrix} (I_p - GK)^{-1} M^{-1} \right\|_{\infty}$$

$$= \sup_{s=j\omega} \sigma_{max} \left\{ \left(\begin{bmatrix} K \\ I_p \end{bmatrix} (I_p - GK)^{-1} M^{-1} \right)(s) \right\}$$

Let $K = PQ^{-1}$ be NRCP factorization of the compensator over $\Re H^{\infty}$. Then it is clear that

$$\begin{bmatrix} K \\ I_p \end{bmatrix} (I_p - GK)^{-1} M^{-1} = \begin{bmatrix} P \\ Q \end{bmatrix} [MQ - NP]$$

and since $\begin{bmatrix} P \\ Q \end{bmatrix}$ is an inner function the resulting norm can be obtained as

$$\frac{1}{\varepsilon} = \left\| [MQ - NP]^{-1} \right\|_{\infty}$$

or equivalently,

$$\varepsilon = \inf_{s=j\omega} \sigma_{min} \{ \Phi(s) \}$$

where

$$\Phi(s) = [MQ - NP](s)$$

Thus we conclude that $\varepsilon = \theta_{sm}$.

The significance of the geometric stability margin is to lend an insight relating the classical Nyquist analysis to the MIMO setting and to clarify the role of the normalization in geometric terms. Thus it is clear from the definition of the geometric stability margin that θ_{sm} is the sine of the minimum principal angle between a certain pair of subspaces and therefore $0 \leq \varepsilon \leq 1$. We suspect that the role of the geometric picture may offer new insights in terms of frequency shaping design for combined stability and performance robustness. In the Phase 1 study we have highlighted these features briefly as part of the flight control benchmark.

2.3. Design Methods for combined performance and stability robustness

Loop shaping is a well established design methodology for control design for MIMO systems with LQG/LTR being one of the better developed techniques. An advantage of loop shaping is that a suitable loop shape for both stability and performance robustness can often be chosen---at least in the case of unstructured model uncertainty---with relative ease. The motivation for loop shaping comes from classical frequency domain design for SISO systems where lead/lag circuits as well as PID circuits provide the component parts for attaining the desired loop shapes and stability margins guide the designer in quantitative choices. For example, following SISO design we expect that low frequency gains should be sufficiently high for typical performance requirements of good tracking at steady state, while high frequency gain should be rapidly attenuated in regions where

17

the model dynamics may neglect significant parasitics. The achievable roll off in SISO systems is related to phase in a direct way as described by Bode. For MIMO systems it is in general also difficult to guarantee good robustness in the gain cross over region---particularly for nonminimum phase plants.

A new method of loop shaping has been proposed by McFarlane and Glover [33] and has been examined for the flight control design considered in this study. In this approach, the results of the problem of optimal robust stabilization of the normalized coprime factors (i.e., maximization of the geometric stability margin) are used as a basis for design. As an example consider the robust stabilization of a simple SISO plant and choose arbitrary stable NLCP factors;

$$G(s) = \frac{1}{s}, \quad M(s) = \frac{s}{s+1}, \quad N(s) = \frac{1}{s+1}$$

and take as compensator

$$K(s) = -k.$$

The class of systems that can be stabilized by K(s) can be described as

$$G_\Delta(s) = \left(M + \Delta_M\right)^{-1}\left(N + \Delta_N\right)$$

with $\left\|\begin{bmatrix}\Delta_M & \Delta_N\end{bmatrix}\right\|_\infty \le \theta_{sm}(G, K)$ where $\theta_{sm}(G, K)$ is the geometric stability margin which can be computed as

$$\theta_{sm}(G, K) = 1 / \left\|\begin{bmatrix}K\\I\end{bmatrix}(I - GK)^{-1}M^{-1}\right\|_\infty.$$

In this case we can obtain

$$\theta_{sm}(1/s, -k) = \begin{cases} \left(1 + k^{-2}\right)^{-1/2}, & \text{for } k \le 1 \\ \left(1 + k^{2}\right)^{-1/2}, & \text{for } k \ge 1. \end{cases}$$

Hence the stability margin is poor if either k<<1 or k>>1 and, in fact, optimal if k=1. In the former case the closed loop pole is moved to -k and hence a small change in the open loop pole--- say to +2k---would not be stabilized by the fixed feedback. In the latter case, the gain is high so that phase errors could cause loss of stability. Note that in both cases the interpretation just described will depend on several factors, including, for example, the scaling of time, inputs, and outputs. Note also that the loop shape, $1/\omega$, has been substantially altered in either case if k<<1 or k>>1.

18

The method proposed in [33] and implemented in this study is as follows:

(i) *Loop shaping*: Choose weighting functions W_i and W_0 such that the weighted or shaped plant $G_s = W_0 G W_i$ has the desired loop shape.

(ii) *Robust Stabilization*: Compute the optimal stability margin $\varepsilon_0 = \max_K \theta_{sm}(G_s, K)$

as in (2.18). If $\varepsilon_0(G_s) \ll 1$, return to (i), otherwise compute a controller K_s which achieves the maximal stability margin for the weighted plant using (2.19)--(2.22).

(iii) *Control Realization*: The final controller is realized by $K = W_i K_s W_0$.

The design method proposed has several useful and assured properties. For example, the direct optimization of the stability margin assures the geometric stability margin is achieved or execeeded at all frequencies. This feature is demonstrated in the examples considered in this report and provides a graphic demonstration of the broadband matching properties of H^∞ optimization. Second, in the high gain region the controller K_s computed for the shaped plant reduces the loop gains (i.e. min/max singular values) by a factor of at most $\varepsilon_0(G_s)$. Third, in the low gain region the controller K_s can increase the loop gains by at most a factor of $1/\varepsilon_0(G_s)$ Moreover, if $\varepsilon_0(G_s) \ll 1$, then $\theta_{sm} \leq \varepsilon_0(G_s) \ll 1$, for any stabilizing controller. Hence, in this case the loop shape is not compatible with the robust stabilization requirement and any controller which achieves it will have a poor stability margin in the gain cross over region, or undesirable decrease in the low frequency gain (i.e., loos of perfromance), or undesirable increase in the high frequency gain (i.e., loss of stability margin).

We therefore interpret the optimal stability margin as an indicator or engineering figure of merit for the compatibility of the loop shaping proposed in step (i). The resulting performance will be robust to any small changes in plant parameters which can be absorbed into the unstructured model uncertainty in terms of the perturbations to the NLCP factors. However, large changes in real parameters arising from changes in the system operating point may be difficult if not impossible to embed in perturbations to the NLCP factors of the plant without making the design overly conservative. An example of this fact is discussed in the flight control benchmark considered in a later section.

3. Worst Case Control Design for Combined Structured-Unstructured Model Uncertainty

In Figure 3.1 we display an uncertain system with feedback controller, K. $\Delta(s)$ is the plant model uncertainty and it is desired that the transfer function from w to z remain bounded less than 1 for all Δ such that $\|\Delta\|_\infty < 1$. The bound can be rescaled to any value and this problem can include both performance and stability robustness.

A sufficient condition for robust performance is that the closed-loop transfer function from $\bar{w} = [v^t, w^t]^t$ to $\bar{z} = [e^t, z^t]^t$ have an H^∞ norm less than 1. This condition is not conservative if robust stability or nominal performance alone are considered, but will become conservative when robust performance is required [16]. H^∞ optimization is an effective tool which can be applied to such problems to maximize the robustness. Additionally, the computational requirements are now understood [35]. The resulting approach is computationally quite tractable and provides controllers with degree no greater than the degree of the model P(s). However, it does not address structured uncertainty.
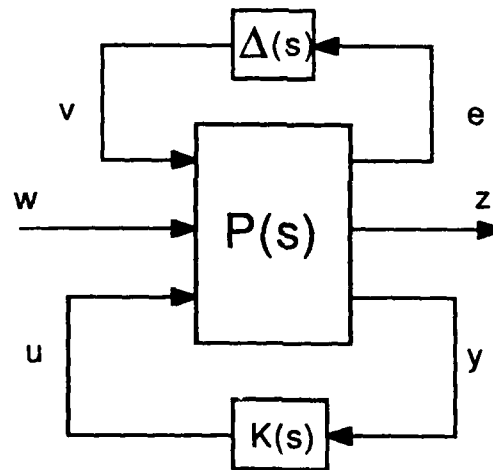
Figure 3.1: Uncertain Structure of Feedback Control Problem.

3.1. Summary of Some Existing Methods for Design
3.1.1. Structured Singular Values

The robust performance problem of Fig. 3.1 for $\|\Delta\|_\infty < 1$ and subject to a specific block diagonal structure for Δ is considered by Doyle in terms of the 'structured singular value' analysis. For a large number of blocks this problem is not tractable, but a good approximation can be obtained by introducing diagonal 'D-scales' on the inputs v and outputs z. These D-scales are

chosen to be functions of frequency that minimize the H^∞ norm of the scaled transfer function $\bar{w} \to \bar{z}$. This can provide an effective analysis tool.

The design problem is more difficult. It can be addressed by alternately minimizing over the D-scales and then over the stabilizing controllers K until convergence. There are few theoretical results to justify this procedure. Real parametric variation can (in principle) also be addressed using a nontrivial modification of the method [36]. Again, this is an analysis tool and computationally more involved than the case of complex (i.e. frequency dependent) structured uncertainties.

3.1.2. Methods Based on Kharitonov's Theorem

Kharitonov's theorem provides a remarkably efficient test for the stability of a class of systems when the closed loop characteristic polynomial can be written as a polynomial with coefficients--- each of which lies in an independent interval of the parameter space. This result has lead to a variety of methods for analysis of interval matrices whose elements are parameters contained in known intervals. However, for more general structures the resulting tests become intractable becouse of the size of the test matrices involved. Such tests are based on determinantal inequalities and involve purely algebraic computations whose complexity leads to algorithms which are NP-complete (in the jargon of computer science.)

3.1.3. Quadratic Stabilization

The work of Peterson and Hollot [37] on quadratic stabilization of uncertain systems considers norm-bounded but possibly time-varying perturbations of a nominal system. Furthermore, they employ a strong stability condition which requires the existence of a quadratic Lyapunov function.

It can be shown that this version of stability is identical to requiring an H^∞ norm bound on the transfer function from the outputs of the perturbations back to the corresponding inputs (as in Fig 3.1). Robust stability then follows from a small gain argument. Results using this procedure can therefore be interpreted in an H^∞ robust stabilization/performance framework.

3.1.4. Combined LQG-H^∞ Design

Bernstein and Haddad [38] consider a combined LQG and H^∞ control design. Their introduction suggest that they are minimizing the H^2 norm subject to a constraint on the H^∞ norm. This is in fact not the case as a careful examination of the paper reveals. Instead they minimize upperbounds rather than the actual norms as claimed. In many circumstances this will result in a good approximation to the original problem. Indeed, in the case when the H^∞ constraint and the H^2 criterion are both applied to the same closed loop transfer function, then (as shown by Mustafa [39]) their criterion is identical to the entropy maximization criterion in H^∞ design as considered by

Mustafa and Glover [40] (see also appendix). The entropy criterion for a closed loop transfer function, H(s), is

$$I(H,\gamma) = -\frac{1}{2\pi\gamma^2} \int_{-\infty}^{\infty} \log\left[\det\{1-\gamma^{-2}H(j\omega)H^*(j\omega)\}\right]d\omega \tag{3.1}$$

Clearly, it is required that $\|H\|_\infty \leq \gamma$ for $I(H,\gamma)$ to be well-defined and it is easily shown that $\sqrt{I(H,\gamma)}$ is an upper bound on the H^2 norm.

The major contribution of these papers is to allow different transfer functions in the H^2 and H^∞ criteria and can therefore address the problem of reduced order compensator design, the main disadvantage being the substantial computational difficulty involved in solving the resulting coupled Riccati equations.

In [41] Yeh et al consider the problem of designing controllers for the combination of both real parametric uncertainty and unmodeled dynamics. The approach utilizes a combination of the methods of Bernstein and Haddad together with the results of Peterson and Hollot. However, since both approachs employ upper bounds one can expect the results to be conservative.

To be specific consider the closed loop system

$$\dot{x} = (A + \Delta A)x + Bw$$
$$z = Cx \tag{3.2}$$

where

$$\Delta A = \sum_{i=1}^{p} D_i \Delta_i E_i, \quad \sigma_{max}(\Delta_i) \leq 1. \tag{3.3}$$

This system can be rewritten in the form of Figure 3.1 by defining,

$$e_i = E_i x, \quad v_i = \Delta_i e_i \tag{3.4}$$

to give,

$$\dot{x} = Ax + \sum_{i=1}^{p} D_i v_i + Bw \tag{3.5}$$

The corresponding Riccati equation employed in [41] is then

$$0 = AQ + QA^t + \gamma^{-2}QC^tCQ + \Omega + BB^t \tag{3.6}$$

22

where

$$\Omega = \sum_{i=1}^{p} D_i \, D_i^t + Q\left(\sum_{i=1}^{p} E_i \, E_i^t\right) Q .$$

(3.7)

However, the existence of $Q \geq 0$ to satisfy (3.7) is precisely a test on the H^∞ norm of the transfer function from w to z in Fig. 3.1. Hence the performance will be robust to the uncertainty as claimed but will also be robust to the unstructured uncertainty.

This approach gives a viable design technique for structured and unstructured uncertainty, however, it will be conservative because it essentially (although not obviously) embeds the structured uncertainty into a larger unstructured uncertainty perturbation (e.g. block of Δ). In fact if the coprime factors M_i and N_i are optimally scaled with frequency, then this scheme becomes identical to the structured singular values.

3.2. Worst Case Design as Minimax Optimal Control Problem

The geometric stability margin $\theta_{sm}(G_s, K)$ has been shown to be a suitable design indicator and engineering figure-of-merit for both performance and stability robustness of closed loop control systems. However, the control design procedure suggested above will be conservative if structured uncertainty due to real parametric variation is present in the model. Instead, in this section, we take the plant model to be of the form $G_\alpha(s) = G(s, \alpha)$, a function of a real parameter vector α. If we assume $\alpha \in \Theta \subseteq \mathfrak{R}^k$, a compact set in the k-dimensional real vector space then the optimal "robust" design solution for stability is to find a compensator K which stabilizes the nominal plant $G_0(s)$ and maximizes the worst case stability margin attained over the set $\alpha \in \Theta \subseteq \mathfrak{R}^k$. Here let $\gamma(\alpha, K) = 1/\theta_{sm}(G_\alpha, K)$ then we wish to find K which solves;

$$\inf_{K} \sup_{\alpha \in \Theta} \gamma(\alpha, K)$$

(3.8)

To see formally that this is appropriate for combined structured and unstructured uncertainty consider the problem as follows: given the design model

(plant) $y = G(\alpha)u$

(comp) $u = Ky$

with u an m-vector of plant inputs and y a p-vector of plant outputs. See Figure 3.2. The structured plant uncertainty is characterized by a l-vector of parameters, $\alpha \in \Theta$, with $\mathfrak{R}^l \supseteq \Theta$.
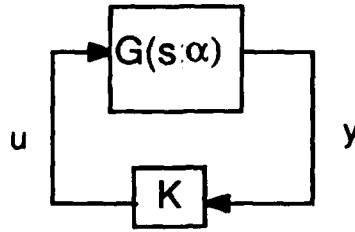
23

Figure 3.2: Robust Control Design Model for Mixed Uncertainty

Problem of Robust Stabilization: Find $K(s)$ $m \times p$ (controller) fixed wrt. α which stabilizes a class of plants $G(\alpha)$ given by:

(uc) Unstructured uncertainty conditions: for each $\alpha \in \Theta$, $G = \tilde{M}^{-1} \tilde{N}$ is taken to be a normalized left coprime factorization (NLCP); i.e., (N,M) are left coprime and

$$\tilde{M} \tilde{M}^* + \tilde{N} \tilde{N}^* = I$$

$$G \in \mathbb{G}_\varepsilon = \{ (\tilde{M} + \Delta_M)^{-1} (\tilde{N} + \Delta_N) : \| [\Delta_M , \Delta_N] \|_\infty < \varepsilon \} \qquad (3.9)$$

(sc) structured uncertainty conditions:

$$G \in \mathbb{G}_\alpha = \{ G(s; \alpha) : \alpha \in \Theta \}, \quad \Re^l \supseteq \Theta. \qquad (3.10)$$

For the mixed (or combined) uncertainty conditions we simply mean
$$G \in \mathbb{G}_\varepsilon \cap \mathbb{G}_\alpha .$$

A closely related but more tractable problem is the maximin (or dual) version of (3.8);

$$\sup_{\alpha \in \Theta} \inf_K \gamma(\alpha, K) = \frac{1}{\theta_{sm}(G_{\alpha_o}, K_o)}, \qquad (3.11)$$

whose solution is now feasible because of the results of Glover and McFarlane [32] as described in Section 2.2 of this report. These results provide a simple and computationally straightforward solution of the first level optimization problem; i.e., the optimal stability margin can be computed for any choice of α. The use of minimax design for parametric model uncertainty has been considered previously in only a few cases which have been reported in the open literature. Examples available provide an insufficient basis for theoretical extension of the results to large, complex problems but do suggest the practicality for relatively simple systems with small number of parameters [43].

Sufficient conditions for the minimax and maximin problems to have the same saddle point solution include the function $\gamma(\alpha, K)$ being convex in K and concave in $\alpha \in \Theta$. It is not

24

apparent that either of these conditions are likely to be satisfied globally. It can however, be shown that if we employ the Youla parametrization for the choice of K (i.e., to find a single controller for all $\alpha \in \Theta$) then the objective will be convex in the Q parameter [20]. The behavior with respect to $\alpha \in \Theta$ is unlikely to be concave except locally. At a saddle point it can be checked whether $\theta_{sm}(G_\alpha, K)$ is locally convex with respect to α. To do this we find the relation $K_o(\alpha)$ by the minimization in (3.11); i.e., the optimal controller depending on the unknown parameters. Then at the point (α_o, K_o) we check that $\theta_{sm}(G_\alpha, K_o)$ is minimized with respect to $\alpha \in \Theta$. Furthermore, if we use the suggested compensator K_o then we have the guaranteed bound

$$\underset{K}{\mathbf{inf}}\, \underset{\alpha \in \Theta}{\mathbf{sup}}\, \theta_{sm}(G_\alpha, K) \geq \theta_{sm}(G_{\alpha_o}, K_o)$$

$$(3.12)$$

and we can evaluate the achieved performance

$$\underset{\alpha \in \Theta}{\mathbf{sup}}\, \theta_{sm}(G_\alpha, K_o)$$

$$(3.13)$$

to establish the saddle point equivalence by comparison with the lower bound (3.12). The combination of the steps (3.11) and (3.13) will in general require extensive evaluations of the stability margins at various candidates (K, α) which may create extensive computational burden. However, as illustrated in the benchmark example, several significant flight control design issues can be addressed using this approach. We emphasize also that since no bounding approximations are used, the structure of the parametric uncertainty is retained in an essential way in the design process. It is also apparent that the worst case design obtained can be directly understood from the model assumptions and the objective of a *robust* solution [42].

The minimax and maximin problems will also be equivalent in the case when

$$\underset{\alpha \in \Theta}{\mathbf{sup}}\, \theta_{sm}(G_\alpha, K) = \varepsilon(G_{\alpha_o}, K) \quad \text{for all K;}$$

$$(3.14)$$

i.e. when the worst case set of parameters is independent of the choice of controller. This is often the case, for example, when the extreme values of the parameter correspond to maximum phase lag or ultimate instability (see example in the next section).

4. Control Design Benchmark-Robust Control for Aircraft with Relaxed Static Stability

4.1. Longitudinal Dynamics

We summarize the basic equations of motion which govern the longitudinal dynamics of an aircraft. Further details may be found in [49-52]. Figure 4.1 identifies the body axes $(X-Z)$[1], the velocity V, the body attitude θ, the flight path angle γ, the angle of attack $\alpha=\theta+\gamma$, and the principle forces acting on the airframe. These include lift, drag, thrust and weight.
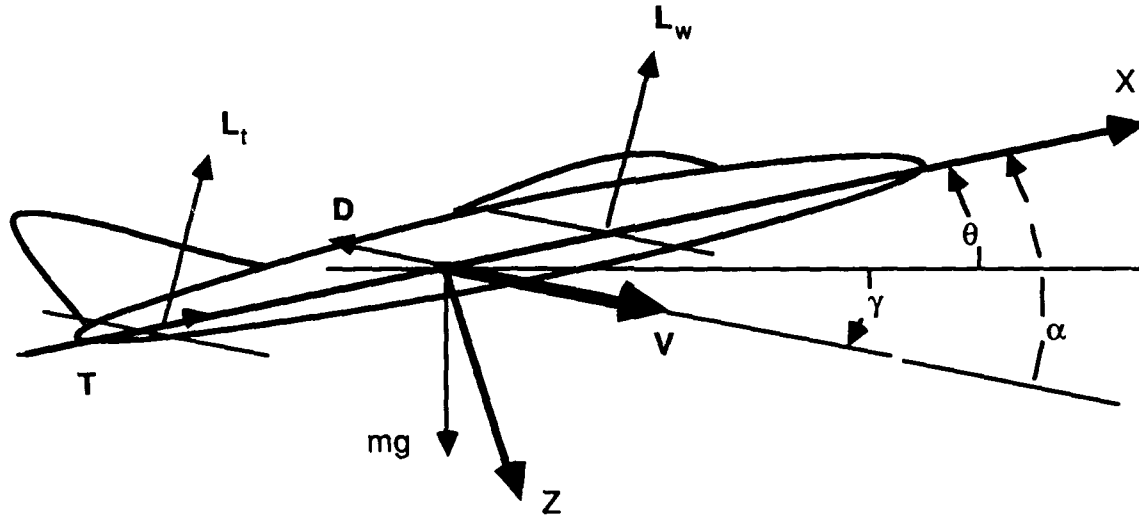

Figure 4.1. Principle Longitudinal Parameters

The basic equations of motion include: linear momentum balance in the X direction, linear momentum balance in the Z direction and angular momentum balance.

$$m(\dot{u}+w\dot{\theta}) = -mg\sin\theta + L_w\sin\alpha + L_t\sin\alpha_t + T - D\cos\alpha \qquad (4.1a)$$

$$m(\dot{w}-u\dot{\theta}) = mg\cos\theta - L_w\cos\alpha - L_t\cos\alpha_t - D\sin\alpha \qquad (4.1b)$$

$$I\ddot{\theta} = M_w + l_wL_w\cos\alpha - l_tL_t\cos\alpha_t - c\dot{\theta} \qquad (4.1c)$$

where α_t is the tail angle of attack and is related to the angle of attack α, pitch rate $\dot{\theta}$, tail angle i_t, downwash angle ε and the elevator deflection angle δ_e via the relation

$$\alpha_t = \alpha + i_t - \varepsilon + \delta_e + (l_t/V)\dot{\theta}$$

We also have

$$l_w + l_t = l*$$

---

[1]The X axis is usually aligned so that $\alpha=0$ corresponds to zero lift.

The lift and drag forces depend on the velocity V, air density ρ and surface area S via the relations

$$L = C_L(\alpha)\frac{1}{2}\rho V^2 S \tag{4.2a}$$

$$D = C_D(\alpha)\frac{1}{2}\rho V^2 S \tag{4.2b}$$

$$M = C_M(\alpha)\frac{1}{2}\rho V^2 S \tag{4.2c}$$

In view of the dependence of the forces and moments on V, α it is convenient to replace u, w in (4.1) by V, α using the transformation relations

$$w = V\sin\alpha \tag{4.3a}$$

$$u = V\cos\alpha \tag{4.3b}$$

Thus, we obtain

$$m(\cos\alpha\dot{V}-V\sin\alpha\dot{\alpha}+V\sin\alpha\dot{\theta}) = -mg\sin\theta + L_w\sin\alpha + L_t\sin\alpha_t + T - D\cos\alpha \tag{4.4a}$$

$$m(\sin\alpha\dot{V}+V\cos\alpha\dot{\alpha}-V\cos\alpha\dot{\theta}) = mg\cos\theta - L_w\cos\alpha - L_t\cos\alpha_t - D\sin\alpha \tag{4.4b}$$

$$I\ddot{\theta} = M_w + l_wL_w\cos\alpha - l_tL_t\cos\alpha_t - c\dot{\theta} \tag{4.4c}$$

Notice that equations (4.4) can be organized in the vector form

$$
\begin{bmatrix}
m\cos\alpha & -mV\sin\alpha & mV\sin\alpha & 0 \\
m\sin\alpha & mV\cos\alpha & -mV\cos\alpha & 0 \\
0 & 0 & 1 & 0 \\
0 & 0 & 0 & I
\end{bmatrix}
\frac{d}{dt}
\begin{bmatrix}
V \\ \alpha \\ \theta \\ \dot{\theta}
\end{bmatrix}
$$

$$
=
\begin{bmatrix}
-mg\sin\theta + L_w\sin\alpha + L_t\sin\alpha_t + T - D\cos\alpha \\
mg\cos\theta - L_w\cos\alpha - L_t\cos\alpha_t - D\sin\alpha \\
\dot{\theta} \\
M_w + l_wL_w\cos\alpha - l_tL_t\cos\alpha_t - c\dot{\theta}
\end{bmatrix}
\tag{4.5}
$$

4.1.1 Nondimensional Equations of Motion

Let us introduce a normalized velocity by identifying a nominal velocity (for example, the maximum cruise velocity) V_0 and define

$$\upsilon := (V/V_0)$$

and also the nondimensional quantities

$$\kappa := (l_w/l^*)$$
$$\Lambda_w := (L_w/mg), \quad \Lambda_t := (L_t/mg), \quad \Delta := (D/mg), \quad \Pi := (T/mg), \quad \Sigma_w := (M_w/l^*mg)$$

Equation (4.5) can now be written

$$
\begin{bmatrix}
\cos\alpha & -\upsilon\sin\alpha & \upsilon\sin\alpha & 0 \\
\sin\alpha & \upsilon\cos\alpha & -\upsilon\cos\alpha & 0 \\
0 & 0 & 1 & 0 \\
0 & 0 & 0 & 1
\end{bmatrix}
\frac{d}{dt}
\begin{bmatrix}
\upsilon \\
\alpha \\
\theta \\
(V_0/g)\dot{\theta}
\end{bmatrix}
$$

$$
= \frac{g}{V_0}
\begin{bmatrix}
-\sin\theta + \Lambda_w\sin\alpha + \Lambda_t\sin\alpha_t + \Pi - \Delta\cos\alpha \\
\cos\theta - \Lambda_w\cos\alpha - \Lambda_t\cos\alpha_t - \Delta\sin\alpha \\
(V_0/g)\dot{\theta} \\
(v_0^2 l^*/gr^2)\{\Sigma_w + \kappa\Lambda_w\cos\alpha - (1-\kappa)\Lambda_t\cos\alpha_t\} - (cV_0/mgr^2)(V_0/g)\dot{\theta}
\end{bmatrix}
$$

Now, let us introduce a nondimensional time, τ, and pitch rate, q,

$$\tau := (g/V_0)t, \quad q := (V_0/g)\dot{\theta}$$

in order to obtain the nondimensional equations

$$
\begin{bmatrix}
\cos\alpha & -\upsilon\sin\alpha & \upsilon\sin\alpha & 0 \\
\sin\alpha & \upsilon\cos\alpha & -\upsilon\cos\alpha & 0 \\
0 & 0 & 1 & 0 \\
0 & 0 & 0 & 1
\end{bmatrix}
\frac{d}{d\tau}
\begin{bmatrix}
\upsilon \\
\alpha \\
\theta \\
q
\end{bmatrix}
$$

28

$$= \begin{bmatrix} -\sin\theta + \Lambda_w\sin\alpha + \Lambda_t\sin\alpha_t + \Pi - \Delta\cos\alpha \\ \cos\theta - \Lambda_w\cos\alpha - \Lambda_t\cos\alpha_t - \Delta\sin\alpha \\ q \\ \dfrac{V_0^2 l^*}{gr^2}\{\Sigma_w + \kappa\Lambda_w\cos\alpha - (1-\kappa)\Lambda_t\cos\alpha_t\} - \dfrac{cV_0}{mgr^2}\,q \end{bmatrix} \qquad (4.6)$$

4.1.2 A Fictitious Aircraft

Level flight corresponds to $\gamma = 0$. We assume that the longitudinal body reference axis corresponds to the wing zero lift line and that level flight at nominal conditions (V_0,ρ_0) corresponds to $\alpha,\theta = \alpha_0$. In this case, the normalized lift forces take the form

$$\Lambda_w = f_w(\alpha)\bar{p}\upsilon^2, \quad \Lambda_t = f_t(\alpha_t)\bar{p}\upsilon^2, \text{ with } f_w(0) = 0, f_t(0) = 0, \bar{p} = (\rho/\rho_0) \qquad (4.7)$$

The normalized drag force is assumed to be of the form

$$\Delta = \left(a + b[f_w(\alpha)]^2\right)\bar{p}\upsilon^2 \qquad (4.8)$$

and the moment is of the form

$$\Sigma_w = \sigma_w(\alpha)\bar{p}\upsilon^2 \qquad (4.9)$$

In the following discussion, numerical computations and examples will be based on the following model aircraft characteristics unless otherwise noted.

$$\bar{p} = 1, \varepsilon = 0, \sigma_w(\alpha) = 0, a = .1, b = .1 \qquad (4.10a)$$

$$f_w = \left(\frac{\alpha-2.08(\alpha-\alpha_0)^3}{\alpha_0}\right), f_t = \varepsilon'\left(\frac{(\alpha-\alpha_0+\delta_e)-3(\alpha-\alpha_0+\delta_e)^3}{\alpha_0}\right), \alpha_0 = .05, \varepsilon' = .1 \qquad (4.10b)$$

$$\frac{V_0^2 l^*}{gr^2} = 300, \frac{cV_0}{mgr^2} = 8 \qquad (4.10c)$$

4.1.3 Static and Dynamic Stability

Equation (4.6) can be written

$$J(x)\dot{x} = f(x,u,\mu) \qquad (4.11)$$

29

where x denotes the state vector, u denotes the control variables and μ denotes a designated set of system parameters. A triple (x^*, u^*, μ^*) is an equilibrium point if

$$f(x^*, u^*, \mu^*) = 0 \tag{4.12}$$

The corresponding perturbation equations are

$$J(x^*)\delta\dot{x} = \frac{\partial f}{\partial x}(x^*, u^*, \mu^*)\delta x + \frac{\partial f}{\partial u}(x^*, u^*, \mu^*)\delta u \tag{4.13}$$

One easily verifies that $\det\{J(x)\} = \upsilon$ for $\upsilon > 0$, so that under these conditions we can rewrite (4.13) in the form

$$\delta\dot{x} = A(\mu^*)\delta x + B(\mu^*)\delta u \tag{4.14}$$

Example. Notice that $\kappa=0$, $\delta_e=.0005$, $\Pi=.1$, $\upsilon=1$, $\alpha=.0495$, $\theta=-.0495$, $q=0$ is an equilibrium point, corresponding to level flight at nominal velocity. The perturbation equations are

$$\frac{d}{d\tau}\begin{bmatrix} \delta\upsilon \\ \delta\alpha \\ \delta\theta \\ \delta q \end{bmatrix} = \begin{bmatrix} -.3960 & -2.949 & -1.0 & 0 \\ -1.980 & -21.80 & 0 & 1.0 \\ 0 & 0 & 0 & 1.0 \\ 0 & -599.2 & 0 & -8.0 \end{bmatrix} \begin{bmatrix} \delta\upsilon \\ \delta\alpha \\ \delta\theta \\ \delta q \end{bmatrix} + \begin{bmatrix} .9987 & .0010 \\ -.0495 & -2.0 \\ 0 & 0 \\ 0 & -599.3 \end{bmatrix} \begin{bmatrix} \delta\Pi \\ \delta_e \end{bmatrix}$$

The dynamical modes are

short period $\qquad \lambda = -14.961 \pm j23.366,$ $\qquad v = \begin{bmatrix} -.0053 \\ -.0300 \\ .0009 \\ -.8550 \end{bmatrix} \pm j \begin{bmatrix} -.0005 \\ .0273 \\ .0360 \\ -.1516 \end{bmatrix}$

phugoid $\qquad \lambda = -.13873 \pm j1.2339,$ $\qquad v = \begin{bmatrix} ..3723 \\ -.0081 \\ -.3847 \\ .5554 \end{bmatrix} \pm j \begin{bmatrix} -.2536 \\ .0043 \\ -.4069 \\ -.4182 \end{bmatrix}$

30

In characterizing equilibria for systems with feedback control it is usual to associate with (4.11) a set of outputs equal in number to the control inputs

$$y = g(x,u,\mu) \qquad (4.15)$$

Then we obtain equilibria by specifying μ^* and solving the following equations for x^*, u^*

$$F(x^*,u^*,\mu^*) = \begin{bmatrix} f(x^*,u^*,\mu^*) \\ g(x^*,u^*,\mu^*) \end{bmatrix} = 0 \qquad (4.16)$$

<u>*Definition*</u> : An equilibrium point (x^*,u^*,μ^*) is *regular* if there exists a neighborhood of μ^* on which there exist unique functions $x(\mu)$, $u(\mu)$ satisfying

$$F(x(\mu),u(\mu),\mu) = 0$$

with $x^*=x(\mu^*)$, $u^*=u(\mu^*)$.

Notice that the implicit function theorem implies that an equilibrium point is regular if

$$\det [D_x F \; D_u F]^* \neq 0 \qquad (4.17)$$

<u>*Definition*</u> : An equilibrium point (x^*,u^*,μ^*) is a *(static) bifurcation point* with respect to $F(x,u,\mu)$ if in each neighborhood of (x^*,u^*,μ^*) there exists (x_1,u_1,μ) and (x_2,u_2,μ) with $(x_1,u_1) \neq (x_2,u_2)$ and $F(x_1,u_1,\mu)=0, F(x_2,u_2,\mu)=0$.

Clearly, an equilibrium point is a bifurcation point only if it is not regular. We can give a useful interpretation to static bifurcation for systems defined by state Equation (4.11) and output Equation (4.15). Let us define

$$C(\mu^*):=\frac{\partial g}{\partial x}(x^*,u^*,\mu^*), \quad D(\mu^*):=\frac{\partial g}{\partial u}(x^*,u^*,\mu^*) \qquad (4.18)$$

so that in terms of perturbation variables the output equation becomes

$$\delta y = C(\mu^*)\delta x + D(\mu^*)\delta u \qquad (4.19)$$

With this notation (4.17) is equivalent to

$$\det \begin{bmatrix} A(\mu^*) & B(\mu^*) \\ C(\mu^*) & D(\mu^*) \end{bmatrix} \neq 0 \tag{4.20}$$

Thus, we have the following conclusion.

Theorem : An equilibrium point (x^*, u^*, μ^*) is a *(static) bifurcation point* only if the linearized system (4.14), (4.19) has a transmission zero at the origin.

We define stability of equilibria for parameter dependent dynamical systems as follows.

Definition : An equilibrium point (x^*, u^*, μ^*) is *(dynamically) stable* if it is regular and stable in the sense of Liapunov.

Notice that this definition incorporates two essential elements. The equilibrium point persists under infinitesimal variations of the parameter μ (regularity), and the state trajectories remain bounded following sufficiently small state perturbations (Liapunov stability).

It is common, and useful, to distinguish between dynamic and static stability. A necessary condition for stability of the equilibrium point (x^*, u^*, μ^*) is that the matrix $A(\mu^*)$ has eigenvalues with nonpositive real parts, so that it must satisfy

$$\det\{-A(\mu^*)\} = (-1)^n \det\{J(x^*)\}\det\{\frac{\partial f}{\partial x}(x^*, u^*, \mu^*)\} \geq 0$$

where n=dim(A). Recall that $\det\{J(x)\} = \upsilon > 0$, so that this condition reduces to

$$(-1)^n \det\{\frac{\partial f}{\partial x}(x^*, u^*, \mu^*)\} \geq 0$$

Accordingly, we introduce the following notion of static stability.

Definition : An equilibrium point (x^*, u^*, μ^*) of (4.11), (4.15) is *statically stable* if it is regular and if $(-1)^n \det\{\frac{\partial f}{\partial x}(x^*, u^*, \mu^*)\} \geq 0$.

Notice that static stability is a necessary but not sufficient condition for stability Also, in the case of aircraft longitudinal dynamics, as defined by (4.6), n=4. Our definition of static stability differs from the conventional one (see Etkin [1]) only in the fact that we explicitly include the requirement that the equilibrium point be regular. It is often the case that aircraft longitudinal static stability reduces approximately to the requirement that the pitch stiffness is negative. Such an example is given below.

4.2. Structured Model Uncertainty of Aircraft Longitudinal Model

Example I: Open Loop Properties. We give a simple example which illustrates the importance of center of gravity location on aircraft longitudinal static stability. Consider the following problem. With the elevator deflection angle δ fixed and the velocity υ specified, we wish to determine values of α, θ (or, equivalently, γ) and Π which satisfy the equilibrium equations[1]. The first equation can always be satisfied by choosing

$$\Pi = \sin(\alpha-\gamma) - \Lambda_w\sin\alpha - \Lambda_t\sin(\alpha+\delta) + \Delta\cos\alpha \tag{4.17}$$

Thus, we need only be concerned with the determination of α and θ from the remaining two equilibrium equations

$$\cos(\theta) - \Lambda_w\cos\alpha - \Lambda_t\cos(\alpha+\delta) - \Delta\sin\alpha = 0 \tag{4.18a}$$

$$\Sigma_w + \kappa\Lambda_w\cos\alpha - (1-\kappa)\Lambda_t\cos(\alpha+\delta) = 0 \tag{4.18b}$$

Let us consider κ to be the only adjustable parameter. Then since α and θ are the dependent variables we have

$$DF = [D_\alpha F\ D_\theta F\ D_\kappa F] = \begin{bmatrix} A & B & 0 \\ C & 0 & D \end{bmatrix}$$

$A = \dfrac{\partial}{\partial\alpha} \left[-\Lambda_w\cos\alpha - \Lambda_t\cos(\alpha+\delta) - \Delta\sin\alpha \right]$

$B = -\sin\theta$

$C = \dfrac{\partial}{\partial\alpha} \left[\Sigma_w + \kappa\Lambda_w\cos\alpha - (1-\kappa)\Lambda_t\cos(\alpha+\delta) \right]$

$D = \Lambda_w\cos\alpha + \Lambda_t\cos(\alpha+\delta)$

---

[1]Notice that q=0 in equilibrium.

33

Notice that $\det\{D_x f\} = -BC = 0$ only if either $\theta = n\pi$ for some integer n or $C=0$. Thus, a static bifurcation occurs only if one of these conditions is satisfied simultaneously with (4.18). We can easi'v illustrate the significance of the case $C=0$ as κ varies. Equation (4.18b) provides a relation between the center of gravity location (κ) and the angle of attack (α). Figures 4.2 and 4.3 illustrate this relation for linear and cubic lift coefficient characteristics, respectively. Both curves reveal similar qualitative behavior. There is a critical cg location κ_c (and an associated α_c, θ_c) corresponding to a local maximum and which may be shown to coincide with $C(\alpha_c, \theta_c, \kappa_c) = 0$. For $\kappa > \kappa_c$ there are no equilibrium solutions and for $\kappa < \kappa_c$ there are two. In the latter case, the equilibrium corresponding to $C<0$ (the one with smaller angle of attack) is stable whereas the the other equilibrium corresponds to $C>0$ and is unstable.
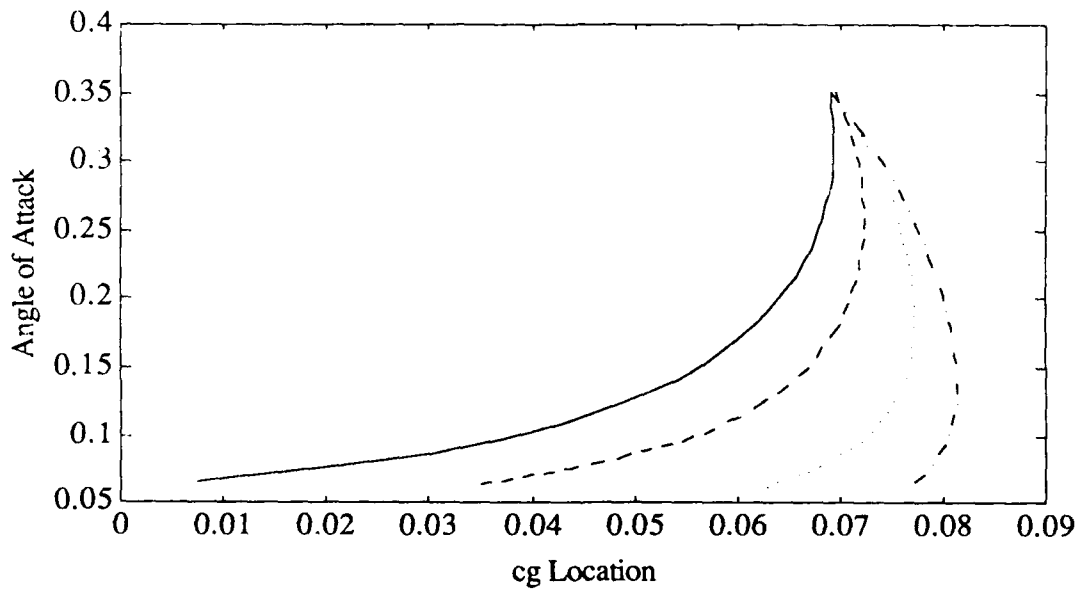

Figure 4.2 Angle of attack, α, vs. center of gravity location, κ, with $\upsilon = .4$ and various values of δ (from left to right $\delta = -0.01, 0.01, 0.03, 0.04$). Note that κ negative means that the center of gravity is forward of the wing center of pressure.
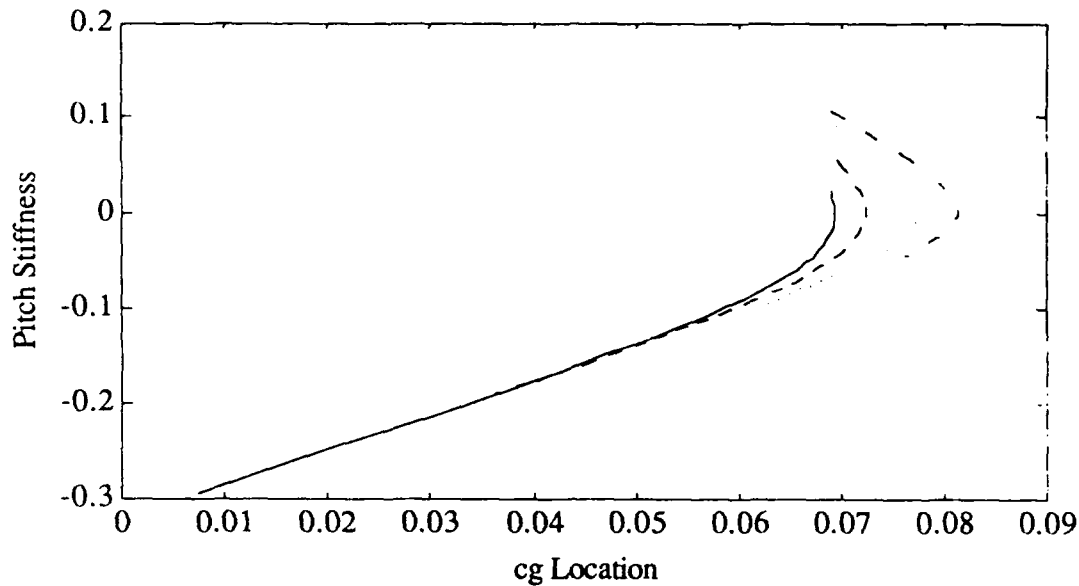
Figure 4.3 Pitch stiffness, C, as a function of cg location, κ. The same parameter values as above.

Note that C may be interpreted as the pitch stiffness. It is a commonly used indicator of aircraft longitudinal static stability [1-4]. In the aviation community static stability is distinct from dynamic stability. An equilibrium point is said to be statically stable if C>0, statically unstable if C<0 and to have neutral static stability if C=0. In the preceeding example neutral static stability corresponds to a parameter value at which the equilibrium point is not regular - indeed, it corresponds to a bifurcation point.

It should be emphasized that this static instability is distinct from aerodynamic stall phenomena. The cubic lift coefficients used in generating Figure 4.3 are illustrated in Figure 4.4. It is readily observed that the critical angle of attack in Figure 4.3 is well below the stall angle of attack for either the wing or the tail.
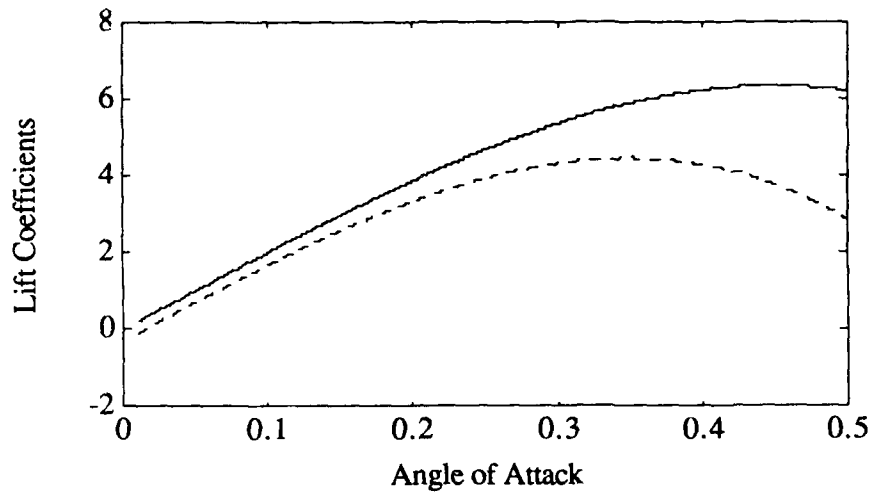
Figure 4.4. Normalized lift coefficients f_w (solid) and f_t/ε' (dashed) plotted as functions of α.

In the following Figures 4.6 through 4.11 we illustrate how velocity affects the equilibrium values of pitch angle and angle of attack.
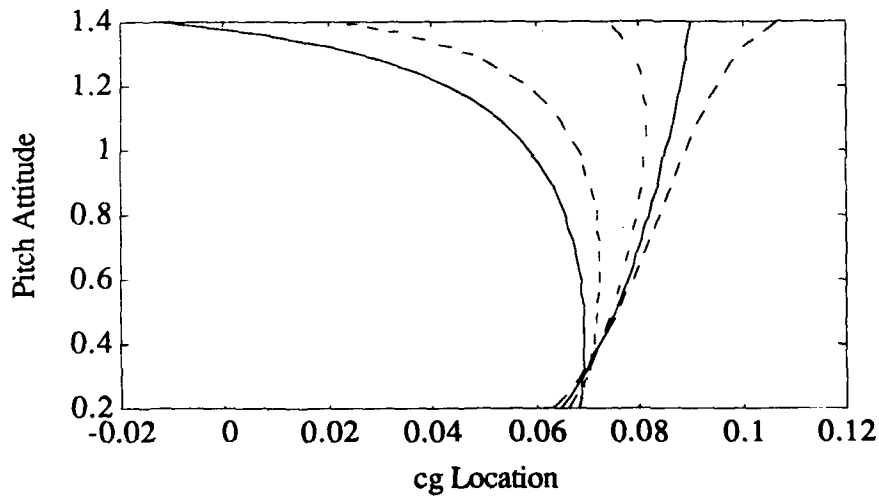

Figure 4.5a Pitch attitude,θ, vs. cg location, κ, with $\upsilon=.4$, and from left to right $\delta=-0.01$, 0.01, 0.03, 0.04, 0.05, 0.06.

Figure 4.5b Angle of attack,α, vs. cg location, κ, with υ=.4, and from left to right δ=-0.01, 0.01, 0.03, 0.04, 0.05, 0.06.

Figure 4.6a Pitch attitude,θ, vs. cg location, κ, with υ=.41, and from left to right δ=-0.01, 0.01, 0.03, 0.04, 0.05, 0.06.

Figure 4.6b Angle of attack,α, vs. cg location, κ, with υ=.41, and from left to right δ=-0.01, 0.01, 0.03, 0.04, 0.05, 0.06.

Figure 4.7a Pitch attitude,θ, vs. cg location, κ, with υ=.42, and from left to right δ=-0.01, 0.01, 0.03, 0.04, 0.05, 0.06.
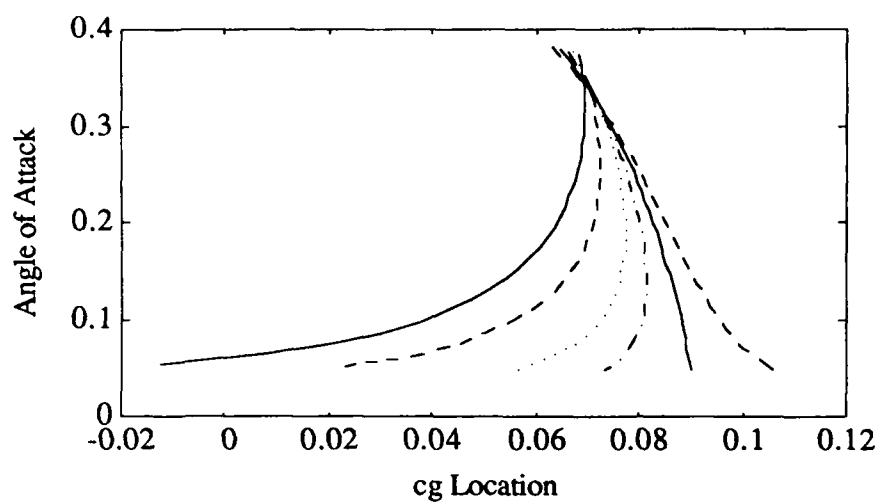
38

Figure 4.7b Angle of attack,α, vs. cg location, κ, with υ=.42, and from left to right δ=-0.01, 0.01, 0.03, 0.04, 0.05, 0.06.
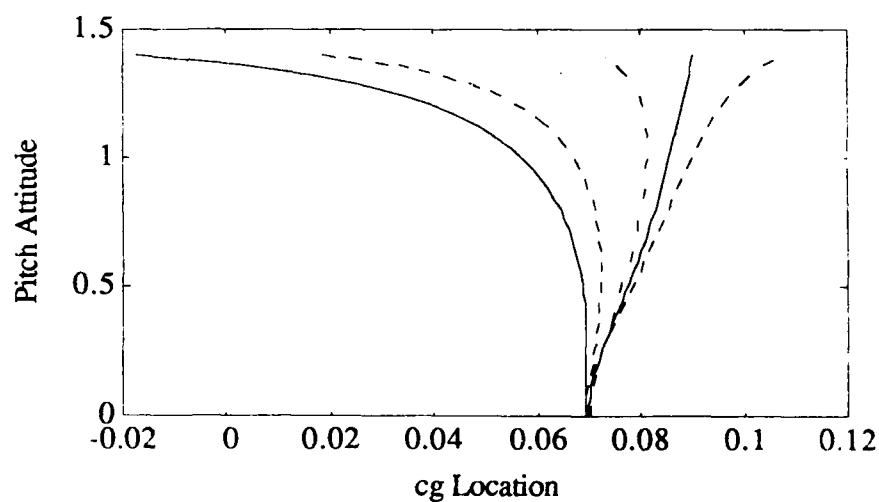

Figure 4.8a Pitch attitude,θ, vs. cg location, κ, with υ=.45, and from left to right δ=-0.01, 0.01, 0.03, 0.04, 0.05, 0.06.
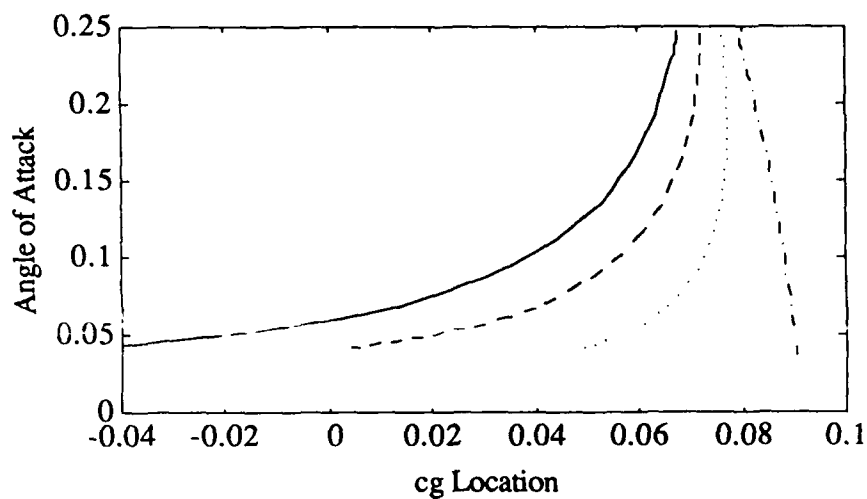
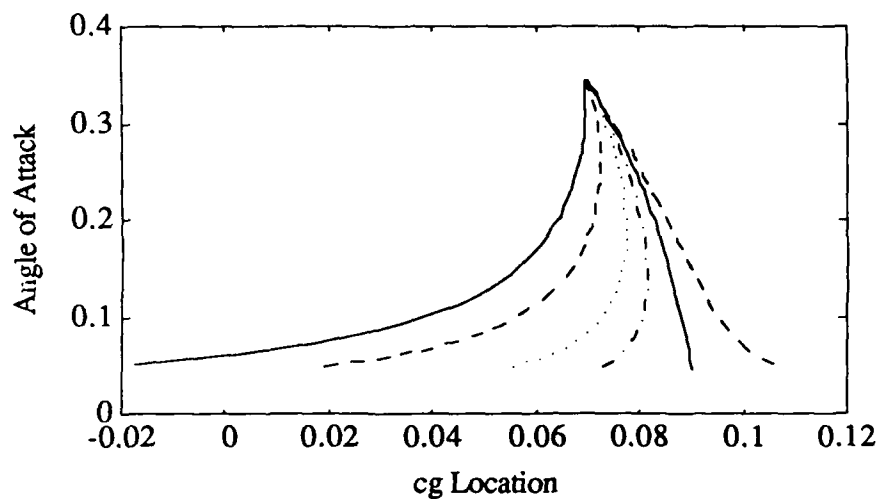Figure 4.8b Angle of attack,α, vs. cg location, κ, with υ=.45, and from left to right δ=-0.01, 0.01, 0.03, 0.04, 0.05, 0.06.
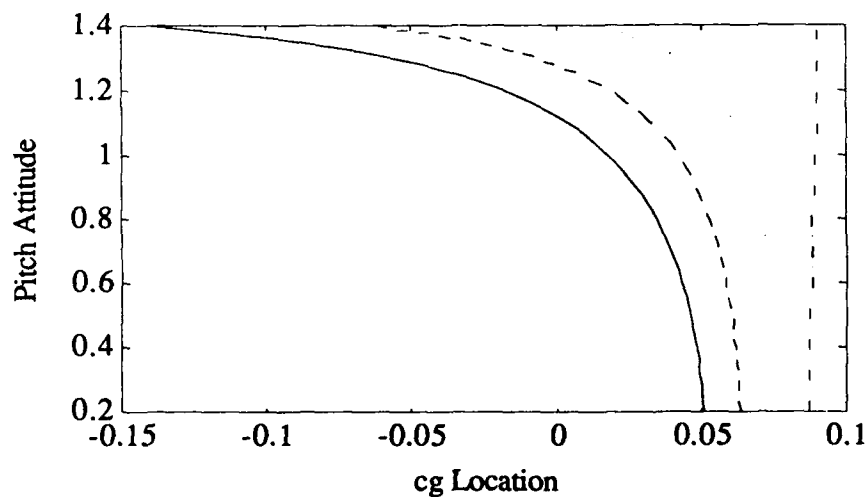
Figure 4.9a Pitch attitude,θ, vs. cg location, κ, with υ=.6, and from left to right δ=-0.01, 0.01, 0.03, 0.04, 0.05, 0.06.
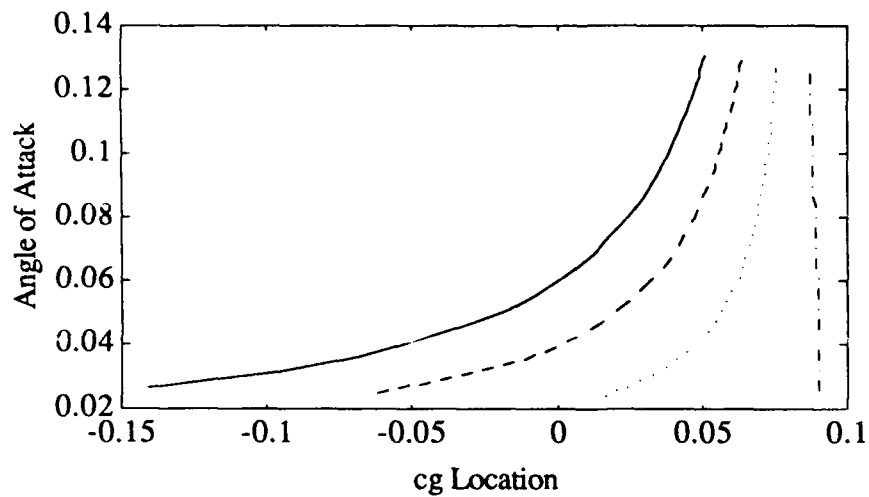
Figure 4.9b Angle of attack,α, vs. cg location, κ, with υ=.6, and from left to right δ = 0.01, 0.01, 0.03, 0.04, 0.05, 0.06.
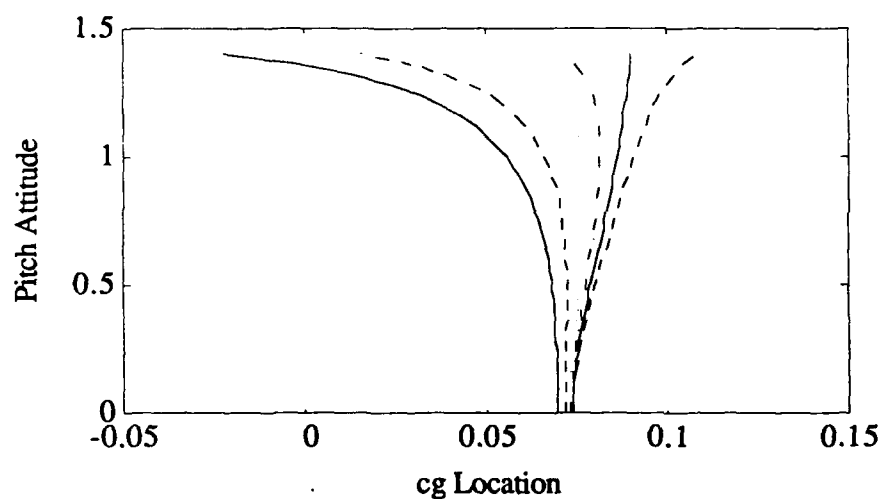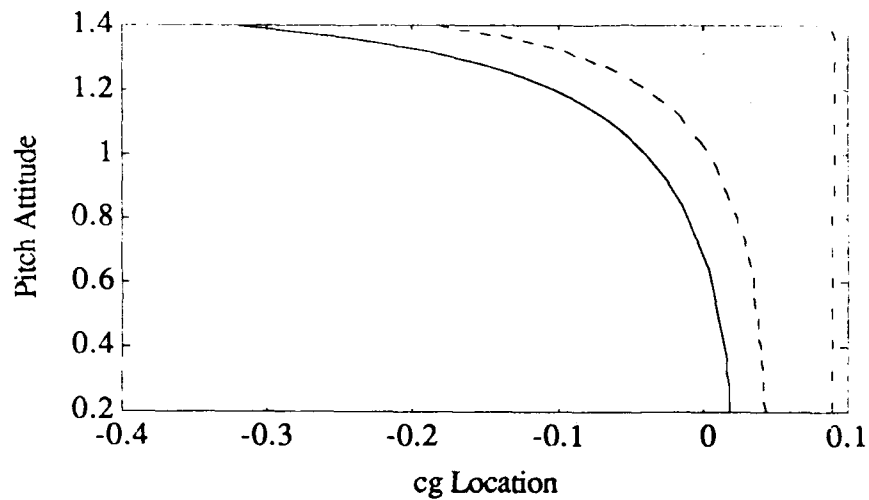

Figure 4.10a Pitch attitude,θ, vs. cg location, κ, with υ=.8, and from left to right δ=-0.01, 0.01, 0.03, 0.04, 0.05, 0.06.
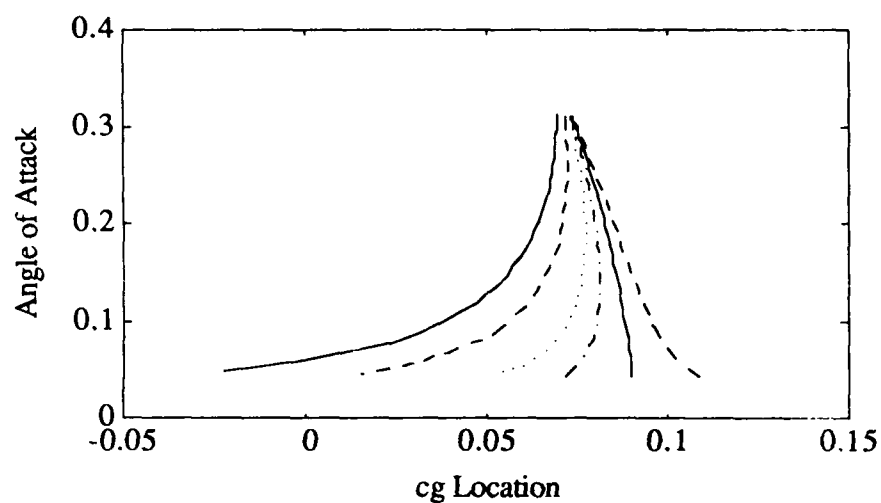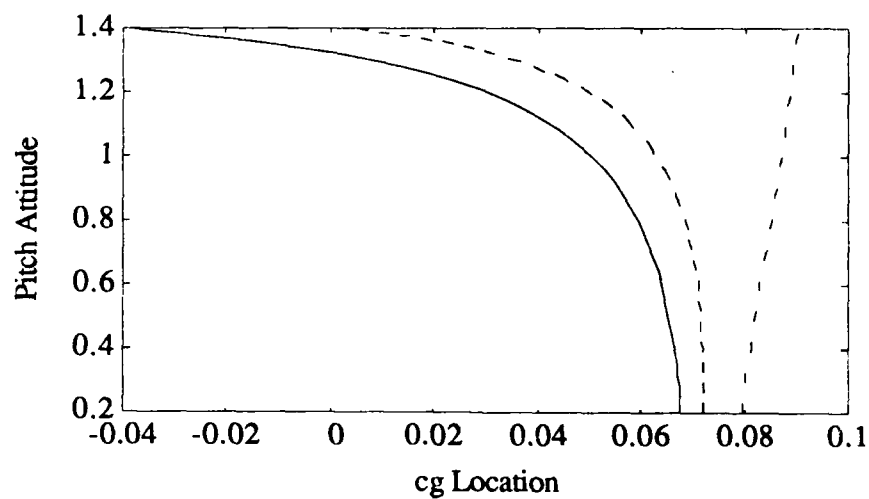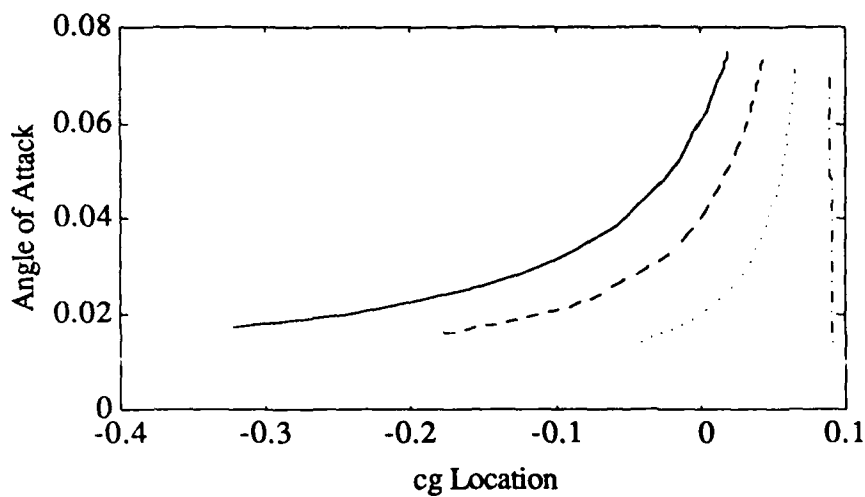
Figure 4.10b Angle of attack,α, vs. cg location, κ, with υ=.8, and from left to right δ=-0.01, 0.01, 0.03, 0.04, 0.05, 0.06.
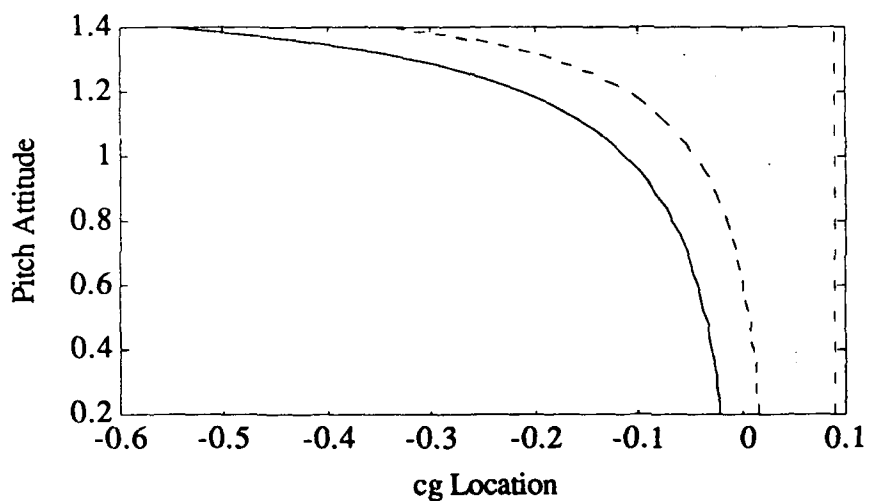
Figure 4.11a Pitch attitude,θ, vs. cg location, κ, with υ=1., and from left to right δ=-0.01, 0.01, 0.03, 0.04, 0.05, 0.06.
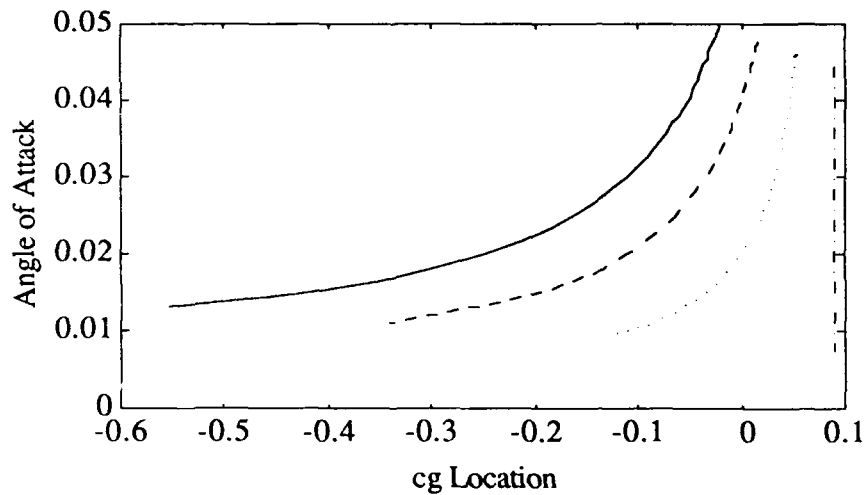
Figure 4.11b Angle of attack,α, vs. cg location, κ, with $\upsilon=1$., and from left to right $\delta=-0.01$, 0.01, 0.03, 0.04, 0.05, 0.06.

We obtain another perspective in Figures 4.12a,b&c where the complete equilibrium curves are illustrated with normalized velocity $\upsilon=.42$ and a elevator deflection angle $\delta=0.03$. These curves should be compared with Figures 4.13 a,b&c, which correspond to $\upsilon=1$.
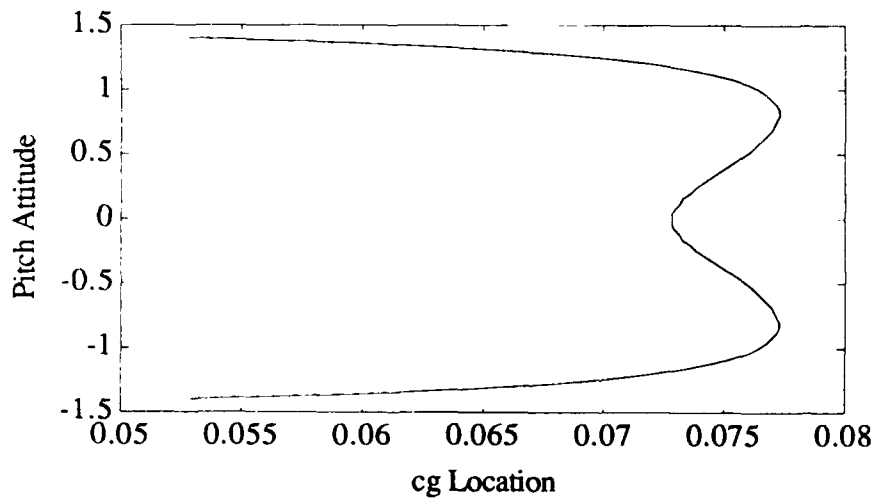
Figure 4.12a Pitch attitude,θ, vs. cg location, κ, with $\upsilon=.42$, and elevator deflection angle $\delta= 0.03$.
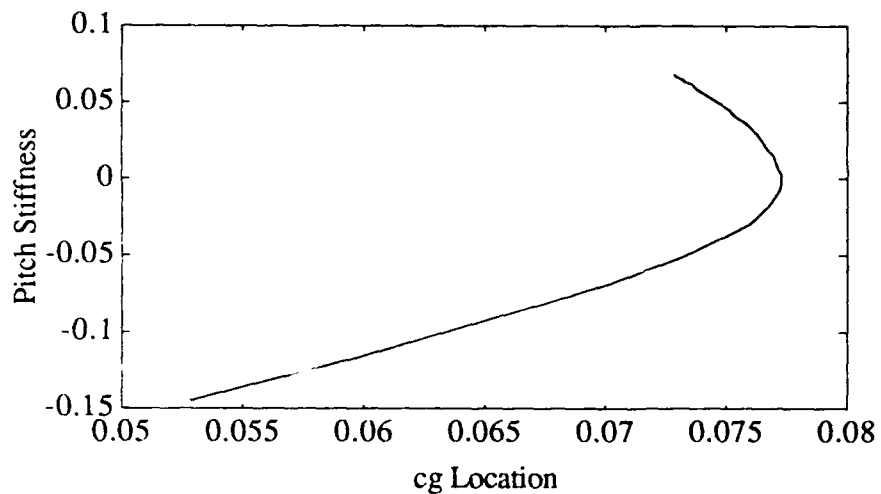
Figure 4.12b Pitch Stiffness, C, vs. cg location, κ, with υ=.42, and elevator deflection angle δ= 0.03.
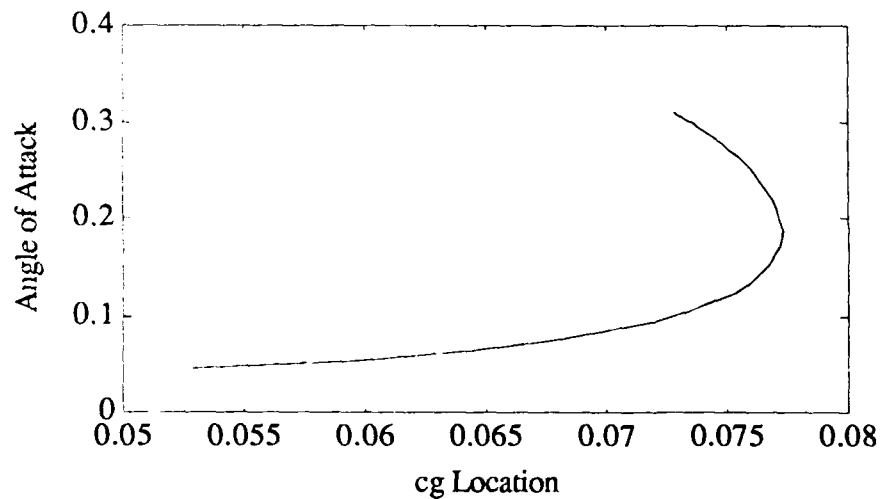
Figure 4.12c Angle of attack,α, vs. cg location, κ, with υ=.42, and elevator deflection angle δ= 0.03.
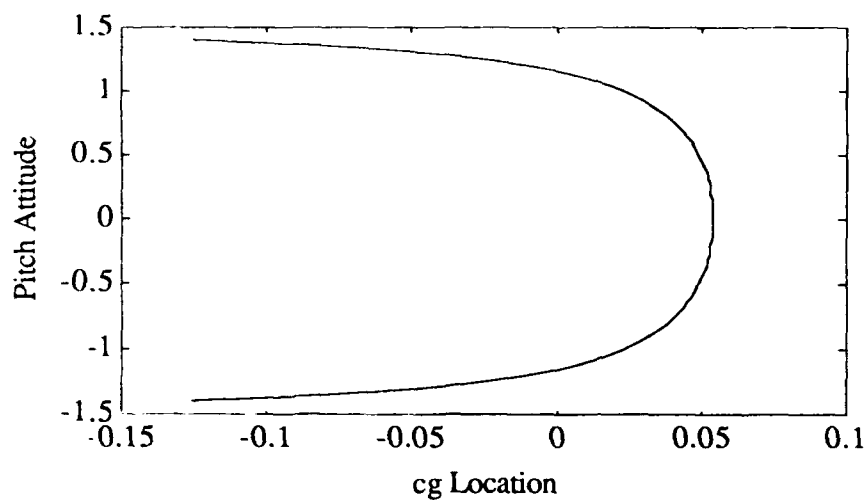
Figure 4.13a Pitch attitude,θ, vs. cg location, κ, with υ=1., and elevator deflection angle δ= 0.03.
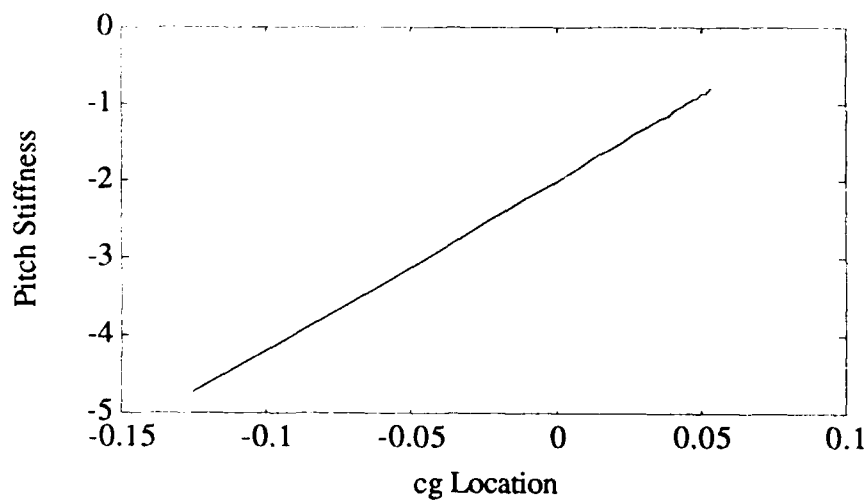
Figure 4.13b Pitch Stiffness, C, vs. cg location, κ, with υ=1., and elevator deflection angle δ= 0.03.
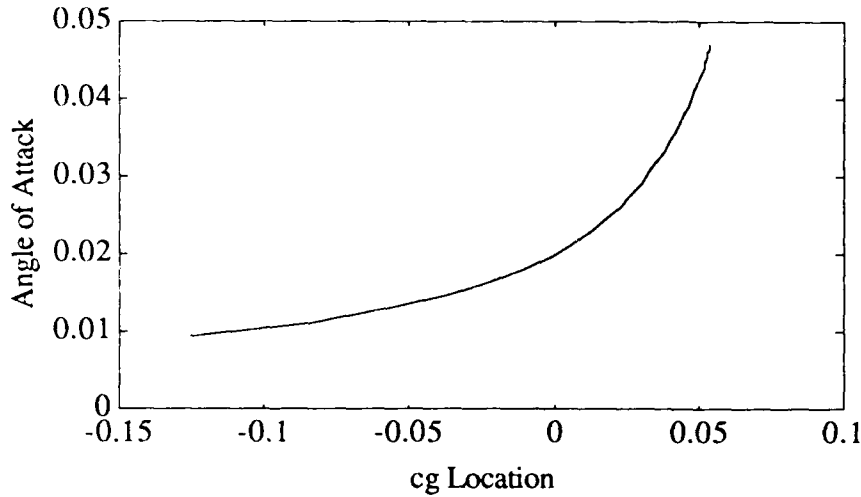
Figure 4.13c Angle of attack,α, vs. cg location, κ, with $\upsilon=1.$, and elevator deflection angle $\delta= 0.03$.

Example II: Closed Loop Properties. A somewhat more pertinent example with respect to control system design is the following. Once again consider the longitudinal dynamics defined by equation (4.6). It is desired to regulate the velocity and flight path angle υ, γ by adjusting the elevator deflection angle and thrust δ, Π. Thus, we define the output equations

$$\begin{bmatrix} y_1 \\ y_2 \end{bmatrix} = \begin{bmatrix} \upsilon\text{-}\upsilon^* \\ \gamma\text{-}\gamma^* \end{bmatrix} = \begin{bmatrix} \upsilon\text{-}\upsilon^* \\ \alpha\text{-}\theta\text{-}\gamma^* \end{bmatrix}$$

Given the desired flight path parameters υ, γ we wish to determine values of α, δ, Π which satisfy the equilibrium equations (4.16), with

$$f(x,u,\mu) := \begin{bmatrix} -\sin\theta + \Lambda_w\sin\alpha + \Lambda_t\sin\alpha_t + \Pi - \Delta\cos\alpha \\ \cos\theta - \Lambda_w\cos\alpha - \Lambda_t\cos\alpha_t - \Delta\sin\alpha \\ q \\ \frac{V_0^2 l^*}{gr^2}\{\Sigma_w + \kappa\Lambda_w\cos\alpha - (1\text{-}\kappa)\Lambda_t\cos\alpha_t\} - \frac{cV_0}{mgr^2}\ q \end{bmatrix} \qquad (4.19a)$$

$$g(x,u,\mu) := \begin{bmatrix} \upsilon\text{-}\upsilon^* \\ \alpha\text{-}\theta\text{-}\gamma^* \end{bmatrix} \qquad (4.19b)$$

46

Once again Π is directly determined from (4.17) and we need only be concerned with the solution properties of the pair of equations

$$\cos(\alpha-\gamma) - \Lambda_w\cos\alpha - \Lambda_t\cos(\alpha+\delta) - \Delta\sin\alpha = 0 \qquad (4.20a)$$

$$\Sigma_w + \kappa\Lambda_w\cos\alpha - (1-\kappa)\Lambda_t\cos(\alpha+\delta) = 0 \qquad (4.20b)$$

Figures 4.14 a&b illustrate the equilibrium values of elevator deflection, δ, and angle of attack, α, as a function of cg location, κ, at cruise conditions $\upsilon=1$, $\gamma=0$.
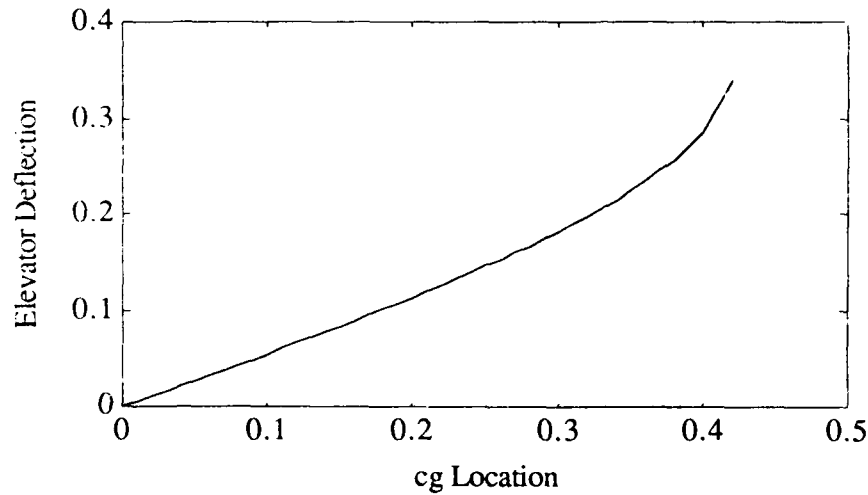
Figure 4.14a Elevator deflection, δ, as a function of cg location, κ, with $\upsilon=1$, $\gamma=0$.
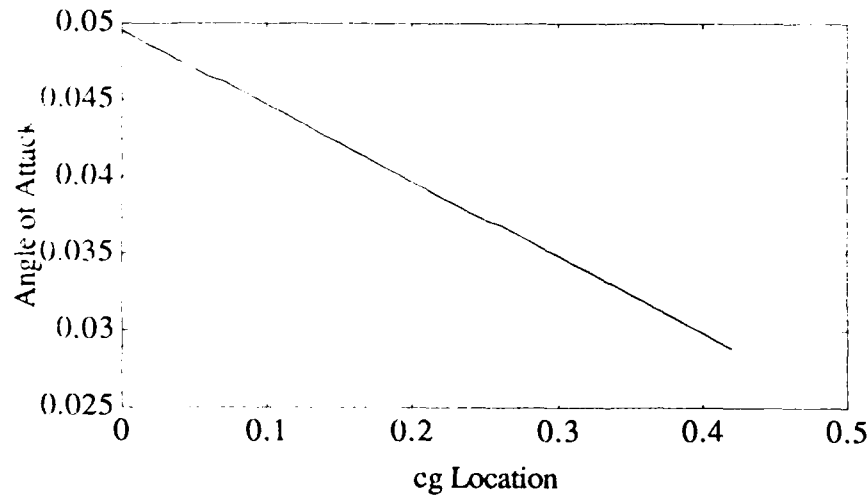
Figure 4.14b Angle of attack, α, as a function of cg location, κ, with $\upsilon=1$, $\gamma=0$.

47

In Figures 4.15a&b we illustrate the eigenvalue locations as a function of cg location, $0 \leq \kappa \leq .4$. Figure 4.15a clearly shows the expected short period and phugoid branches. A loss of static stability occurs at approximately $\kappa = .12$. Interestingly enough, although the Jacobian $D_x f(x^*, u^*, \mu^*)$ is singular, this does not correspond to a bifurcation point because the Jacobian $D_{x,\mu} F(x^*, u^*, \mu^*)$ is not.
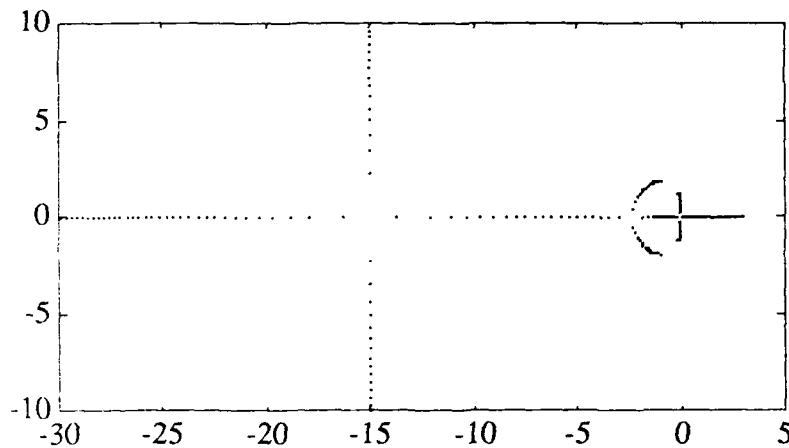
Figure 4.15a Open loop eigenvalue locations as a function of cg location, κ, at cruise conditions.
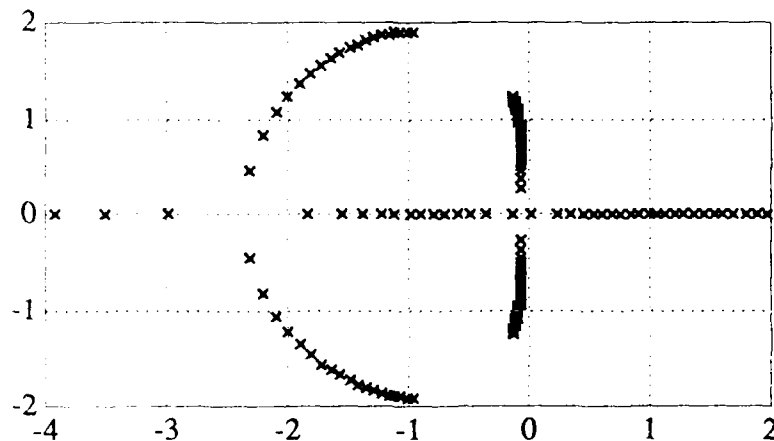
Figure 4.15b Near origin blowup of open loop eigenvalue locations as a function of cg location, κ, at cruise conditions. This figure clearly illustrates occurrence of a divergence instability as the cg moves toward the rear of the aircraft and one of the phugoid roots crosses into the right half plane. This occurs at approximately $\kappa = .12$.

4.3. Worst Case Design Analysis for Aircraft with Relaxed Static Stability

The linear dynamic model for the aircraft described in the previous section taken about the nominal operating condition k=0 is statically and dynamically stable. The linear perturbation equations can be written in the state space form as

$$\dot{x} = A_\kappa x + B_\kappa u$$
$$y = C_\kappa x$$

with state $x=[\upsilon,\gamma,\theta,q]^t$, control $u=[\Pi,\delta_e]^t$. For $\kappa=0$ we obtain the equilibrium conditions for level flight in terms of the state vector,

$$x_{eq} = \begin{bmatrix} 1. \\ 0.0497523 \\ 0.0497523 \\ 0 \end{bmatrix}$$

and the control

$$u_{eq} = \begin{bmatrix} 0.0002477 \\ 0.0996290 \end{bmatrix}$$

The linear perturbation model coefficients are then obtained:

$$A_0 = \begin{bmatrix} -0.1990115 & -0.9945490 & -1. & 0. \\ -1.9900905 & -22.099498 & 0. & 1. \\ 0. & 0. & 0. & 1. \\ 0. & -599.25016 & 0. & -1. \end{bmatrix}$$

$$B_0 = \begin{bmatrix} 0.0004955 & 0.9987626 \\ -1.9999999 & -0.0497317 \\ 0. & 0. \\ -599.25016 & 0. \end{bmatrix}$$

The model exhibits the characteristic pair of underdamped short period and phugoid dynamic modes;

Open loop poles at $\kappa=0$

$$-11.587041 + 22.020408i$$

49

$$- 11.587041 - 22.020408i$$
$$- 0.0622142 + 1.3864461i$$
$$- 0.0622142 - 1.3864461i$$

The choice of outputs defined by

$$C = \begin{bmatrix} 1. & 0. & 0. & 0. \\ 0. & -1. & 1. & 0. \end{bmatrix}$$

gives a real transmission zeros at 77.196225 and - 78.196225. The right half plane transmission zero which will ultimately limit the bandwidth of the closed loop system for robust stabilization. The pole zero plot is shown in Figure 4.16.
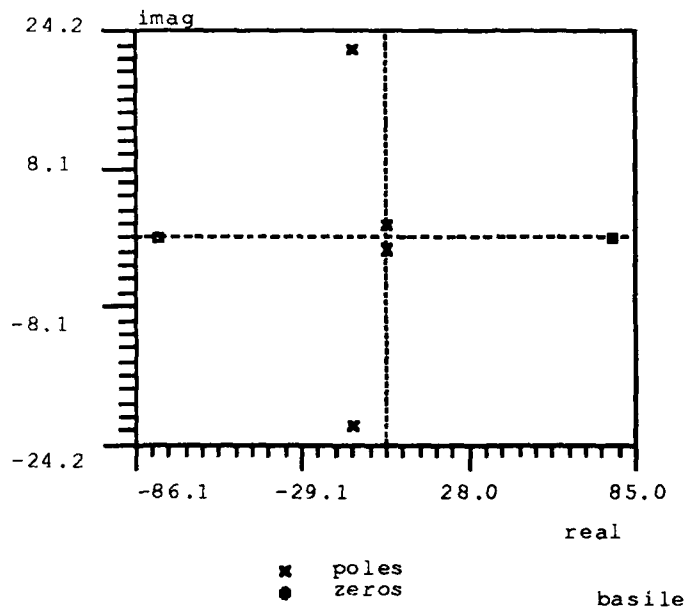
Figure 4.16: Pole-zero plot for nominal statically stable aircraft.

If the CG shifts aft by .12 relative to the effective nominal moment arm for tail controlled pitch motion the aircraft becomes both statically and dynamically unstable. The resulting pole-zero plot is shown in Figure 4.17, although the equilibria shift only slightly to :

50

$$x_{eq} = \begin{bmatrix} 1. \\ 0.0438289 \\ 0.0438289 \\ 0. \end{bmatrix}$$

and

$$u_{eq} = \begin{bmatrix} 0.0669217 \\ 0.0804625 \end{bmatrix}$$
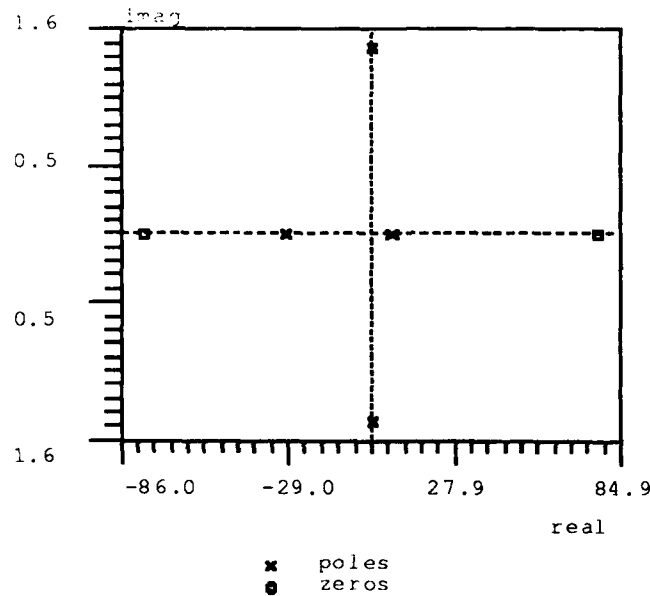
Figure 4.17: Pole-zero plot for statically unstable aircraft configuration.

To procede with the minimax (worst case) design we first determine the minimum achievable stability margin based on the optimization procedure and its dependence on the unknown parameter $0 \leq \kappa \leq 0.12$. This dependence is shown in Figure 4.18. The optimal geometric stability margin is dependent on the CG shift as shown. For this range of the independent parameter the worst case condition is the aft most location of the CG as expected.
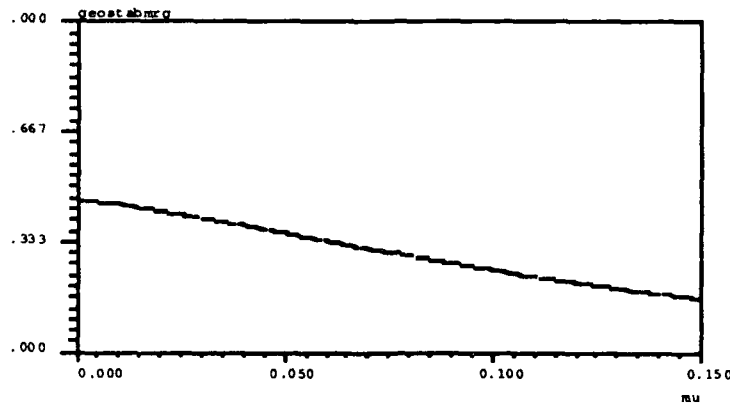
Figure 4.18: Optimal Stability Margin Dependence on k.

The optimal robust geometric stability margin can be given the interpretation of providing a bound on the allowable perturbation to a normalized left coprime factorization of the plant. One can therefore ask if the unstructured uncertainty condition for robust synthesis can provide conditions for stabilization of the flight dynamics model with aftward shift in the CG of 0.12. From the above the optimal stability margin variation is continuous and monotonically decreasing with the aft shift. Taking the aft-most location as worst case we can compute a maximum additive plant perturbation directly in terms of the normalized left coprime factors of the plant for the nominal case

$$G_0(s) = \tilde{M}_0^{-1}(s)\tilde{N}_0(s)$$

and for the case at k=0.12;

$$G_\kappa(s) = \tilde{M}_\kappa^{-1}(s)\tilde{N}_\kappa(s)$$

then we can obtain the required bounds by plotting the singular values of

$$[\tilde{M}_0 \ \tilde{N}_0] (j\omega) - [\tilde{M}_\kappa \ \tilde{N}_\kappa] (j\omega)$$

as shown in Figure 4.19.
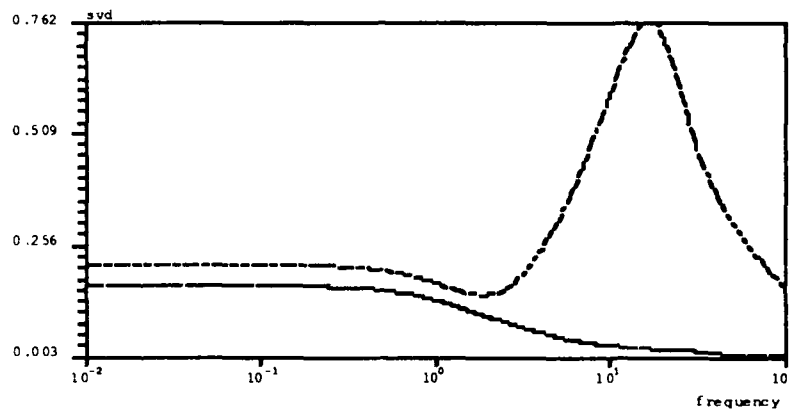
Figure 4.19: Singular Values of NCP Factor Perturbation

Thus using the unstructured model uncertainty description obtained from the geometric stability margin and the expected perturbation to the NLCP factors we see that the required bound is ε_{sm}=0.7619. This means that to design a stabilizing compensator using a totally unstructured requirement is so conservative in this case that it cannot in fact be obtained! Indeed, from the above plot of optimal stability margin vs. CG shift we see that no operating point obtains an optimal geometric stability margin in excess of 0.56. This is typical of unstructured uncertainty modeling and robust control synthesis. However, it is significant to note that using the geometric stability margin and the optimal robust stabilization problem a unique, quantitative criterion for robust stabilization is obtained which addresses the problem without examining frequency dependent data.

To illustrate the options for design using the optimal robust stabilization formulation we first consider scaling and its effect on the closed loop design. We first consider the design for a fixed, nominal operating point.

The MIMO open loop system has gains displayed as frequency dependent singular value plot as shown in Figure 4.20.

53
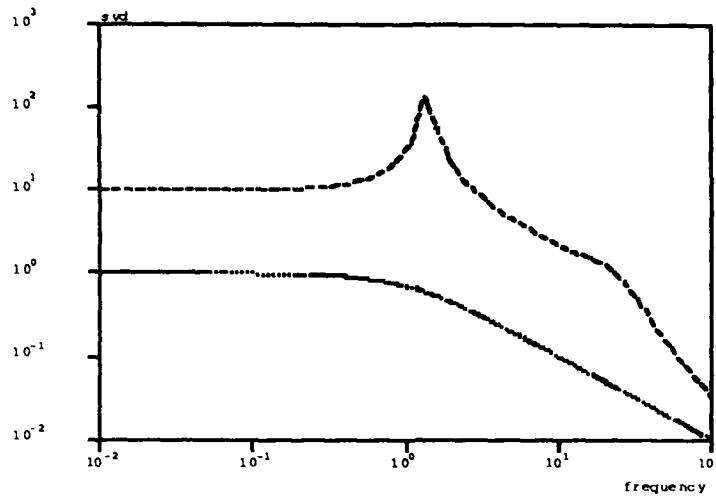
Figure 4.20: Singular value Loop Gains for nominal Plant Transfer Function.

Given the ultimate bandwidth limitation imposed by the right half plane zero at -77 we choose a nominal crossover frequency of $\omega=10$. Rescaling the inputs and outputs proceeds first by consideration of the relative importance of changes in each channel. For the nondimensional model the inputs consist of thrust and deflection of the tail control surface and the outputs include velocity and flight path angle. Scaling to obtain equalization of each channel follows from the choice of nominal value and relevant changes as:

$$
\begin{matrix}
& \text{nominal} & \text{relative} \\
u = \begin{bmatrix} \Pi \\ \delta_c \end{bmatrix} & \begin{bmatrix} 0 \\ 0 \end{bmatrix} & \begin{bmatrix} 0.1 \\ 0.5236 \end{bmatrix} \\
y = \begin{bmatrix} \upsilon \\ \gamma \end{bmatrix} & \begin{bmatrix} 1 \\ 0 \end{bmatrix} & \begin{bmatrix} 0.1 \\ .0873 \end{bmatrix}
\end{matrix}
$$

Let the input/output scaling be given by the diagonal matrices as :

$$
u = S_i \tilde{u} = \begin{bmatrix} .1 & 0 \\ 0 & .5236 \end{bmatrix} \tilde{u}
$$

$$
y = S_o \tilde{y} = \begin{bmatrix} .05 & 0 \\ 0 & .0873 \end{bmatrix} \tilde{y}
$$

then the transfer function becomes $\tilde{G}(s) = S_o^{-1} G(s) S_i$.

54

Finally, to specify desired crossover frequency we reduce the effective plant gain in each channel so that the maximum singular value at desired crossover satisfies . The resulting scaled plant has gains as shown in Figure 4.21 for the worst case parameter value of k=.12.
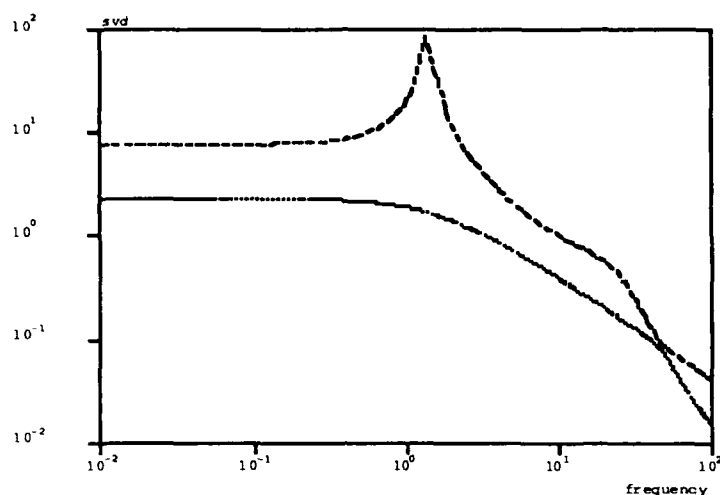
Figure 4.21: Singular Value Loop Gains of Scaled Plant.

The optimal geometric stability margin for the scaled plant is now computed as ε_{sm}=.2772. We note that the procedure described previously suggests that the system has compatible loop shape. We can now obtain a suboptimal controller for any desired level of stability robustness as $\gamma \geq 1/.561$=1.783. We take the suboptimal level γ=1.8 and obtain by the (2.19)--(2.22) the controller realization as:

$$A_c = \begin{bmatrix} -137.81869 & -159.443 & 157.59503 & 0.0071676 \\ 202.57323 & 240.27344 & -262.55426 & 0.9675697 \\ 687.31722 & 884.00473 & -884.00473 & 1 \\ 4043.8865 & 4666.5232 & -5317.9173 & -10.610107 \end{bmatrix}$$

$$B_c = \begin{bmatrix} -6.694682 & 13.840263 \\ 10.200762 & -22.84293 \\ 34.365861 & -77.173613 \\ 196.7627 & -440.94193 \end{bmatrix}$$

55

$$C_c = \begin{bmatrix} 4.7375856 & 9.371697 & -11.645754 & -0.4191080 \\ 18.620063 & -0.4424553 & -0.2898523 & -0.0357794 \end{bmatrix}$$

To illustrate that the resulting suboptimal controller achieves the required stability margin over a broad range of frequencies we plot the singular values of

$$\Phi(j\omega) = [\tilde{M}Q - \tilde{N}P](j\omega)$$

where $K(s) = P(s)Q^{-1}(s)$ is a normalized right coprime factorization for the achieved controller $K(s) = C_c[sI-A]^{-1}B_c$ (see Figure 4.22). To highlight the broadband solution obtained from this problem we plot separately the maximum singular value of F (i.e. the geometric stability margin) in Fig. 4.22a and minimum singular value in Fig. 4.22b.
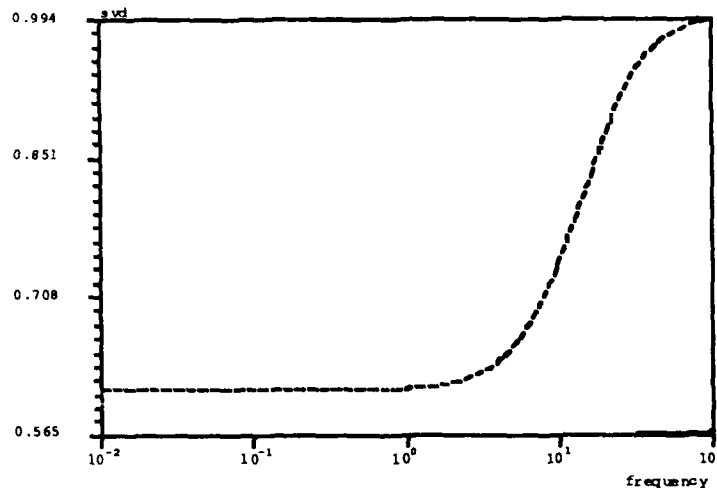
Figure 4.22a: Maximum Singular Value of Φ
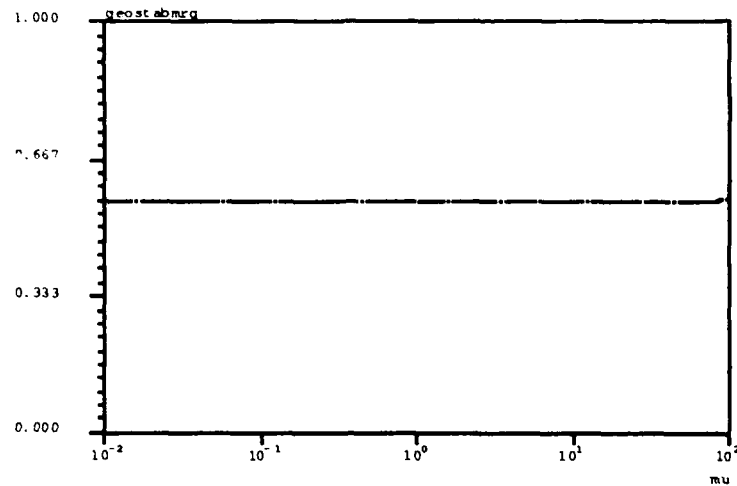
Figure 4.22b: Minimum Singular Value of Φ.

Finally, the achieved loop gains are displayed by plotting the singular values of K(s)G(s) in Figure 4.23.
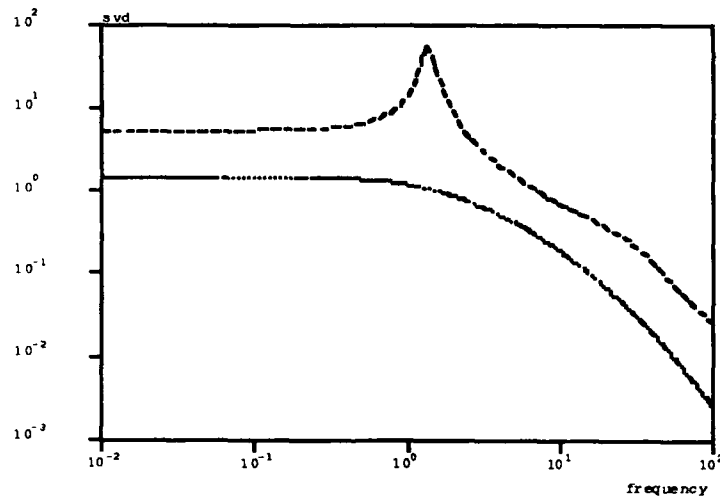
Figure 4.23: Achieved loop transmission gains.

For direct comparison we superimpose the desired loop shape with that achieved from the suboptimal compensator for the scaled plant response.
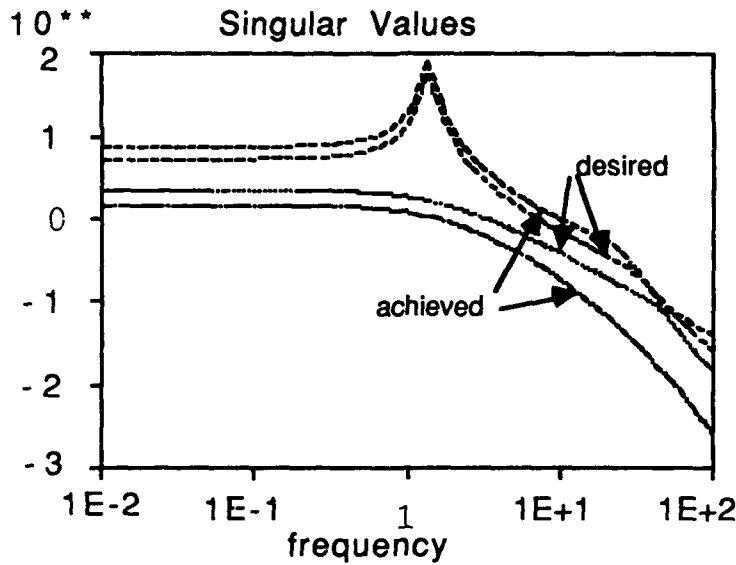
Figure 4.24: Achieved/desired loop transmission gains

4.4. Performance Considerations for Aircraft Flight Control

In this problem we introduce two modifications of the previous problem. First to illustrate design for performance robustness we introduce a requirement for integral action in each channel. Second, to test the worst case parametric design problem we perform the design for the worst case operating point at $\kappa=.12$. We also assume there is a dominant source of modeling error which is characterized as relative error in terms of bounds on multiplicative perturbation at the system output. We assume this is given by a specification that the model is to be considerd accurate to 10% for frequencies less than 2. Beyond $\omega>2$ the model relative error increases at 20dB/decade. Thus the relative bound $l_m>\|D_m\|$ is greater than 1 for $\omega>50$.

To motivate the choice of weighting functions we consider the requirement for steady error reduction and consequences for integral action in each loop. From the discussion in Blight, Gangsaas and Richardson [1] we see such requirements are apparent in LQG/LTR type designs but the application is much more difficult to implement than using the present method. To balance the requirements for integral action with loop crossover at $\omega=10$ we performed a simple tradeoff with PI type weighting in each channel to obtain the desired loop shape. The weighting considered has the form:

$$W_1(s) = \begin{bmatrix} \frac{1}{\tau_i s}+1 & 0 \\ 0 & \frac{1}{\tau_i s}+1 \end{bmatrix}$$

58

A value of $\tau_i = .7$ was chosen.

It became apparent that from the perspective of multiplicative model errors at the outputs the high frequency attenuation needed to be increased. We therefore added first order rolloff in terms of the lead/lag weights:

$$
W_2(s) = \begin{bmatrix} \dfrac{\tau_z s + 1}{\tau_p s + 1} & 0 \\ 0 & \dfrac{\tau_z s + 1}{\tau_p s + 1} \end{bmatrix}
$$

where values of 8 and 80. were chosen for the lead zero, resp. lag pole. This permitted increased rolloff in the region after cutoff without serious attenuation near the desired cutoff frequency. The shaped loop gain in displayed in Figure 4.25.
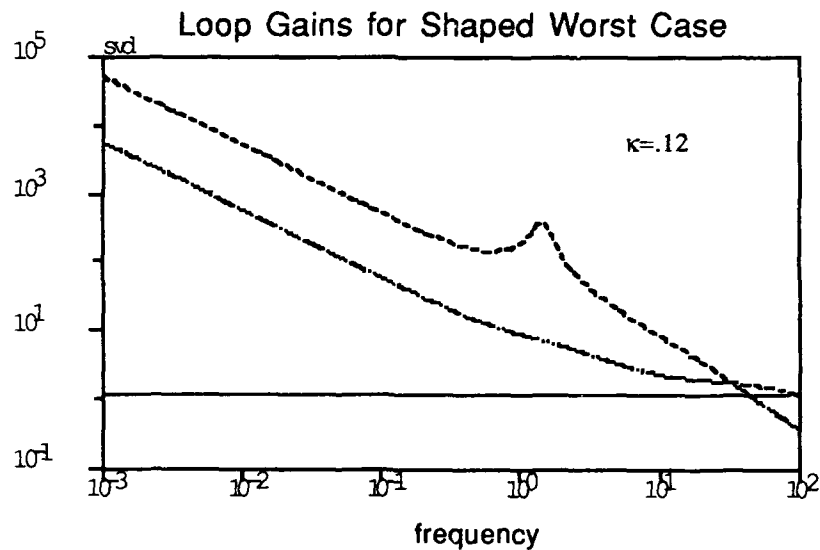
Figure 4.25: Desired loop shape with weightings.

The shaped transfer function dynamics are summarized in terms of the transmission poles and zeros in Table 4.1.

Table 4.1: Shaped Transmission Poles and Zeros

poles	zeros
- 80.	77.196225
- 80.	- 78.196225
0	- 8.
0	- 8.
- 29.556023	- 0.7
6.7912262	- 0.7
- 0.2004232 + 1.4435674i	
- 0.2004232 - 1.4435674i	

For this loop shape we compute the optimal stability margin as ε_{sm}=0.2772. Then we choose the desired suboptimal level for controller synthesis as $\gamma \geq 1/.2772$. Here we take γ=3.65 and synthesize the suboptimal robust control for the weighted plant. Incorporating the weighting functions into the controller K(s) we obtain the achieved loop gains as displayed in Figure 4.26. It can be seen that the specifications given in teims of relative model uncertainty at the outputs (multiplicative errors) together with performance specification for integral action and cross over frequency at least ω=10 have been achieved.
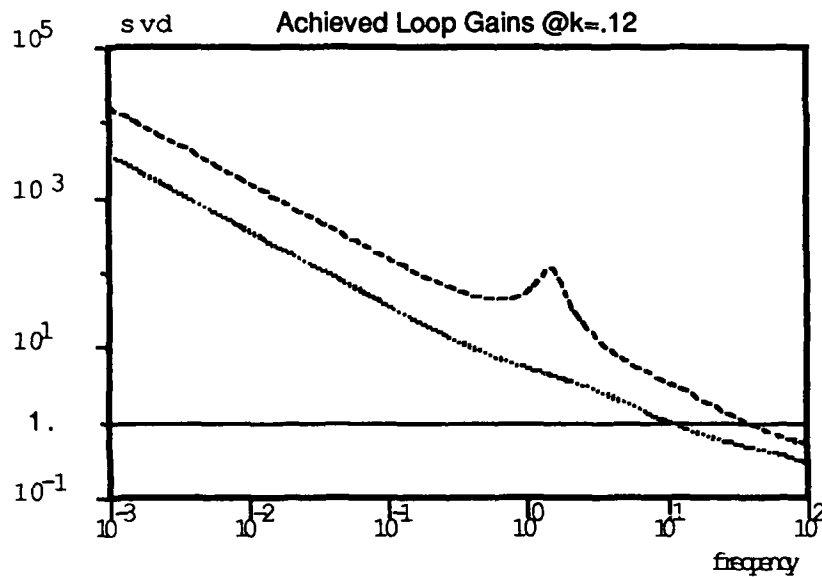
Figure 4.26: Acheived Loop Gains for shaped worst case design.

To check the assumptions implicit in the minimax/maximin equivalence for parametric robustness we evaluate the stability margin achieved by the worst case design at the nominal, stable configuration of κ=0 (the other extreme of the parameter variation in this case). The resulting stability margin achieved is ε_{sm}=0.2583 as seen from Figure 4.27.

Achieved Stability Margin for stable config
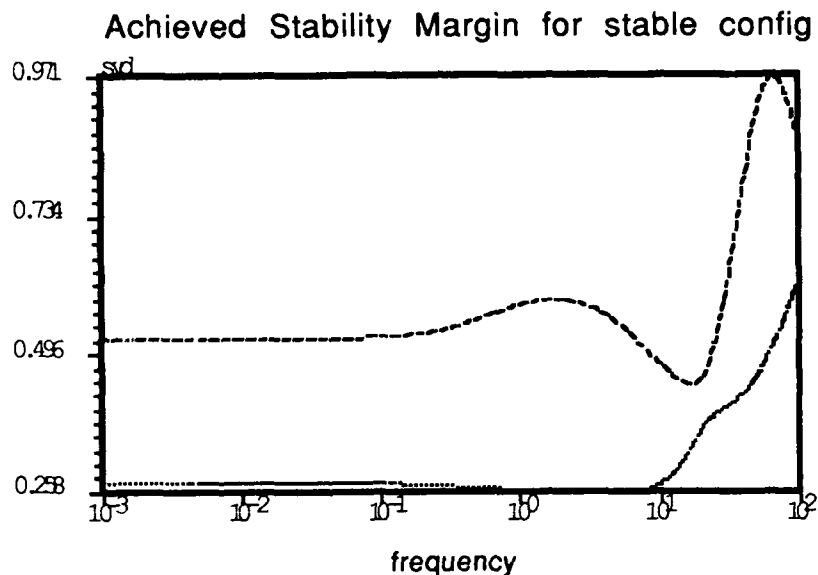
Figure 4.27: Achieved Stability Margin @k=0.

Finally, to illustrate the effect of the worst case design on the nominal, stabel aircraft configuration we display the achieved loop gains for this case in Figure 4.28.

Achieved Loop Gains for k=0
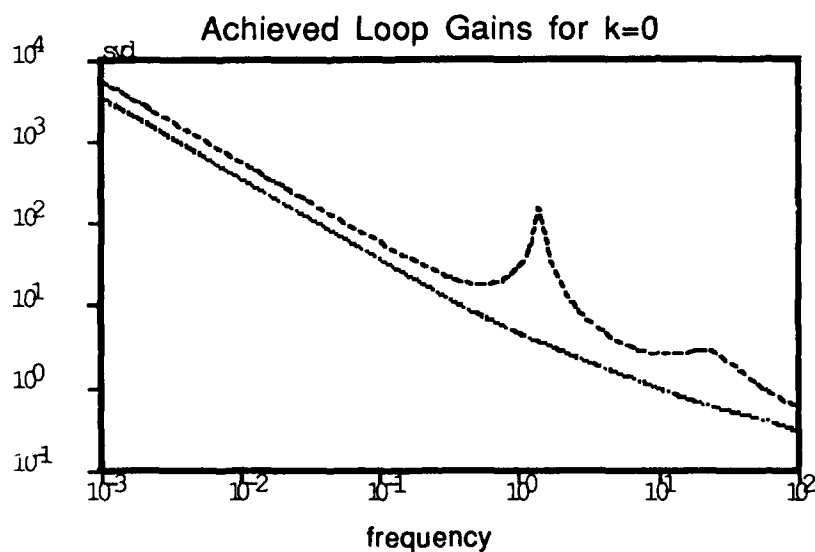
Figure 4.28: Achieved Loop Gains for stable configuration.

61

The closed loop system poles for the nominal stable configuration with the control as designed above can be computed as:

Closed Loop Poles for nominal (stable) aircraft

- 1819.4462
- 270.14803 + 29.621817i
- 270.14803 - 29.621817i
- 78.048361
- 7.222071 + 25.390096i
- 7.222071 - 25.390096i
- 12.391449
- 7.4595557
- 2.0803007
- 2.0285601
- 0.7878369
- 0.6121988

5. Conclusions and Directions for Future Research

5.1. Nonlinear Control Design for Robust Flight Control

In order to achieve enhanced maneuverability and efficiency, future aircraft will operate close to or even beyond open loop stability boundaries. For example, reduction of horizontal tail size in order to achieve reduced fuel consumption results in loss of longitudinal static stability for sufficiently aft c.g. locations [1]. Fighter aircraft may operate at high angle of attack or at high roll rate where nonlinear effects cause loss of stability [6]. Such aircraft require augmentation by automatic flight control systems which induce the desired handling qualitites over the full range of flight conditions.

Feedback controllers for these applications are typically conceived to be linear, perhaps with some form of gain scheduling. However, when operating near stability boundaries the system dynamics are nonlinear in an essential way. It is well known, for instance, that a linear perturbation model is a reliable indicator of stability only if none of its eigenvalues lie on the imaginary axis [9]. Otherwise nonlinear effects are crucial. Some recent studies in flight mechanics characterize aircraft loss of stability in terms of elementary local bifurcations [10-11]. Thus, divergence instability is typically associated with a saddle-node bifurcation and a change in the equilibrium

62

point structure while flutter is associated with a Hopf bifurcation and the appearance of a limit cycle. Such phenomenon, of course, are fundamentally nonlinear.

Unfortunately, these studies deal almost exclusively with open loop dynamics under parameter variation and very little general theory is availiable concerning the design of feedback controls near bifurcation points. We can, however, draw some obvious inferences although our remarks will be confined to static instability (divergence). It is known that linear feedback can be used to stabilize a divergence instability. McRuer et al [4] note that in aircraft such stabilization requires high gain, wide bandwidth control. Such controllers may be sensitive to actuator saturation and excitation of high frequency parasitics. It is our view that these problems assume exagerated proportions because of the attempt to force a linear solution on an intrinsically nonlinear problem.

Note also that when the system operates near a saddle-node bifurcation point, the stable equilibrium point is necessarily close to the boundary of the domain of attraction (the neighboring unstable equilibrium is on the boundary.) It follows that the system may be unacceptably sensitive to external disturbances. Performance can sometimes be dramatically improved by nonlinear feedback. In fact, the substantial improvement obtained by Garrard and Jordan [6] in recovery from stall by using a nonlinear feedback can be explained by this observation.

Techniques for the design of nonlinear feedback control systems are still very limited and tend to be tailored to specific situations. The most promising approaches appear to be those associated with methods of exact linearization. This procedure is based on some early work of Krener [44] and others demonstrating that a large class of state equation models for nonlinear dynamical systems can be exactly linearized by a combination of nonlinear state feedback and a nonlinear transformation of state coordinates. Once the system is linearized all methods of control system design for linear dynamics become applicable. The inverse transformation is then implemented in conjunction with the linear compensator so that the overall controller is nonlinear. Meyer and his coworkers have articulated the application of these ideas to certain problems in flight control as an alternative to gain scheduling.

Another approach termed input-output linearization has evolved from work of Hirschorn [45]. The notion of input-output linearization as developed by Kravaris and Chung [46]) is based on the so-called Byrnes-Isidori canonical form [47] for nonlinear systems. This approach produces a linear input-output model and may have certain advantages especially when frequency domain design methods are to be used for compensator design. The attractiveness of such methods is further

enhanced by recent frequency domain formulations of Hopf bifurcation analysis [12] with application to multivariable nonlinear control system analysis [54].

Although these methods may be formally applied at or near bifurcation points such applications have not been studied. It is interesting to note that another approach to linearization which has generated some interest in recent years, the extended linearization method of Rugh [59] fails in an obvious way at bifurcation points.

The essentials of the approach are most easily understood in terms of the single input single output problem. Consider a nonlinear dynamical system in the form

$$\dot{x} = f(x) + g(x)u \tag{5.5a}$$

$$y = h(x) \tag{5.5b}$$

where f, g are smooth vector fields on R^n and h is a smooth function mapping $R^n \to R$. Now, differentiate (5.5b) to obtain

$$\dot{y} = \frac{\partial h}{\partial x}(f(x) + g(x)u) \tag{5.6}$$

If the scalar coefficient of u is zero, we differentiate (5.6) and continue in this way until a nonzero coefficient first appears.

This process can be succinctly described by introducing some conventional notation of differential geometry and analytical mechanics. We need only the concept of Lie derivative. First, the Lie (directional) derivative of the scalar function h with respect to the vector field f is defined as

$$L_f(h) = \langle dh, f \rangle = \frac{\partial h}{\partial x} f(x) \tag{5.7}$$

Since the Lie derivative is itself a scalar function on R^n, higher order derivatives may be successively defined

$$L_f^k(h) = L_f(L_f^{k-1}(h)) = \langle dL_f^{k-1}(h), f \rangle \tag{5.8}$$

Now, (5.6) can be written

64

$$\dot{y} = \langle dh, f \rangle + \langle dh, g \rangle u = L_f(h) + L_g(h)u \tag{5.9}$$

If $L_g(h) = 0$, then differentiate (5.9) to obtain

$$\ddot{y} = \langle dL_f(h), f \rangle + \langle dL_f(h), g \rangle u = L_f^2(h) + L_g(L_f(h))u \tag{5.10}$$

If $L_g(L_f(h)) = 0$, then differentiate (5.10). If $L_g(L_f^{k-1}(h)) = 0$ for $k = 1,.., r-1$, but $L_g(L_f^{r-1}(h)) \neq 0$,

then the process ends with

$$\frac{d^r y}{dt^r} = L_f^r(h) + L_g(L_f^{r-1}(h))u \tag{5.11}$$

The number r is called the "relative degree" or "characteristic number" of (5.5). Note that if we define the coordinates $z \in R^r$

$$z_k = L_f^{k-1}(h), \qquad k = 1,..,r$$

then Equations (5.9) through (5.11) can be written

$$\dot{z} = \begin{bmatrix} 0 & 1 & 0 & . & 0 \\ 0 & 0 & 1 & 0 & . \\ . & . & 0 & 1 & 0 \\ . & . & . & . & 1 \\ 0 & 0 & . & . & 0 \end{bmatrix} z + \begin{bmatrix} 0 \\ 0 \\ . \\ 0 \\ \alpha(x) + \rho(x)u \end{bmatrix} \tag{5.12}$$

where

$$\alpha(x) = L_f^r(h), \text{ and } \rho(x) = L_g(L_f^{r-1}(h))$$

Formally, the system (5.12) may be linearized and simultaneously stabilized in the input-output sense as follows. Choose the control

$$u = \Phi(x,v) = (v - \sigma(x))/\rho(x) \tag{5.13}$$

where

$$\sigma(x) = \sum_{k=0}^{r-1} \beta_k L_f^k(h) + L_f^r(h), \qquad \rho(x) = L_g(L_f^{r-1}(h))$$

and β_k, $k = 0,..., r-1$ are real numbers corresponding to the coefficients of any Hurwitz polynomial. Then the relationship between the new control input v and the output y is defined by the linear r-dimensional (completely controllable and observable, companion form) system

$$\dot{z} = \begin{bmatrix} 0 & 1 & 0 & . & 0 \\ 0 & 0 & 1 & 0 & . \\ . & . & 0 & 1 & 0 \\ . & . & . & . & 1 \\ -\beta_0 & -\beta_1 & . & . & -\beta_{r-1} \end{bmatrix} z + \begin{bmatrix} 0 \\ 0 \\ . \\ 0 \\ 1 \end{bmatrix} v \qquad (5.14a)$$

$$y = [\, 1 \quad 0 \quad . \quad . \quad 0 \,] z \qquad (5.14b)$$

These calculations are readily extended to MIMO case [55, 56].

The importance of this construction is that linear dynamic compensators may now be designed for the resulting linear system using any applicable linear method. The exact linearization is global if the transformations admit unbounded control u; otherwise, the linearization is local. However, it should be emphasized that unlike traditional linearization about a fixed operating point or trim condition (based formally on Taylor series expansion) the approach just described linearizes the system dynamics about a nominal model. Open questions in the available theory for such linearization includes the effect of such control constraints and parametric uncertainty.

5.2. Linear Mode Design and Critical Nonlinear Dynamics

For the limited scope of the phase 1 study we have focused on computational studies for relaxed static stability aircraft where the parametric uncertainty is related to the shift of CG during flight operations. The underlying nonlinear dynamics illustrate the role of parameters in determining the dynamic properties of the resulting family of linear perturbation models. What is evident from our analysis and numerical computations so far is the significance of the transmission zeros to this parameter. Certainly in the region which we considered for variation of κ the transmission zero are relatively insensitive by comparison with the system poles. However, this does change as the variation of κ is extended to approach the static bifurcation point for the system equilibria. It has been shown that in feedback systems static bifurcation is associated with the passing of a real zero through the origin. This differs from the conventional case in dynamical sytem theory where static bifurcation is associated with a real eigenvalue passing through the origin. In this region we expect the sensitivity of the system optimal stability margin to be significant, indicating a difficult control design problem. It is our conjecture that part of the limitation evidenced in such regions comes

66

from the linear mode design approach where we are essentially trying to design a single fixed (and therefore robust) linear compensator for the linear plant. The requirement for stability of the linear mode design has the implicit objective to maintain the system state near the desired equilibrium or trim condition. Near a bifurcation of the equilibria under parametric variation we expect the domain of attraction to change depending on the type of bifurcation. Clearly, the underlying nonlinear dynamics will be significant for control of the system dynamics in such operating regimes.

Such considerations have lead engineers to develop various methods for gain scheduling--most of which are ad hoc. On the other hand the previous discussion on feedback linearizing control for certain nonlinear systems provides a complete analytical basis for control design based on linearization about a nominal system model rather than about an equilibrium operating point in the system state space. Despite the abstract basis for the theory of feedback linearization, its practical application provides an analytical basis for gain scheduling the linear mode design. Both methods are essentially model-based control design schemes and therefore robustness considerations are important in applications. Flight control systems often employ gain scheduling with respect to various measurable system parameters (e.g. velocities, angle of attack, etc.) for operation in nonlinear regimes. It is our view that methods for integrated design of multiloop controllers based on methods related to feedback linearization may provide enhanced capabilities for such high performance flight control problems as recovery from stall. In the Phase 2 effort we will propose to study methods for robust design and implementation of such nonlinear control laws.

5.3. Research Directions for multiparameter worst case design

The worst case design procedure based on the maximin design is computationally feasible if the number of real parameters is small since the evaluation of the optimal controller dependence on α is simple. It is therefore suggested that in applications the plant be modeled with the less significant real parametric uncertainty embedded in the unstructered uncertainty bounds. This is the practical aspect of the methods we will propose to investigate and develop in Phase 2: that we seek a pragmatic approach to implement the available methods in optimization based approachs to robust control synthesis for structured uncertainty together with more well developed methods for structured uncertainty. We believe that this blend can be developed with respect to a significant class of flight control problems where dynamic degrees of freedom are relativly small.

The focus of the Phase 1 study has been on developing a method for robust stabilization of models subject to combined real parametric uncertainty and parasitic (unmodeled) dynamics. Our efforts were directed toward eliminating the source of conservatism abundant in such design methods

while retaining the essential feature of robust design in the engineering context. We feel that the optimal worst case design methods described above addresses these concerns in principle. The result however, is a computationally difficult problem in the general case. Our approach in the benchmark designs has been pragmatic. We also believe that the essential features of the nonlinear dynamics of flight control designs will serve to restrict consideration of the variation of physically based real parameters which effect the aircraft dynamics. Nevertheless, we feel that a focus of the Phase 2 proposal should be in the area of algorithm development for the minimax (worst case) design for realistic combination of structured uncertainty (arising from physical parameters) and unstructured uncertainty (arising from unmodeled dynamics).

We also feel that the entropy interpretation of the results of Bernstein and Haddad --and therefore the results obtained in Yeh et al [41] -- may offer additional perspectives on how inherent conservatism of such designs can be reduced. The analysis achieved to date represents only a special case for these problems.

The loop shaping procedure has been shown to be effective with many desireable properties. However, the choice of loop shape has not been adequately addressed. In particular, the modification of loop shape to incorporate knowledge about system uncertainties, the question of how loop shape affects ε_{max}, and the role and use of loop shaping for decoupling and scaling are all potentially fruitful directions of inquiry.

6. References

[1] J.D. Blight, D. Gangsaas, and T.M. Richardson, "Control Law Synthesis for an Airplane with Relaxed Static Stability," *J. Guid, Cntrl and Dynamics*, Vol 9, 1986, pp. 546--554.

[2] S. N. Singh and A.A.R. Coelho, "Nonlinear Control of Mismatched Uncertain Systems and Application to Control of Aircraft," *J. Dynamic Systems, Measurement and Control*, Vol. 106, 1984, pp. 203--210.

[3] R. Freymann, "Interactions Between Aircraft Structure and Active Control," *J. Guid. Cntrl and Dynamics*, Vol.10, 1987, pp. 447--452.

[4] D. McRuers, D. Johnston, and T. Myers, "A Perspective on Superaugmented Flight Control: Advantages and Problems," *J. Guid, Cntrl and Dynamics*, Vol 9, 1986, pp. 530--540.

[5] W. E. Schmitendorf, "Design Methodology for Robust Stabilizing Controllers," *J. Guid, Cntl, and Dynamics*, Vol .10, 1987, pp. 250--254.

[6] W.L. Garrard and J.M. Jordan, "Design of Nonlinear Automatic flight Control Systems," *Automatica*, 1977, pp. 497--505.

[7] J.H. Vincent, "Direct Incorporation of Flying Qualities Into Multivariable Control System Design," Paper No. AIAA-84-1830-CP, *AIAA Guid/Cntrl Conf.*, Aug 1984.

[8] K. Wilhelm and D. Schafranek, "Landing Approach Handling Qualities of Transport Aircraft with Relaxed Static Stability," *J. of Aircraft*, Vol. 23, 1986, pp. 756--762.

[9] J. Guckenheimer and P. Holmes, *Nonlinear Oscillations, Dynamical Systems and Bifurcations of Vector Fields*, Springer-Verlag, 1983.

[10] R.K. Mehra, W.C. Kessel, and J.V. Carrol, *Global Stability and Control of Aircraft at High Angles of Attack*, Cambridge: Scientific Systems, 1977.

[11] W.H. Hui and M. Tobak, "Bifurcation Analysis of Aircraft Pitching Motions About Large Mean Angles of Attack," *J. Guid Cont*, Vol 7, 1984, pp. 106--113.

[12] A. Mees and L.O. Chua, "The Hopf Bifurcation Theorem and its Application to Nonlinear Oscillations in Circuits and Systems," *IEEE Trans Circuits and Systems*, Vol. CAS-26, 1979, pp. 235--254.

[13] C. Nett, C. Jacobsen, and M. Balas, "A Connection Between State--Space and Doubly--Coprime Fractional Representations," *IEEE Trans. Auto. Control*, Vol. AC-29(1984), pp. 831-832.

[14] D. Meyer and G. Franklin, "A Connection Between Normalized Coprime Factorizations and Linear Quadratic Regulator Theory," *IEEE Trans. Auto. Control*, Vol. AC-32 (1987). pp. 227-228.

[15] J.C. Doyle and G. Stein, "Multivariable Feedback Design: Concepts for a Classical/Modern Synthesis," *IEEE Trans on Auto Cntrl*, Vol.AC-26, No.1, (1981), pp. 4-16.

[16] J.C. Doyle, J.E. Wall and G. Stein, "Performance and Robustness Analysis for Structured Uncertainty," *Proc 21st IEEE CDC*, (1982), pp. 629-636.

[17] C.A. Desoer & M. Vidyassagar, *Feedback Systems: Input-Output Properties*, Academic Press, Inc. 1975.

[18] G.W. Stewart, *Introduction to Matrix Computations*, Academic PRess, Inc., 1973.

[19] N. A. Lehtomaki, N.R. Sandell, & M. Athans, "Robustness Results in Linear-Quadratic-Gaussian Based Multivariable Control Designs", *IEEE Trans. Auto. Cntrl.*, Vol. AC-26, Feb. 1981, pp. 75-92.

[20] B. A. Francis, *Notes on H^{∞}-Optimal Linear Feedback Systems*, Linkoping Univ., (Aug. 1983).

[21] R. E. Brockett and C. I. Byrnes, "The Nyquist Criterion, Root Loci and Pole Placement by Output Feedback: A Geometric Viewpoint," *IEEE Trans. Aut. Control*, AC-26 (1981), pp.271-283.

[22] W. H. Bennett and J.S. Baras, "A New Geometric Stability Margin," *Proc. 24th IEEE CDC,* Ft. Lauderdale, Florida, (1985), pp. 519-526.

[23] W.H. Bennett, "Robust Stabilization: A Geometric Perspective without Forming a Return Difference Test," *Proc. Math. Theory of Networks and Systems,* Pheonix, AZ, June (1987).

[24] A. Bjorck and G.H. Golub, "Numerical Methods for Computing Angles Between Linear Subspaces," *Math of Comp.,* Vol. 17, No. 123, (1973), pp. 579-594.

[25] M. Vidyasagar, *Control System Synthesis: A Factorization Approach,* (1985) MIT Press.

[26] M. Vidyasagar, "The Graph Metric for Unstable Plants and Robustness Estimates for Feedback Stability," *IEEE Trans Auto Cntrl,* Vol AC-29, 1984, pp. 403--417.

[27] M. Vidyasagar, H. Schneider, and B. Francis, "Algebraic and Topological Aspects of Feedback Stabilization," *IEEE Trans Auto Cntrl,* Vol AC-27, 1982, pp. 880--894.

[28] D.C. Youla, et al, "Modern Wiener-Hopf Design of Optimal Controllers---Parts I and II", (1976) *IEEE Trans Auto Cntl.*

[29] K. Glover, "Robust Stabilization of Linear Multivariable Systems: Relations to Approximation", (1986) *Int. J. Control.*

[30] K. Glover, "All Optimal Hankel-norm Approximations of Linear Multivariable Systems and Their L^∞)-error Bounds," *Int. J. Control,* Vol. 39, No, 6, (1984), pp. 1115-1193.

[31] K. Glover and D. McFarlane, "Robust Stabilization of Normalized Coprime Factors: An Explicit H^∞) Solution," *Proc. ACC,* (1988).,

[32] K. Gover and D. McFarlane, "Robust Stabilization of Normalized Coprime Factor Plant Descriptions with H^∞-Bounded Uncertainty," Submitted to *IEEE Trans. on Auto. Cntrl.,* June, 1988.

[33] D. McFarlane and K. Glover, "An H^∞ Design Procedure using Robust Stabilization of Normalized Coprime Factors," *Proc. IEEE CDC,* Dec. 1988.

[34] D. McFarlane, K. Glover, and M. Norton, "Robust Stabilization of Flexible Space Structures: An H^∞ Coprime Factor Approach," Cambridge Univ. Rep. CUED/F-INFENG/TR.5 (1988).

[35] K. Glover and J.C. Doyle, "State-space Formulae for all Stabilizing Controllers that Satisfy an H^∞ -norm Bound and Relations to Risk Sensitivity," *Systems & Control Letters,* Vol. 11, 1988, pp. 167-172.

[36] M.K.H. Fan, A. L. Tits, & J.C. Doyle, "Robustness in the Presence of Joint Parametric Uncertainty and Unmodeled Dynamics," *Proc. ACC.,* 1988, pp. 1195-1200.

[37] I.R. Peterson & C.V. Hollot, "A Riccati Equation Approach to the Stabilization of Uncertain Systems," *Automatica,* Vol. 22, 1986, pp. 397-411.

[38] D.S. Bernstein & W. M. Haddad, "LQG Control with an H^∞ Performance Bound: A Riccati Equation Approach," *Proc. 1988 ACC,* pp. 796-802.

[39] D. Mustafa & K. Glover, "Derivation of the Maximum Entropy H$^\infty$ controller and a State-space Formula for its Entropy," to appear *Systems and Control Letters*, 1989.

[40] D. Mustafa & K. Glover, "Controllers Which Satisfy a Closed Loop H$^\infty$ Norm and Minimize an Entropy Integral," *Proc. IEEE CDC.*, 1988, pp. 959-965.

[41] H.-H. Yeh, S.S. Banda, A.C. Bartlett, Lt. S. A. Eide, "Robust Design of Multivariable Feedback Systems with Real-Parameter Uncertainty and Unmodeld Dynamics," *Proc. 1989 ACC*.

[42] H. Kwakernak, "Minimax Frequency Domain Performance and Robustness Optimization of Linear Feedback Systems," (1985) *IEEE Trans Auto Cntl*.

[43] V. Manousiouthakis, "On a Minimax Approach to Robust Controller Synthesis and Model Selection," *Proc. ACC*, (1988), pp. 2353-2356.

[44] A.J. Krener, "On the Equivalence of Control Systems and Linearization of Nonlinear Systems," *SIAM J. Cont. and Opt.*, Vol 11, 1973, pp. 670.

[45] R.M. Hirschorn, "Invertibility of Nonlinear Control Systems," *SIAM J. Cont. and Opt.*, Vol. 17, 1979, pp. 289--297.

[46] C. Kravaris and C.B. Chung, "Nonlinear State Feedback Synthesis by Global Input/Output Linearization," *AIChE J.*, 1987.

[47] C.I. Byrnes and A. Isidori, "Global Feedback Stabilization of Nonlinear Systems," *Proc. 24th IEEE CDC*, 1985, pp. 1031--1037.

[48] G. Meyer, R. Su, and L.R. Hunt, "Application of Nonlinear Transformations to Automatic Flight Control." *Automatica*, Vol 20, 1984, pp. 103--107.

[49] Etkin, B., *Dynamics of Atmospheric Flight*, New York: John Wiley & Sons, 1972.

2. Blakelock, J. H., *Automatic Control of Aircraft and Missiles*, New York: John Wiley & Sons, 1965.

[50] Hacker, T., *Flight Stability and Control*, New York: American Elsevier, 1970.

[51] v. Karman, T., and Biot, M. A., *Mathematical Methods in Engineering*, New York: McGraw-Hill, 1940.

[52] Sobel, K. M. and Shapiro, E. Y., "A Design Methodology for Pitch Pointing Flight Control Systems," *J. Guidance, Control and Dynamics*, Vol. 8, March-April 1985, pp. 181-187.

[53] Namachchivaya, N. Sri and Ariaratnam, S. T., "Non-Linear Stability Analysis of Aircraft at High Angles of Attack," *Int. J. Non-Linear Mechanics*, Vol. 21, No. 3, 1986, pp.217-288.

[54] Kwatny, H. G., and Siu, T., "Chattering in Variable Structure Feedback Systems," *Proc. 10th IFAC World Congress*, 1987.

[55] Fernandez R., B., and Hedrick, J. K., "Control of Multivariable Non-Linear Systems by the Sliding Mode Method," *Int. J. Control*, Vol. 46, No. 3, 1987, pp. 1019-1040.

[56] Charlet, B., "Stability and Robustness for Nonlinear Systems Decoupled and Linearized by Feedback," *Systems and Control Letters*, N0.8, 1987, pp. 367-374.

[57] Safanov, M. G. and Athans, M., "A Multiloop Generalization of the Circle Criterion for Stability Margin Analysis," *IEEE Tans. Auto. Contr.*, Vol. AC-26, NO. 2, April 1981, pp. 415-421.

[58]. Fan, M. K. H., and Tits, A. L., "Characterization and Efficient Computation of the Structured Singular Value," *IEEE Trans. Auto. Contr.*, Vol. AC-31, No. 8, August, 1986, pp. 734-743.

[59]. Rugh, W. J., "An Extended Linearization Approach to Nonlinear System Inversion," *IEEE Trans. Auto. Contr.*, Vol. AC-31, No. 8, August 1986, pp 725-733.

[60]. Desoer, C. A., Liu, R.-W., Murray, J., and Saeks, R., "Feedback System Design: The Fractional Representation Approach to Analysis and Synthesis," *IEEE Trans Auto Contr*, Vol. AC-25, No. 3, June 1980, pp. 399-412.

Appendix

This appendix includes two papers prepared by Dr. Keith Glover of Cambridge University which were presented at the 27th IEEE CDC in Austin, Texas in December 1988. This work is partly supported by the subject contract.

AN H∞ DESIGN PROCEDURE USING ROBUST STABILIZATION

OF NORMALIZED COPRIME FACTORS

by

Duncan McFarlane [†] and Keith Glover [†]

[†] Department of Engineering, University of Cambridge,
Trumpington Street, Cambridge, CB2 1PZ, United Kingdom.

ABSTRACT - A two stage H_∞ based design procedure has been described which uses a normalized coprime factor approach to robust stabilization of linear systems. A loop-shaping procedure is also incorporated to allow the specification of performance characteristics. Theoretical justification of this technique is given and an outline given of the design methodology.

1. INTRODUCTION

In a number of recent papers it has been shown that H_∞ optimization can be applied to the problem of robust stabilization of unstructured uncertainty. (See Francis [4], and the references therein.) This paper describes a design technique based on the robust stabilization of a particular representation of unstructured uncertainty, namely that of *normalized* 'stable factor' or 'coprime factor' perturbations. (See Vidyasagar [15], for a suitable introduction to coprime factors, and [7] for a complete solution to the normalized coprime factor robust stabilization problem.) The design technique, which also allows performance objectives to be incorporated, has two stages: (1) A loop-shaping approach 'shapes' the nominal plant singular values to give desired open-loop properties, and (2) The normalized coprime factor robust stabilization technique mentioned above is used to stabilize the shaped plant.

2. THE NORMALIZED LEFT COPRIME FACTOR ROBUSTNESS PROBLEM

We firstly summarize the main results of [6], [7] for the normalized LCF robust stabilization problem. It has been shown [14], [16] that an attractive way of representing unstructured uncertainty in a plant is via coprime factor perturbations. That is, if the nominal plant is

$$G = \bar{M}^{-1}\tilde{N} \qquad (2.1)$$

then a perturbed plant is written

$$G_\Delta = (\bar{M} + \Delta_M)^{-1}(\tilde{N} + \Delta_N) \qquad (2.2)$$

where $\bar{M}$, $\tilde{N}$ is a left coprime factorization (L.C.F.) of G, and Δ_M, Δ_N are stable, unknown transfer functions representing the uncertainty and satisfying $\|[\Delta_M, \Delta_N]\|_\infty < \epsilon$ where $\epsilon > 0$ (See Fig 2.1) A design objective is then to find a feedback controller K which stabilizes all such G_Δ for a given ϵ. Following [16], this can be rewritten in the framework of an H_∞ optimization problem: Find a stabilizing controller K such that

$$\left\| \begin{bmatrix} (I - GK)^{-1}\bar{M}^{-1} \\ K(I - GK)^{-1}\bar{M}^{-1} \end{bmatrix} \right\|_\infty \leq \epsilon^{-1} \qquad (2.3)$$
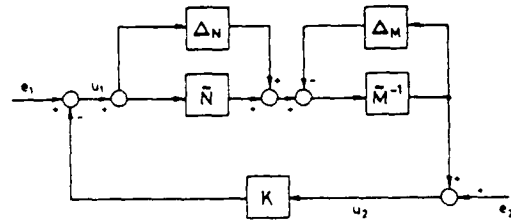
Figure 2.1 Coprime Factor Uncertainty

where K is chosen over all controllers which stabilize G. The solution for the largest achievable ϵ ($= \epsilon_{max}$) is generally iterative [16], *but*, if the left coprime factorization (LCF) of G is *normalized*, meaning

$$\bar{M}(j\omega)\bar{M}(j\omega)^* + \tilde{N}(j\omega)\tilde{N}(j\omega)^* = I \text{ for all } \omega \qquad (2.4)$$

then it is possible to show ([6], [7]) that a maximum value of ϵ can be obtained by a non-iterative method, and is given by

$$\epsilon_{max} = \left(1 - \|[\bar{M}, \tilde{N}]\|_H^2\right)^{0.5} \qquad (2.5)$$

where $\|\bullet\|_H$ denotes the Hankel Norm, and ϵ_{max} is called the *maximum stability margin*.

Remark 2.1 It can be simply shown that the problem in (2.3) is equivalent to the 'four block' problem:

$$\left\| \begin{bmatrix} K \\ I \end{bmatrix} (I - GK)^{-1}[G, I] \right\|_\infty \leq \epsilon^{-1},$$

and hence this also has a minimum solution given by (2.5).

3. LOOP SHAPING METHODS

In feedback design many performance and robust stability objectives can be written as requirements on the maximum singular values of particular closed-loop transfer functions. The principal idea of 'Loop Shaping' is that the magnitude (or maximum singular values) of these *closed-loop* transfer functions can be directly determined (over appropriate frequency ranges) by the singular values of the corresponding *open-loop* transfer function. (The reader is referred to [3] for a comprehensive introduction to loop shaping methods.)

For example, for a plant, G, and controller, K, if $\underline{\sigma}(GK) \gg 1$ (typically at low frequency) then
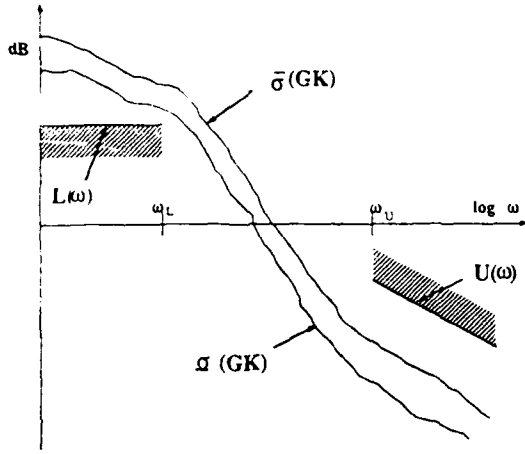
Figure 3.1 Loop Shaping Specifications

$$\bar{\sigma}((I - GK)^{-1}) \lesssim 1/\underline{\sigma}(GK) \qquad (3.1)$$

$$\bar{\sigma}((I - GK)^{-1}G) \lesssim \bar{\sigma}(G)/\underline{\sigma}(GK) \qquad (3.2)$$

and if $\underline{\sigma}(GK) \ll 1$ (typically at high frequency) then

$$\bar{\sigma}(K(I - GK)^{-1}) \lesssim \bar{\sigma}(K) \qquad (3.3)$$

$$\bar{\sigma}(GK(I - GK)^{-1}) \lesssim \bar{\sigma}(GK). \qquad (3.4)$$

For good performance we require $\bar{\sigma}((I - GK)^{-1})$ and $\bar{\sigma}((I - GK)^{-1}G)$ to be small (particularily at low frequency) and for good robust stability properties we require $\bar{\sigma}(K(I - GK)^{-1})$ and $\bar{\sigma}(GK(I - GK)^{-1})$ to be small (at high frequency in particular). A typical closed-loop design specification can therefore be illustrated as in Figure 3.1, and the desired closed-loop behaviour can be achieved by manipulation of the open loop gains, $\bar{\sigma}(GK)$, $\underline{\sigma}(GK)$.

However, this open-loop shaping approach is complicated by the need to ensure stability of the resulting closed-loop system. This requires that plant phase properties also be considered, and the loop shape can be shown to be limited by such stability requirements. This is examined in [1] for the SISO case, and in [3] for a MIMO extension. Further, these requirements are even more restrictive if the nominal plant has RHP poles or zeros. (See [12] for example.)

A loop-shaping approach that is somewhat simpler from the designers point of view is that used in the Loop Transfer Recovery (LTR) method in LQG design. (See [9] and [2].) In this method, the designer specifies a desired singular value loopshape, and the guaranteed stability properties of the LQG compensator ensure stability. LTR however, cannot systematically deal with plants with RHP zeros (see [13]), and is limited in that it can only guarantee performance and robust stability properties at either plant input or plant output.

The design technique that is proposed in this paper is similar in philosophy to LTR: The designer specifies a desired loop shape and then the 'shaped' plant is further compensated by a controller using the normalized LCF robust stabilization method of Section 2 to ensure closed-loop stability.

4. THE DESIGN PROCEDURE

4.1 Outline of the Design Procedure

We will now formally state the design procedure that was proposed in Section 1. The objective of this approach is to incorporate the simple performance/robustness trade-off obtained in loop shaping, with the guaranteed stability properties of H_∞ design methods.

'The Loop Shaping Design Procedure (LSDP)'

(1) Loop Shaping - using a precompensator, W_1, and/or a post-compensator, W_2, the singular values of the nominal plant are 'shaped' to give a desired open-loop shape. The nominal plant, G, and 'shaping functions' W_1, W_2 are combined to form the 'shaped plant', G_S where $G_S = W_2 G W_1$. (See Figure 4.1a.) We assume that W_1 and W_2 are such that G_S contains no hidden modes.

(2) Robust Stabilization - a feedback controller, K_∞, which robustly stabilizes the normalized left coprime factorization of G_S, with stability margin ϵ $(= \gamma^{-1})$, is synthesised, using the approach outlined in Section 2. (See Figure 4.1b.)

(3) The final feedback controller, K, is then constructed by combining the H_∞ controller, K_∞, with the shaping functions, W_1 and W_2 such that $K = W_1 K_\infty W_2$. (See Figure 4.1c.)

Note that, in contrast to the classical loop shaping approach, the loop shaping here is done *without* explicit regard for the nominal plant phase information. That is, closed-loop stability requirements are disregarded at this stage. Also, the robust stabilization is done *without* frequency weighting. The parameter ϵ can be seen as an *indicator* of the success of the loop shaping, where we note by (2.5), $\epsilon < 1$ always. A small value of ϵ $(\epsilon \ll 1)$
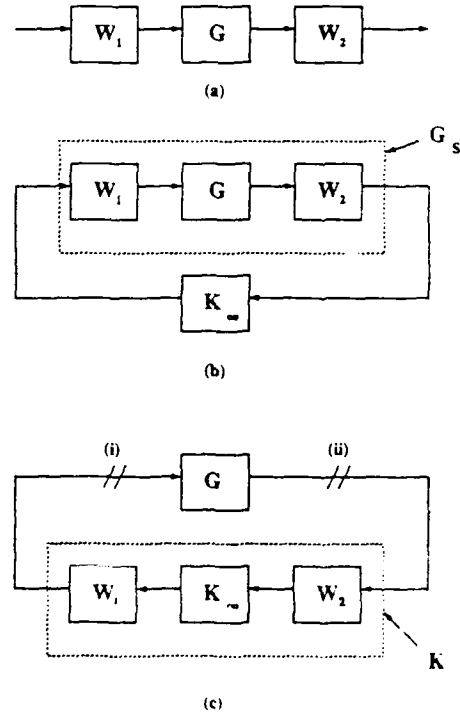

(a)

(b)

(c)

Figure 4.1 The Design Procedure (a) Shaped Plant, (b) Robust Stabilization, (c) Final Controller.

in Stage (2) always indicates incompatibility between the specified loop shape, the nominal plant phase, and robust closed-loop stability. Hence the loop shaping of Stage (1) is connected to the robust stabilization of Stage (2) via the indicator ϵ.

A typical design works as follows: The designer inspects the open-loop singular values of the nominal plant, and shapes these by pre and/or post compensation until nominal performance (and possibly robust stability) specifications are met. (Recall that the open-loop shape is related to closed-loop objectives.) A feedback controller, K_∞, with associated stability margin (for the shaped plant) $\epsilon \leq \epsilon_{max}$, is then synthesized. If ϵ is small, then the desired performance is incompatible with robust stability requirements, and the loop shape should be adjusted accordingly, and K_∞ re-evaluated. (In Section 5, the explicit dependence of performance and robust stability objectives on ϵ will be shown.) This procedure is both simple and systematic, and only assumes knowledge of elementary loop shaping principles on the part of the designer.

4.2 Comments on the Design Procedure

The following comments refer to the design procedure given in Section 4.1.

1. In the Loop Shaping Design Procedure we have interpreted the measure ϵ as a design indicator rather than as a specific stability margin for the notional perturbations on the normalized LCF of the shaped plant. In Section 5 we will show that any stabilizing controller achieving $\epsilon \ll 1$ will lead to deterioration in the achieved loop-shape compared with the specified loop shape at low or high frequencies, or will imply poor robust stability properties in the selected cross-over frequency region.

2. The procedure is applicable to stable or unstable, minimum or non minimum phase plants, provided they satisfy the minimum requirement for any design - that is, there are no unstable hidden modes. In particular, if a plant is non-minimum phase, the standard performance restrictions will still exist in the design procedure: It is well known, (see [8] or [5] for example) that the presence of a non minimum phase (RHP) zero in the nominal plant limits the achievable bandwidth and restricts low frequency behaviour. In the Loop Shaping Design Procedure, a loop shape which is incompatible with these generic restrictions will lead to a 'small' ϵ value in Stage (2). To illustrate this, consider the following example:

Let a nominal plant be given by $G = \frac{s-1}{s(s+2)}$, and we select $W = k$, a constant, as the shaping function. The shaped plant is then $G_S = WG = \frac{k(s-1)}{s(s+2)}$. By [8] we know that the closed-loop bandwidth has a practical limit of $1 r/s$ because of the RHP zero at $s = 1$ in G. Noting that the crossover frequency of the open-loop shape reflects the closed-loop bandwidth, we now select four values of k, the largest yielding a crossover frequency that is incompatible with the bandwidth limitations. The resulting ϵ values after Stage (2) of the Loop Shaping Design Procedure are

$$k = .1 \qquad \epsilon = 0.6814$$
$$k = 1 \qquad \epsilon = 0.5038$$
$$k = 5 \qquad \epsilon = 0.2177$$
$$k = 20 \qquad \epsilon = 0.0684$$

The value of ϵ associated with $k = 20$ is extremely small, indicating an 'incompatible loop shape'. This is confirmed by
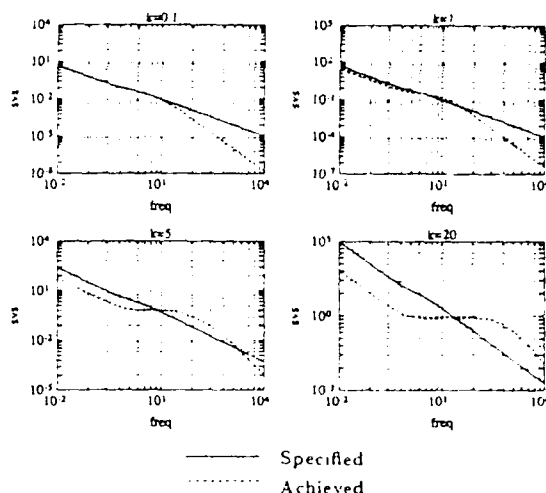
Figure 4.2 Specified and Achieved Loop Shapes-RHP Zeros Example

comparing the specified and achieved loop shapes for each case in Figure 4.2.

In the next section, we give theoretical justification for using the loop shaping design procedure.

5. PROPERTIES OF THE DESIGN METHOD

5.1 Controller Magnitude Bounds

In the previous section we specified the desired loop shape by $W_2 G W_1$ (Fig. 4.1a), but the actual loop shape achieved is in fact given by $W_1 K_\infty W_2 G$ at plant input (point (i), Fig 4.1c), and $G W_1 K_\infty W_2$ at plant output (point (ii), Fig. 4.1c). We will now show that the degradation in the loop shape caused by the H_∞ controller K_∞ is limited at those frequencies where the desired loop shape is sufficiently large or sufficiently small:

5.1.1 Low Frequency Behaviour

At low frequency (in particular $\omega \in (0, \omega_i)$) the deterioration in loop shape at plant output can be obtained by comparing $\underline{\sigma}(G W_1 K_\infty W_2)$ with $\underline{\sigma}(W_2 G W_1)$. Note that:

$$\underline{\sigma}(GK) = \underline{\sigma}(G W_1 K_\infty W_2) \geq \underline{\sigma}(W_2 G W_1)\underline{\sigma}(K_\infty)/c(W_2) \tag{5.1}$$

Similarly, for loop shape deterioration at plant input we compare $\underline{\sigma}(W_1 K_\infty W_2 G)$ with $\underline{\sigma}(W_2 G W_1)$ and we have

$$\underline{\sigma}(KG) = \underline{\sigma}(W_1 K_\infty W_2 G) \geq \underline{\sigma}(W_2 G W_1)\underline{\sigma}(K_\infty)/c(W_1) \tag{5.2}$$

In each case, $\underline{\sigma}(K_\infty)$ is required to obtain a bound on the deterioration in the loop shape at low frequency. Note that the condition numbers $c(W_1)$ and $c(W_2)$ are selected by the designer, and are commonly ot order one.

The following result shows that $\underline{\sigma}(K_\infty)$ is explicitly bounded by functions of ϵ and $\underline{\sigma}(G_S)$, the minimum singular value of the shaped plant. We assume here that the shaped plant G_S has an equal number of inputs and outputs. For convenience, the parameter, γ, defined $\gamma \triangleq \epsilon^{-1}$ will be used in the following analysis.

Theorem 5.1 *Any controller, K_∞, satisfying*

$$\left\| \begin{bmatrix} K_\infty \\ I \end{bmatrix} (I - G_S K_\infty)^{-1} \tilde{M}_s^{-1} \right\|_\infty \le \gamma$$

where $(\tilde{N}_s, \tilde{M}_s)$ is a normalized LCF of G_S, also satisfies

$$\underline{\sigma}(K_\infty(j\omega)) \ge \frac{\underline{\sigma}^2(G_S(j\omega)) - (\gamma^2 - 1)}{\sqrt{\gamma^2 - 1}(1 + \underline{\sigma}^2(G_S(j\omega))) + \gamma^2 \underline{\sigma}(G_S(j\omega))} \quad (5.3)$$

for all ω such that

$$\underline{\sigma}(G_S(j\omega)) \ge \sqrt{\gamma^2 - 1}.$$

(Lengthy proofs are omitted in this paper, and the reader is referred to [11] for full details.)

The main implication of Theorem 5.1 is that the bound on $\underline{\sigma}(K_\infty)$ depends only on the selected loop shape, and the stability margin. The value of γ directly determines the frequency range over which this result is valid - a small γ is desirable, as we would expect. Further, if we consider those frequencies where $\underline{\sigma}(G_S) \gg \sqrt{\gamma^2 - 1}$, we have the following asymptotic result:

Corollary 5.2 *Following the notation of Theorem 5.1, if $\underline{\sigma}(G_S(j\omega)) \gg \sqrt{\gamma^2 - 1}$, then*

$$\underline{\sigma}(K_\infty(j\omega)) \gtrsim \frac{1}{\sqrt{\gamma^2 - 1}}.$$

Proof: This follows immediately from equation (5.3), by noting that $\underline{\sigma}(G_S(j\omega)) \gg \sqrt{\gamma^2 - 1}$ implies that $\underline{\sigma}^2(G_S(j\omega)) \gg 1$, and also that $\underline{\sigma}^2(G_S(j\omega))(\gamma^2 - 1)^{1/2} \gg \gamma^2 \underline{\sigma}(G_S(j\omega))$. ∎

5.1.2 High Frequency Behaviour

At high frequency (in particular $\omega \in (\omega_u, \infty)$) the deterioration in plant output loop shape can be obtained by comparing $\bar{\sigma}(GW_1 K_\infty W_2)$ with $\bar{\sigma}(W_2 G W_1)$. Note that, analogously to (5.1) and (5.2) we have

$$\bar{\sigma}(GK) = \bar{\sigma}(GW_1 K_\infty W_2) \le \bar{\sigma}(W_2 G W_1)\bar{\sigma}(K_\infty)c(W_2). \quad (5.4)$$

Similarly, the corresponding deterioration in plant input loop shape is obtained by comparing $\bar{\sigma}(W_1 K_\infty W_2 G)$ with $\bar{\sigma}(W_2 G W_1)$ where

$$\bar{\sigma}(KG) = \bar{\sigma}(W_1 K_\infty W_2 G) \le \bar{\sigma}(W_2 G W_1)\bar{\sigma}(K_\infty)c(W_1). \quad (5.5)$$

Hence in each case, $\bar{\sigma}(K_\infty)$ is required to obtain a bound on the deterioration in the loop shape at high frequency. In an analogous manner to Theorem 5.1, we now show that $\bar{\sigma}(K_\infty)$ is explicitly bounded by functions of γ, and $\bar{\sigma}(G_S)$, the maximum singular value of the shaped plant.

Theorem 5.3 *Any controller, K_∞, satisfying*

$$\left\| \begin{bmatrix} K_\infty \\ I \end{bmatrix} (I - G_S K_\infty)^{-1} \tilde{M}_s^{-1} \right\|_\infty \le \gamma$$

where $(\tilde{N}_s, \tilde{M}_s)$ is a normalized LCF of G_S, also satisfies

$$\bar{\sigma}(K_\infty(j\omega)) \le \frac{\sqrt{\gamma^2 - 1}(1 + \bar{\sigma}^2(G_S(j\omega))) + \gamma^2 \bar{\sigma}(G_S(j\omega))}{1 - (\gamma^2 - 1)\bar{\sigma}^2(G_S(j\omega))} \quad (5.6)$$

for all ω such that

$$\bar{\sigma}(G_S(j\omega)) \le \frac{1}{\sqrt{\gamma^2 - 1}}.$$

Again, if we consider those frequencies at which $\bar{\sigma}(G_S) \ll \frac{1}{\sqrt{\gamma^2 - 1}}$, then we have the following result:

Corollary 5.4 *Following the notation of Theorem 5.3, if $\bar{\sigma}(G_S(j\omega)) \ll \frac{1}{\sqrt{\gamma^2 - 1}}$, then*

$$\bar{\sigma}(K_\infty(j\omega)) \lesssim \sqrt{\gamma^2 - 1} \quad (5.7)$$

Proof: This follows immediately from (5.6) by noting that $\bar{\sigma}(G_S) \ll \frac{1}{\sqrt{\gamma^2 - 1}}$ implies $\bar{\sigma}^2(G_S) \ll 1$, and $\gamma^2 \bar{\sigma}(G_S) \ll (\gamma^2 - 1)^{1/2}$. ∎

Remark 5.5 The approximate results in Corollaries 5.2 and 5.4 show that at frequencies where $\underline{\sigma}(G_S) \gg 1$ or $\bar{\sigma}(G_S) \ll 1$, the deterioration in the loop shape due to K_∞ is bounded by a function of γ (or equivalently ϵ) only. Noting that γ 'small' (implying ϵ 'large') indicates a minimal deterioration in the loop shape, it is confirmed that ϵ indicates the compatibility between the specified loop shape and closed-loop stability requirements.

Remark 5.6 Note that in Theorem 5.3 it is not necessary to assume that G_S is a square transfer function matrix. Hence, high frequency loop shape properties can be guaranteed for a plant of any dimension.

We have shown in this section that the values of γ (alternatively ϵ) achieved in the Loop Shaping Design Procedure will directly affect the singular values of the H_∞ controller K_∞. Although the precise relationship between γ and the shaping functions W_1 and W_2 is not known, we have shown that a large γ value indicates incompatibility between the selected loop shape and the closed-loop stability requirements. Such an incompatibility can lead to extensive deterioration in the specified loop shape. Under such circumstances, the designer would be required to 'relax' the original loop shape specification, until a more compatible loop shape is achieved.

5.2 Using γ/ϵ as a Design Indicator

In Section 5.1 we evaluated bounds on the *maximum* loop shape deterioration at low and high loop gains, for a given γ ($= \epsilon^{-1}$), and a specified loop shape. In this section we take a contrary approach: Given any stabilizing controller, K_a, there exists a frequency ω_o, such that

$$\bar{\sigma}\left(\begin{bmatrix} K_a \\ I \end{bmatrix} (I - G_S K_a)^{-1} \tilde{M}_s^{-1} \right)(j\omega_o) = \gamma \ge \gamma_{min},$$

and we evaluate the *minimum* deterioration in loop shape that can be expected, if any, for this γ, and examine the effect of γ on robust stability at this frequency. We summarize these ideas in the following theorem.

Theorem 5.7 *Let $\gamma_{min}^{-1} = \epsilon_{max}$ be the optimal stability margin for the normalized LCF robust stabilization problem, as given in (2.5). Then, for any stabilizing controller, K_a, there exists a frequency, ω_o, such that*

$$\bar{\sigma}\left(\begin{bmatrix} K_a \\ I \end{bmatrix} (I - G_S K_a)^{-1} \tilde{M}_s^{-1} \right)(j\omega_o) = \gamma \ge \gamma_{min}$$

and hence

(i) There exists a perturbed system

$$G_\Delta = W_2^{-1}(\tilde{M}_s + \Delta_M)^{-1}(\tilde{N}_s + \Delta_N)W_1^{-1}$$

with

$$\|[\Delta_N, \Delta_M]\|_\infty \le \gamma_{min}^{-1} \tag{5.9}$$

which destabilizes the system. Further,

(ii) if $\underline{\sigma}(G_S(j\omega_o)) > (\gamma_{min}^2 - 1)^{-1/2}$, then

$$\underline{\sigma}(K_a(j\omega_o)) \le \frac{\sqrt{\gamma_{min}^2 - 1}(1 + \underline{\sigma}^2(G_S(j\omega_o))) + \gamma_{min}^2 \underline{\sigma}(G_S(j\omega_o))}{(\gamma_{min}^2 - 1)\underline{\sigma}^2(G_S(j\omega_o)) - 1}$$

and

(iii) if $\overline{\sigma}(G_S(j\omega_o)) < (\gamma_{min}^2 - 1)^{1/2}$, then

$$\overline{\sigma}(K_a(j\omega_o)) \ge \frac{\gamma_{min}^2 - 1 - \overline{\sigma}^2(G_S(j\omega_o))}{\sqrt{\gamma_{min}^2 - 1}(1 + \overline{\sigma}^2(G_S(j\omega_o))) + \gamma_{min}^2 \overline{\sigma}(G_S(j\omega_o))}$$

Remark 5.8 Theorem 5.7 shows that γ/ϵ is a design indicator for the entire frequency range: Firstly, if the coprime factor robust stability is poor (that is $\epsilon \ll 1$ or $\gamma \gg 1$) at a frequency where $\tilde{N}_s$ and $\tilde{M}_s$ are of comparable size, then (i) shows that only a small relative perturbation on either $\tilde{N}_s$ or $\tilde{M}_s$ is permitted. However, if $\tilde{M}_s \gg \tilde{N}_s$, then the notional destabilizing perturbation could correspond to a very large relative perturbation in $\tilde{N}_s$, implying that robust stability properties may in fact be acceptable despite $\gamma \gg 1$. However, in this case, we have $\overline{\sigma}(G_S) \ll 1$ and part (iii) of Theorem 5.7 applies, showing that the loop gain is necessarily and undesirably increased. Conversely, if $\tilde{M}_s \ll \tilde{N}_s$, then the notional destabilizing perturbation could correspond to a very large relative perturbation in $\tilde{M}_s$, again implying that robust stability properties may in fact be acceptable despite $\gamma \gg 1$. However, in this case, we have $\underline{\sigma}(G_S) \gg 1$ and part (ii) of Theorem 5.7 applies, showing that the loop gain is necessarily and undesirably decreased.

In the next section we examine the closed-loop behaviour achieved using the Loop Shaping Design Procedure, and confirm that the loop shaping approach gives guarantees on particular closed-loop objectives.

5.3 Behaviour of Standard Closed-Loop Objectives

In Section 3 we stated that a feature of the classical loop shaping design approach is that it is possible, by open-loop singular value shaping, to ensure that a number of standard closed-loop design objectives are 'well behaved'. The following result demonstrates that this is also the case for the Loop Shaping Design Procedure outlined in Section 4.1:

Theorem 5.9 *Let G be the nominal plant and let $K = W_1 K_\infty W_2$ be the associated controller obtained from the Loop Shaping Design Procedure of Section 4.1. Then*

$$\overline{\sigma}(K(I - GK)^{-1}) \le \gamma\overline{\sigma}(\tilde{M}_s)\overline{\sigma}(W_1)\overline{\sigma}(W_2) \tag{5.10}$$

$$\overline{\sigma}((I - GK)^{-1}) \le \gamma\overline{\sigma}(\tilde{M}_s)c(W_2) \tag{5.11}$$

$$\overline{\sigma}(K(I - GK)^{-1}G) \le \gamma\overline{\sigma}(\tilde{N}_s)c(W_1) \tag{5.12}$$

$$\overline{\sigma}((I - GK)^{-1}G) \le \frac{\gamma\overline{\sigma}(\tilde{N}_s)}{\underline{\sigma}(W_1)\underline{\sigma}(W_2)} \tag{5.13}$$

and

$$\overline{\sigma}((I - KG)^{-1}) \le 1 + \gamma\overline{\sigma}(\tilde{N}_s)c(W_1) \tag{5.14}$$

$$\overline{\sigma}(G(I - KG)^{-1}K) \le 1 + \gamma\overline{\sigma}(\tilde{M}_s)c(W_2) \tag{5.15}$$

where $(\tilde{N}_s, \tilde{M}_s)$ is a normalized LCF of $G_S = W_2 G W_1$, and $c(\bullet)$ denotes the condition number.

Remark 5.10 Note that because $(\tilde{N}_s, \tilde{M}_s)$ is a *normalized* LCF of G_S we have that $\overline{\sigma}(\tilde{N}_s) \le 1$ and $\overline{\sigma}(\tilde{M}_s) \le 1$ for all frequencies. Noting also that γ has a finite value (typically $1 < \gamma < 5$ in practice), and that the shaping functions are selected by the designer, then it can be seen that, by (5.10) - (5.15), all of the closed-loop objectives are guaranteed to have bounded magnitude. We say that in this case the objectives are *well behaved*. For the simple case of $W_1 = I$ and $W_2 = I$ it can be readily seen that in (5.10) - (5.13), $\tilde{N}_s$ ($= \tilde{N}$) and $\tilde{M}_s$ ($= \tilde{M}$) provide frequency weighting. The frequency shapes are 'natural' for many problems: for example at frequencies where $\overline{\sigma}(\tilde{M}_s)$ is small (indicating a nominal plant pole near the imaginary axis), then $\overline{\sigma}((I - GK)^{-1})$ and $\overline{\sigma}(K(I - GK)^{-1})$ are small. So the behaviour of the standard closed-loop transfer functions $(I - GK)^{-1}$, $K(I - GK)^{-1}$, $K(I - GK)^{-1}G$, and $(I - GK)^{-1}G$ is compatible with sensible closed-loop design.

5.4 Bounds on the Normalized Coprime Factors

We now state a technical result which demonstrates that $\overline{\sigma}(\tilde{N}_s)$ and $\overline{\sigma}(\tilde{M}_s)$ are related to the nominal plant G and the shaping functions W_1 and W_2.

Lemma 5.11 *Let the shaped plant, $G_S = W_2 G W_1$, have a normalized LCF given by $(\tilde{N}_s, \tilde{M}_s)$. Then*

$$\overline{\sigma}(\tilde{N}_s) = \left(\frac{\overline{\sigma}^2(W_2 G W_1)}{1 + \overline{\sigma}^2(W_2 G W_1)}\right)^{1/2} \tag{5.16}$$

and

$$\overline{\sigma}(\tilde{M}_s) = \left(\frac{1}{1 + \underline{\sigma}^2(W_2 G W_1)}\right)^{1/2}. \tag{5.17}$$

Remark 5.12 The value of this Lemma is that the bounds on the closed-loop objectives in Theorem 5.9 can be rewritten in terms of γ, G, W_1, and W_2 only. It can now be clearly seen how the loop shaping influences the closed-loop properties. Noting that if $\underline{\sigma}(W_2 G W_1) \gg 1$ then $\overline{\sigma}(\tilde{M}_s) \simeq 1/\underline{\sigma}(W_2 G W_1)$, $\overline{\sigma}(\tilde{N}_s) \simeq 1$ and that if $\overline{\sigma}(W_2 G W_1) \ll 1$ then $\overline{\sigma}(\tilde{M}_s) \simeq 1$, $\overline{\sigma}(\tilde{N}_s) \simeq \overline{\sigma}(W_2 G W_1)$, then the bounds in Theorem 5.9 can be re-evaluated to show the effects of W_1 and W_2 on closed-loop behaviour in frequency regions of high and low loop gain.

6. SUMMARY OF RESULTS

In this paper we have incorporated the normalized LCF robust stabilization problem into a loop shaping based design technique. This enables both performance and robust stability objectives to be traded-off, and preserves the exact solution associated with this particular H_∞ problem. The design method is straightforward and systematic, incorporating only the simpler aspects of 'classical' loop shaping. The normalized LCF robust stabilization problem has been shown to be particularly well suited for this approach because the H_∞ controller synthesized causes only a limited deterioration of the specified loop shape. Coprime factor model reduction techniques can be simply incorporated into this framework. As a final comment, it should be noted that the Loop Shaping Design Procedure is restricted to a

particular set of H_∞ objectives. However, it can be shown that the design technique yields simple and effective controllers. (See [10] and [11].)

7. REFERENCES

[1] Bode, H. (1945) 'Network Analysis & Feedback Amplifier Design', *Van Nostrand, Princeton.*

[2] Doyle, J., and Stein, G., (1979) 'Robustness with Observers', *IEEE Trans. Auto. Control,* 24.4:607-611.

[3] Doyle, J., and Stein, G. (1981) 'Multivariable Feedback Design: Concepts for a Classical/Modern Synthesis', *IEEE Trans. Auto. Contr.,* 26.1:4-16.

[4] Francis, B. (1987) 'A Course in H_∞ Control Theory', *Springer Verlag, Berlin.*

[5] Freudenberg, J., Looze, D. (1987) 'Frequency Domain Properties of Scalar and Multivariable Feedback Systems', *Springer Verlag, Berlin.*

[6] Glover, K. and McFarlane, D. (1988a) 'Robust Stabilization of Normalized Coprime Factors: An Explicit H^∞ Solution', *Proceedings 1988 American Control Conference, Atlanta, Georgia*

[7] Glover, K. and McFarlane, D. (1988b) 'Robust Stabilization of Normalized Coprime Factor Plant Descriptions with H_∞ -Bounded Uncertainty', *submitted for publication.*

[8] Horowitz, I. (1963) 'Synthesis of Feedback Systems', *Academic Press.*

[9] Kwakernaak, H. and Sivan, R. (1972) 'Linear Optimal Control Systems', *Wiley.*

[10] McFarlane, D., Glover, K., and Noton, M. (1988) 'Robust Stabilization of a Flexible Space-Platform: An H_∞ Coprime Factorization Approach', *'Control 88', IEE Conference, Oxford.*

[11] McFarlane, D., Glover, K. (1988) 'A Loop Shaping Design Procedure using H_∞ Synthe sis', *under preparation.*

[12] Maciejowski, J. (1988) 'Multivariable Feedback Design', *under preparation.*

[13] Stein, G., and Athans, M. (1987) 'The LQG/LTR Procedure for Multivariable Feedback Design', *IEEE Trans. Auto. Control,* 32.2.:105-114.

[14] Vidyasagar, M. (1984) 'The Graph Metric for Unstable Plants and Robustness Estimates for Feedback Stability', *IEEE Trans. Auto. Control,* 29:403-417.

[15] Vidyasagar, M. (1985) 'Control System Synthesis: A Coprime Factorization Approach', *MIT Press.*

[16] Vidyasagar,M., Kimura,H. (1986) 'Robust Controllers for Uncertain Linear Multivariable Systems', *Automatica,* 85-94.

Proceedings of the 27th Conference
on Decision and Control
Austin, Texas • December 1988

TA3 - 8:30

CONTROLLERS WHICH SATISFY A CLOSED-LOOP H∞-NORM BOUND AND MAXIMIZE AN ENTROPY INTEGRAL

Denis Mustafa   and   Keith Glover

Department of Engineering, University of Cambridge
Trumpington Street, Cambridge, CB2 1PZ, UK

Abstract

The problem of maintaining the H_∞ norm of a standard closed loop below a prespecified tolerance level whilst maximizing an entropy integral (at a point in the right half plane) is posed and solved by way of the equivalent error system distance problem. All error systems with infinity norm below the tolerance level are parametrized as the linear fractional map of an all pass matrix and an arbitrary stable contraction. We derive the maximum entropy choice for the contraction and a value for the maximum entropy. For the maximum entropy at infinity, it is proved that the arbitrary contraction must be set to zero (the 'central' solution); the maximum entropy in this case is an explicit formula in terms of the realization of the error system. Some motivational remarks are made and links between entropy, H_2 norms and H_2 optimal control are given.

Notation

C_+	The open right half plane.
$\mathcal{R}$	(Prefix) Real-rational.
$\mathcal{R}H_2$	Hardy space of real-rational transfer function matrices analytic and square-integrable on vertical lines in the right-half plane.
$\mathcal{R}H_\infty$	Hardy space of real-rational transfer function matrices analytic and bounded in the right half plane.
G^*	$:= \overline{G(-\bar{s})}^T$, the parahermitian conjugate.
$\sigma_i(G)$	$:= \lambda_i^{1/2}(G^*G)$, the ith singular value of G.
$\|G\|_2$	$:= \left[\frac{1}{2\pi}\int_{-\infty}^{\infty} Trace(G^*(j\omega)G(j\omega))\,d\omega\right]^{\frac{1}{2}}$, H_2-norm.
$\|G\|_\infty$	$:= \sup_\omega \sigma_{max}(G(j\omega))$, H_∞-norm.
$X = Ric\begin{pmatrix} A & -BB^* \\ -C^*C & -A^* \end{pmatrix}$	is the stabilizing solution of the Riccati equation $XA + A^*X - XBB^*X + C^*C = 0$
$(\ )_{ME}$	Denotes maximum entropy.
$(\ )_{opt}$	Denotes H_∞ optimal.
$(\ )_{H_2}$	Denotes H_2 optimal.
$\left(\frac{A\|B}{C\|D}\right)$	$:= D + C(sI-A)^{-1}B$, state-space realization.

A square transfer function matrix $G(s)$ is said to be *all pass* if

$$G^*(j\omega)G(j\omega) = I, \quad \forall\omega.$$

The Laplace transform variable s will be suppressed to keep typography simple. Dependence of transfer functions on s is understood.

I. Introduction

This paper is concerned with *suboptimal* H_∞ control with a *maximum entropy* criterion. The theory of *optimal* H_∞ control has received much attention over recent years; for full details the interested reader is referred to Francis [6] and the references therein. Figure 1 illustrates the usual configuration, where the 'standard plant' P, consisting of the actual plant, suitable weighting functions and interconnections, maps exogenous inputs w and control inputs u to controlled outputs z and measured outputs y. As is usual in H_∞ control problems, we assume that

$$P = \begin{matrix} {}^{m_1} & {}^{m_2} \\ {}_{p_1}\begin{pmatrix} P_{11} & P_{12} \\ P_{21} & P_{22} \end{pmatrix} \end{matrix}; \quad m_1 \geq p_2, \ p_1 \geq m_2.$$
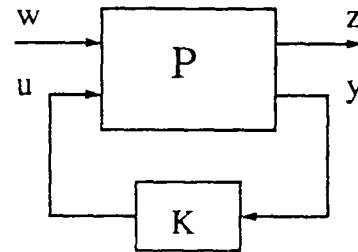

Figure 1. The standard H_∞ configuration.

The closed loop transfer function matrix G from w to z is given by the linear fractional map

$$G = \mathcal{F}(P, K)$$
$$:= P_{11} + P_{12}K(I - P_{22}K)^{-1}P_{21} \quad (1)$$

of the appropriately partitioned standard plant P and the controller K. The optimal H_∞ control problem is to find a stabilizing controller K_{opt} which minimizes the infinity-norm of this transfer function i.e., K_{opt} satisfies

$$inf\{\|\mathcal{F}(P, K)\|_\infty : K \text{ stabilizes } P\} := \gamma_{opt}$$
$$= \|\mathcal{F}(P, K_{opt})\|_\infty. \quad (2)$$

Motivated by the belief that optimal H_∞ control is not always appropriate we consider here the suboptimal problem obtained by relaxing the infimum in (2) to the bound

$$\|\mathcal{F}(P, K)\|_\infty \leq \gamma \quad (3)$$

where $\gamma > \gamma_{opt}$. In general, there is a class of controllers which satisfy this bound; such nonuniqueness is dealt with in this paper by specifying that the *entropy* of the closed loop transfer function must be maximized.

The entropy is defined as follows. For any transfer function matrix G which satisfies $\|G\|_\infty \leq \gamma$ the entropy of G at a point $s_0 \in C_+$ is defined by

$$I(G; \gamma; s_0)$$
$$:= \frac{\gamma^2}{2\pi} \int_{-\infty}^{\infty} \ln|det(I - \gamma^{-2}G^*(j\omega)G(j\omega))| \left[\frac{Re\,s_0}{|s_0 - j\omega|}\right]^2 d\omega. \quad (4)$$

This definition is equivalent to that of Arov and Krein [1], [2] except for an extra $Re\,s_0$ term to ensure non-zero entropy when $s_0 \to \infty$. It is easily seen that the entropy is well-defined (since $\|G\|_\infty \leq \gamma$ implies $0 \leq I - \gamma^{-2}G^*(j\omega)G(j\omega) \leq I$) and nonpositive; that $I(G; \gamma; s_0) = 0$ if and only if $G = 0$; and that the entropy of G is invariant under unitary scaling of G

Our maximum entropy H_∞ control problem is then:

Find, out of all controllers K which stabilize P and satisfy

$$\|\mathcal{F}(P,K)\|_\infty \leq \gamma \tag{5}$$

the K which maximizes the entropy $I(G;\gamma;s_0)$ of the closed loop transfer function matrix $G = \mathcal{F}(P,K)$ at a point $s_0 \in \mathcal{C}_+$.

Maximum entropy has been studied in a wide variety of contexts; its applications to extension problems (Arov and Krein [1], [2]) and to contractive interpolants (Dym and Gohberg [4], [5]) are pertinent here – we use an adaptation of the method of [2]. The use of maximum entropy in H_∞ control has been considered by Limebeer and Hung [9] for the 'one-block case' where both P_{12} and P_{21} are square. No such assumptions are made here, the analysis is valid for 'one-,' 'two-,' and 'four-block' problems.

As with optimal H_∞ problems (see [6]) we approach the problem by reducing our original problem to a 'distance problem'. To do this, we use the parametrization of all stabilizing controllers of Youla *et al.* [12] to reduce (5) to the equivalent model-matching problem of finding $\dot{Q} \in \mathcal{R}H_\infty$ such that

$$\|T_1 + T_2 \dot{Q} T_3\|_\infty \leq \gamma \tag{6}$$

and then exploit the unitary invariance of the H_∞ norm to reduce (6) to the distance problem

$$\left\| \begin{pmatrix} R_{11} & R_{12} \\ R_{21} & R_{22} + \dot{Q} \end{pmatrix} \right\|_\infty \leq \gamma, \quad \dot{Q} \in \mathcal{R}H_\infty \tag{7}$$

where $R = \begin{pmatrix} R_{11} & R_{12} \\ R_{21} & R_{22} \end{pmatrix}$ is antistable and is known in terms of the standard plant P.

If we define the error system E by

$$E := \begin{pmatrix} R_{11} & R_{12} \\ R_{21} & R_{22} + \dot{Q} \end{pmatrix} \tag{8}$$

we know that $I(G;\gamma;s_0) = I(E;\gamma;s_0)$ because entropy is unitarily invariant, therefore the closed loop transfer function G and the error system E have the same entropy, allowing us to solve our original closed loop problem (5) by solving the following error system distance problem:

Find the error system E as defined in equation (8) which satisfies $\|E\|_\infty \leq \gamma$ and maximizes $I(E;\gamma;s_0)$.

The arrangement of the paper is as follows. In the next section we briefly motivate H_∞ control and maximum entropy. Section III contains the main results. By parametrizing all solutions of the error system distance problem we are able to derive the unique maximum entropy solution together with a value for its entropy. This is firstly done for the general case of entropy at any $s_0 \in \mathcal{C}_+$ and then for the important special case of $s_0 \to \infty$. This latter case yields particularly explicit and appealing results. Proofs of certain lemmas have been relegated to the appendix whenever the inclusion of the proof in the main body of the text would be intrusive.

II. Motivation

Here we briefly state some relevant background details. Recall that we want our controller to stabilize P and keep the infinity-norm of the closed loop $\mathcal{F}(P,K)$ below a level γ (where $\gamma > \gamma_{opt}$). Such control problems lead to a class of possible controllers and so there is scope for another criterion. Our approach is to use the controller which maximizes the closed loop entropy. The closed loop entropy (4) is a useful measure of how close $G = \mathcal{F}(P,K)$ is to the worst case of $G^*(j\omega)G(j\omega) = \gamma^2 I \quad \forall\omega$, where the bound is achieved at every frequency, for in this case the entropy is $-\infty$.

As G moves away from this worst case towards $G = 0$ the entropy becomes finite and decreases in magnitude until at $G = 0$ the entropy equals zero. Maximizing the entropy at any particular γ is an effective way of driving G away from the $G^*(j\omega)G(j\omega) = \gamma^2 I, \forall\omega$, case towards the more desirable $G = 0$ case. Of course, our standard plant must be stabilized as well. Furthermore, if we rewrite the entropy as

$$I(G;\gamma;s_0) = \frac{\gamma^2}{2\pi} \int_{-\infty}^{\infty} \sum_i ln|1 - \gamma^{-2}\sigma_i^2(G(j\omega))| \left[\frac{Re\, s_0}{|s_0 - j\omega|} \right]^2 d\omega \tag{9}$$

it is clear that all the singular values $\sigma_i(G)$ of G are included, unlike the infinity norm which depends only on the largest singular value.

The term $[(Re\, s_0)/|s_0 - j\omega|]^2$ in the entropy integral is a frequency weighting with a shape dependent on the position of the point s_0 in the right half plane. In order to obtain real-rational controllers s_0 should be a real number; allowing $s_0 \to \infty$ makes the frequency weighting equal to unity for all frequencies, a notable special case we will return to later.

An interesting link with the H_2 norm is provided by the following lemma.

Lemma 2.1. *For any G which satisfies $\|G\|_\infty < \gamma$ we have*

(i) $\{-I(G;\gamma;s_0)\}^{1/2} \geq \|G(Re\, s_0)/(s_0 + s)\|_2$

(ii) $\{-I(G;\gamma;\infty)\}^{1/2} \geq \|G\|_2$ if G is strictly proper

and equality in both cases is achieved when $\gamma \to \infty$

Proof: Appendix. $\triangle\triangle\triangle$

Part (i) of this lemma shows us that the square root of the magnitude of the entropy at s_0 is an upper bound on a frequency weighted H_2 norm, whilst part (ii) is a similar result for the entropy at infinity and the usual (unweighted) H_2 norm, if it exists. In both (i) and (ii), relaxing the H_∞ norm constraint entirely by allowing $\gamma \to \infty$ gives equality. In other words, the frequency weighted (respectively unweighted) H_2 norm minimization problem is exactly the maximum entropy at s_0 (resp. at ∞) problem, with $\gamma \to \infty$. Thus the imposition of the maximum entropy constraint allows us to use γ to trade off between H_∞ optimal ($\gamma \to \gamma_{opt}$) and H_2 optimal ($\gamma \to \infty$) solutions.

III. Derivation of the maximum entropy solution

In this section we solve the following maximum entropy distance problem, as posed earlier.

Let $s_0 \in \mathcal{C}_+$ and

$$R = \begin{matrix} p_1 - m_2 \\ p_2 \end{matrix} \begin{pmatrix} \overset{m_1 - p_2}{R_{11}} & \overset{m_2}{R_{12}} \\ R_{21} & R_{22} \end{pmatrix} \tag{10}$$

be given, where

$$R^* \in \mathcal{R}H_\infty, \quad m_1 \geq p_2, \quad p_1 \geq m_2.$$

Define the error system E by

$$E := \begin{pmatrix} R_{11} & R_{12} \\ R_{21} & R_{22} + \dot{Q} \end{pmatrix} \quad \dot{Q} \in \mathcal{R}H_\infty \tag{11}$$

and let

$$\gamma_{opt} = \inf \{ \|E\|_\infty : \dot{Q} \in \mathcal{R}H_\infty \}. \tag{12}$$

Then for $\gamma > \gamma_{opt}$, find $\dot{Q} \in \mathcal{R}H_\infty$ such that $\|E\|_\infty \leq \gamma$ and the entropy $I(E;\gamma;s_0)$ is maximized.

We have seen that this problem is equivalent to finding a stabilizing controller K which keeps $\|\mathcal{F}(P, K)\|_\infty \leq \gamma$ and maximizes the closed loop entropy.

Solution proceeds by firstly parametrizing all possible E which satisfy the bound $\|E\|_\infty \leq \gamma$. Ball and Cohen [3] provide such a parametrization in terms of a linear fractional map of a J-*unitary* matrix and an arbitrary, stable contraction Φ (that is, $\Phi \in \mathcal{R}H_\infty$ and $\|\Phi\|_\infty \leq 1$), but it is more convenient to use the parametrization of Glover and Doyle [8] in terms of the linear fractional map of an *all pass* matrix and an arbitrary, stable contraction Φ. By adapting the method of [2] we are able to derive the unique choice of Φ which maximizes the entropy and a value for the maximum entropy, for both the general case of $s_0 \in \mathcal{C}_+$ and when $s_0 \to \infty$.

III.1 The general case

Here we solve the maximum entropy distance problem for arbitrary $s_0 \in \mathcal{C}_+$ and E proper, but not necessarily strictly proper. The class of error systems E over which the entropy must be maximized is parametrized in the following lemma.

Lemma 3.1. [8] *All solutions*

$$E = \begin{matrix} p_1 - m_2 I \\ m_2 I \end{matrix} \begin{pmatrix} \overset{m_1 - p_2}{R_{11}} & \overset{p_2}{R_{12}} \\ R_{21} & R_{22} + \hat{Q} \end{pmatrix}$$

with

$$R^\cdot, \hat{Q} \in \mathcal{R}H_\infty, \quad m_1 \geq p_2, \quad p_1 \geq m_2,$$

to the distance problem $\|E\|_\infty \leq \gamma$ *where* $\gamma > \gamma_{opt}$, *are given by:*

$$E = \gamma \mathcal{F}(R_{aa} + Q_{aa}, \Psi), \tag{13}$$

where

$$\Psi := \begin{matrix} p_1 - m_2 I \\ m_2 I \end{matrix} \begin{pmatrix} \overset{m_1 - p_2}{0} & \overset{p_2}{0} \\ 0 & \Phi \end{pmatrix}, \quad \Phi \in \mathcal{R}H_\infty, \quad \|\Phi\|_\infty \leq 1.$$

Also,

$$R_{aa} + Q_{aa}$$

$$:= \begin{matrix} p_1 I \\ m_1 I \end{matrix} \begin{pmatrix} \overset{m_1}{[R_{aa} + Q_{aa}]_{11}} & \overset{p_1}{[R_{aa} + Q_{aa}]_{12}} \\ [R_{aa} + Q_{aa}]_{21} & [R_{aa} + Q_{aa}]_{22} \end{pmatrix} \tag{14}$$

$$:= \begin{matrix} p_1 - m_2 I \\ m_2 I \\ m_1 - p_2 I \\ p_2 I \end{matrix} \begin{pmatrix} \overset{m_1 - p_2}{\gamma^{-1}R_{11}} & \overset{p_2}{\gamma^{-1}R_{12}} & \overset{p_1 - m_2}{R_{13}} & \overset{m_2}{0} \\ \gamma^{-1}R_{21} & \gamma^{-1}(R_{22} + Q_{22}) & R_{23} + Q_{23} & Q_{24} \\ R_{31} & R_{32} + Q_{32} & R_{33} + Q_{33} & Q_{34} \\ 0 & Q_{42} & Q_{43} & Q_{44} \end{pmatrix} \tag{15}$$

Further, $R_{ij}^\cdot, Q_{ij} \in \mathcal{R}H_\infty$, $R_{aa} + Q_{aa}$ *is all pass,* $Q_{44}(\infty) = 0$ *and* $\|Q_{44}\|_\infty < 1$.

State space realizations of R_{ij} and Q_{ij} are available in [8], in terms of the realization of $\begin{pmatrix} R_{11} & R_{12} \\ R_{21} & R_{22} \end{pmatrix}$ and the solutions to two algebraic Riccati equations. In this section we will not need these realizations.

The next lemma relates the entropy of the linear fractional map of an all pass matrix J and an arbitrary stable contraction Ψ to the entropy of Ψ itself.

Lemma 3.2. *Suppose* $J = \begin{pmatrix} J_{11} & J_{21} \\ J_{21} & J_{22} \end{pmatrix}$ *is all pass,* $\Psi \in \mathcal{R}H_\infty$, $\|\Psi\|_\infty \leq 1$ *and* $det(I - J_{22}\Psi)$ *is a unit in* $\mathcal{R}H_\infty$. *Then*

$$I(\gamma\mathcal{F}(J, \Psi); \gamma; s_0) = \gamma^2 I(\Psi; 1; s_0) + \gamma^2 I(J_{11}; 1; s_0) - \gamma^2 (Re\ s_0) ln|det(I - J_{22}(s_0)\Psi(s_0))|. \tag{16}$$

Proof: Throughout this proof take $s = j\omega$. The assumption that $det(I - J_{22}\Psi)$ is a unit in $\mathcal{R}H_\infty$ together with the all pass nature of J ensures that (Redheffer [10])

$$[\gamma\mathcal{F}(J, \Psi)]^\cdot [\gamma\mathcal{F}(J, \Psi)] \leq \gamma^2 I, \tag{17}$$

so the entropy $I(\gamma\mathcal{F}(J, \Psi); \gamma; s_0)$ is well defined. Using

$$J^\cdot(j\omega)J(j\omega) = I \tag{18}$$

in block-partitioned form, it is straightforward to show that

$$I - \gamma^{-2} [\gamma\mathcal{F}(J, \Psi)]^\cdot [\gamma\mathcal{F}(J, \Psi)]$$
$$= J_{21}^\cdot [I - J_{22}\Psi]^{-\cdot} [I - \Psi^\cdot\Psi] [I - J_{22}\Psi]^{-1} J_{21}. \tag{19}$$

From this, and the fact that for any square real-rational transfer function matrix G

$$ln|det(G^\cdot G)| = ln|det(G)| + ln|det(G^\cdot)| = 2 ln|det(G)|, \tag{20}$$

we obtain

$$ln|det(I - \gamma^{-2} [\gamma\mathcal{F}(J, \Psi)]^\cdot [\gamma\mathcal{F}(J, \Psi)])|$$
$$= ln|det(I - \Psi^\cdot\Psi)| + ln|det(J_{21}^\cdot J_{21})| - 2 ln|det(I - J_{22}\Psi)|. \tag{21}$$

Substituting this into the definition of $I(\gamma\mathcal{F}(J, \Psi); \gamma; s_0)$ and using the (1,1) block of (18) to write $J_{21}^\cdot J_{21} = I - J_{11}^\cdot J_{11}$, $\forall s = j\omega$, it follows that

$$I(\gamma\mathcal{F}(J, \Psi); \gamma; s_0) = \gamma^2 I(\Psi; 1; s_0) + \gamma^2 I(J_{11}; 1; s_0)$$
$$- \frac{\gamma^2}{\pi} \int_{-\infty}^{\infty} ln|det(I - J_{22}(j\omega)\Psi(j\omega))| \left[\frac{Re\ s_0}{|s_0 - j\omega|}\right]^2 d\omega. \tag{22}$$

By assumption, $det(I - J_{22}\Psi)$ is a unit in $\mathcal{R}H_\infty$, which permits the use of Poisson's Integral Theorem (Rudin [11], p343) to evaluate the integral in (22), giving

$$I(\gamma\mathcal{F}(J, \Psi); \gamma; s_0) = \gamma^2 I(\Psi; 1; s_0) + \gamma^2 I(J_{11}; 1; s_0)$$
$$- \gamma^2 (Re\ s_0) ln|det(I - J_{22}(s_0)\Psi(s_0))| \tag{23}$$

as claimed. $\triangle\triangle\triangle$

We are now in a position to derive the unique, stable, contractive Φ in the parametrization of all error systems which maximizes the entropy $I(E; \gamma; s_0)$.

Theorem 3.3. *Consider the class of error systems E which satisfy the condition* $\|E\|_\infty \leq \gamma$ *as parametrized in Lemma 3.1 by*

$$E = \gamma\mathcal{F}(R_{aa} + Q_{aa}, \begin{pmatrix} 0 & 0 \\ 0 & \Phi \end{pmatrix}), \quad \Phi \in \mathcal{R}H_\infty, \|\Phi\|_\infty \leq 1. \tag{24}$$

Then the entropy $I(E; \gamma; s_0)$ *attains its maximum over this class of E with the unique choice*

$$\Phi = Q_{44}^\cdot(s_0). \tag{25}$$

82

Proof: Here we adapt the proof in [2] to the present setting. Lemma 3.1 gives all error systems in the form (24), where $\mathbf{R_{aa}} + \mathbf{Q_{aa}}$ is all pass. Also,

$$det(\mathbf{I} - [\mathbf{R_{aa}} + \mathbf{Q_{aa}}]_{22} \begin{pmatrix} 0 & 0 \\ 0 & \Phi \end{pmatrix}) = det(\mathbf{I} - \mathbf{Q_{44}}\Phi)$$

which is a unit in $\mathcal{RH_\infty}$ because both $\mathbf{Q_{44}}$ and Φ are in $\mathcal{RH_\infty}$ with $\|\mathbf{Q_{44}}\|_\infty < 1$ and $\|\Phi\|_\infty \leq 1$ (Lemma 3.1). Hence we may apply Lemma 3.2 to E to obtain

$$\mathbf{I}(\mathbf{E}; \gamma; s_0) = \gamma^2 \mathbf{I}(\Phi; 1; s_0) + \gamma^2 \mathbf{I}([\mathbf{R_{aa}} + \mathbf{Q_{aa}}]_{11}; 1; s_0) \\ - \gamma^2(Re\, s_0)ln|det(\mathbf{I} - \mathbf{Q_{44}}(s_0)\Phi(s_0))|. \quad (25)$$

If $\mathbf{Q_{44}^*}(s_0) = 0$ then

$$\mathbf{I}(\mathbf{E}; \gamma; s_0) = \gamma^2 \mathbf{I}(\Phi; 1; s_0) + \gamma^2 \mathbf{I}([\mathbf{R_{aa}} + \mathbf{Q_{aa}}]_{11}; 1; s_0) \quad (26)$$

which is clearly maximized by the unique choice $\Phi = 0 = \mathbf{Q_{44}^*}(s_0)$, and there is nothing more to prove. So, henceforth in this proof assume $\mathbf{Q_{44}}(s_0) \neq 0$.

Define the constant matrix $\mathbf{H} = \begin{pmatrix} H_{11} & H_{12} \\ H_{21} & H_{22} \end{pmatrix}$ by

$$\mathbf{H} = \begin{pmatrix} -\mathbf{Q_{44}^*}(s_0) & (\mathbf{I} - \mathbf{Q_{44}^*}(s_0)\mathbf{Q_{44}}(s_0))^{1/2} \\ (\mathbf{I} - \mathbf{Q_{44}}(s_0)\mathbf{Q_{44}^*}(s_0))^{1/2} & \mathbf{Q_{44}}(s_0) \end{pmatrix} \quad (27)$$

where $(\cdot)^{1/2}$ denotes Hermitian square root. It is easy to verify that $\mathbf{H}$ is unitary and that

$$det(\mathbf{I} - \mathbf{H}_{12}\Phi(s)) = det(\mathbf{I} - \mathbf{Q_{44}}(s_0)\Phi(s))$$

which is a unit in $\mathcal{RH_\infty}$.

Let us map the unit ball in $\mathcal{RH_\infty}$ onto itself by the linear fractional map

$$\tilde{\Phi} = \mathcal{F}(\mathbf{H}, \Phi), \quad \Phi \in \mathcal{RH_\infty}, \quad \|\Phi\|_\infty \leq 1. \quad (28)$$

Note that this maps $\Phi = \mathbf{Q_{44}^*}(s_0)$ onto $\tilde{\Phi} = 0$.

Lemma 3.2 is applicable:

$$\mathbf{I}(\tilde{\Phi}; 1; s_0) = \mathbf{I}(\Phi; 1; s_0) + \mathbf{I}(\mathbf{Q_{44}^*}(s_0); 1; s_0) \\ - (Re\, s_0)ln|det(\mathbf{I} - \mathbf{Q_{44}}(s_0)\Phi(s_0))|. \quad (29)$$

Use this together with (25) to relate the entropy of E to the entropy of $\tilde{\Phi}$:

$$\mathbf{I}(\mathbf{E}; \gamma; s_0) = \gamma^2 \mathbf{I}(\tilde{\Phi}; 1; s_0) \\ + \gamma^2 \mathbf{I}([\mathbf{R_{aa}} + \mathbf{Q_{aa}}]_{11}; 1; s_0) - \gamma^2 \mathbf{I}(\mathbf{Q_{44}^*}(s_0); 1; s_0), \quad (30)$$

from which it is immediate that $\mathbf{I}(\mathbf{E}; \gamma; s_0)$ is maximized by the unique choice $\tilde{\Phi} = 0$. But $\tilde{\Phi} = 0 \leftrightarrow \Phi = \mathbf{Q_{44}^*}(s_0)$ from above, and the theorem is proved. $\triangle\triangle\triangle$

Denote maximum entropy quantities by $(\cdot)_{ME}$. An expression for the maximum entropy follows with ease from the above proof.

Corollary 3.4.

$$\mathbf{I}(\mathbf{E}_{ME}; \gamma; s_0) \\ = \gamma^2 \mathbf{I}([\mathbf{R_{aa}} + \mathbf{Q_{aa}}]_{11}; 1; s_0) - \gamma^2 \mathbf{I}(\mathbf{Q_{44}^*}(s_0); 1; s_0) \quad (31) \\ = \gamma^2(Re\, s_0)\{ln|det(\mathbf{R_{21}^*}(s_0))| + ln|det(\mathbf{Q_{12}}(s_0))| \\ - (1/2)ln|det(\mathbf{I} - \mathbf{Q_{44}^*}(s_0)\mathbf{Q_{44}}(s_0))|\}. \quad (32)$$

Proof: Equation (31) follows immediately from equation (30) on setting $\tilde{\Phi} = 0$. To show (32), recall that $\mathbf{R_{aa}} + \mathbf{Q_{aa}}$ is all pass i.e.,

$$(\mathbf{R_{aa}} + \mathbf{Q_{aa}})^*(\mathbf{R_{aa}} + \mathbf{Q_{aa}}) = \mathbf{I}, \quad \forall s = j\omega. \quad (33)$$

The $(1,1)$ block of this gives, $\forall s = j\omega$,

$$\mathbf{I} - [\mathbf{R_{aa}} + \mathbf{Q_{aa}}]_{11}^* [\mathbf{R_{aa}} + \mathbf{Q_{aa}}]_{11} \\ = [\mathbf{R_{aa}} + \mathbf{Q_{aa}}]_{21}^* [\mathbf{R_{aa}} + \mathbf{Q_{aa}}]_{21} \quad (34)$$

so that, along the imaginary axis,

$$ln|det(\mathbf{I} - [\mathbf{R_{aa}} + \mathbf{Q_{aa}}]_{11}^* [\mathbf{R_{aa}} + \mathbf{Q_{aa}}]_{11})| \\ = 2\, ln|det[\mathbf{R_{aa}} + \mathbf{Q_{aa}}]_{21}| \quad (35) \\ = 2\, ln|det(\mathbf{R_{21}^*})| + 2\, ln|det(\mathbf{Q_{12}})|, \quad (36)$$

where (36) follows from (35) on examination of the structure of $\mathbf{R_{aa}} + \mathbf{Q_{aa}}$ in Lemma 3.1.

Substituting (36) into the definition of entropy, we see that

$$\gamma^2 \mathbf{I}([\mathbf{R_{aa}} + \mathbf{Q_{aa}}]_{11}; 1; s_0) = \frac{\gamma^2}{\pi} \int_{-\infty}^{\infty} \{ln|det(\mathbf{R_{21}^*}(j\omega))| \\ + ln|det(\mathbf{Q_{12}}(j\omega))|\} \left[\frac{Re\, s_0}{|s_0 - j\omega|}\right]^2 d\omega \quad (37)$$

Since $\mathbf{R_{21}^*}$ and $\mathbf{Q_{12}}$ are units in $\mathcal{RH_\infty}$ [8], Poisson's integral theorem may be used to evaluate (37) as

$$\gamma^2 \mathbf{I}([\mathbf{R_{aa}} + \mathbf{Q_{aa}}]_{11}; 1; s_0) = \gamma^2(Re\, s_0)(ln|det(\mathbf{R_{21}^*}(s_0))| \\ + ln|det(\mathbf{Q_{12}}(s_0))|). \quad (38)$$

The second term in (31) is

$$-\gamma^2 \mathbf{I}(\mathbf{Q_{44}^*}(s_0); 1; s_0) \\ = -\frac{\gamma^2}{2\pi} ln|det(\mathbf{I} - \mathbf{Q_{44}}(s_0)\mathbf{Q_{44}^*}(s_0))| \int_{-\infty}^{\infty} \left[\frac{Re\, s_0}{|s_0 - j\omega|}\right]^2 d\omega \\ = -\frac{\gamma^2}{2\pi} ln|det(\mathbf{I} - \mathbf{Q_{44}}(s_0)\mathbf{Q_{44}^*}(s_0))|.\pi.(Re\, s_0)$$

and this with (38) gives (32). $\triangle\triangle\triangle$

III.2 Entropy at infinity

We turn our attention in this section to the important special case which occurs when $s_0 \to \infty$ along the real axis. The entropy at infinity of G, ($\|G\|_\infty \leq \gamma$) is then

$$\mathbf{I}(\mathbf{G}; \gamma; \infty) = \frac{\gamma^2}{2\pi} \int_{-\infty}^{\infty} ln|det(\mathbf{I} - \gamma^{-2}\mathbf{G}^*(j\omega)\mathbf{G}(j\omega))| d\omega \quad (39)$$

which is finite if G is strictly proper. For our problem, where we maximize the entropy of the error system E, this means that the maximum entropy at infinity is finite if $\mathbf{E}_{ME}$ is strictly proper; this occurs when R in the distance problem (13) is strictly proper, which in turn occurs when $\mathbf{P_{11}}(\infty) = 0$ in the standard configuration of figure 1. This corresponds to no direct feedthrough terms from the exogenous inputs w to controlled outputs z.

The results for the maximum entropy problem at infinity are particularly simple. The maximum entropy solution is found by setting the arbitrary stable contraction Φ to zero, by choosing the 'central solution' out of the set of possible E and an explicit formula for the maximum entropy is derived in terms of the state space realizations inherent in the solution of the distance problem of Lemma 3.1; these state space realizations are stated in the next lemma.

Lemma 3.5. [8] *Consider the distance problem of Lemma 3.1 in the case* $R(\infty) = 0$. *Suppose* R *has a realization*

$$R = \begin{array}{c} {}^{2n}I \\ p_1-m_2I \\ m_2I \end{array} \overset{\overset{2n \quad m_1-p_2 \quad p_2}{}}{\begin{pmatrix} A & B_1 & B_2 \\ C_1 & 0 & 0 \\ C_2 & 0 & 0 \end{pmatrix}}. \qquad (40)$$

Then $R_{aa} + Q_{aa}$ *in the parametrization of all solutions to the distance problem* $\|E\|_\infty \le \gamma$ *in Lemma 3.1 has a realization*

$$R_{aa} + Q_{aa} = \left(\begin{array}{c|c} \check{A} & \check{B} \\ \hline \check{C} & \check{D} \end{array} \right) \qquad (41)$$

where

$$\check{A} := \begin{pmatrix} A & 0 \\ 0 & \hat{A} \end{pmatrix}$$

$$\check{B} := \begin{pmatrix} \gamma^{-1/2}B_1 & \gamma^{-1/2}B_2 & -\gamma^{-3/2}XC_1^* & 0 \\ 0 & \gamma^{-3/2}Z^{-*}YB_2 & -\gamma^{-1/2}C_1^* & \gamma^{-1/2}Z^{-*}C_2^* \end{pmatrix}$$

$$\check{C} := \begin{pmatrix} \gamma^{-1/2}C_1 & 0 \\ \gamma^{-1/2}C_2 & -\gamma^{-3/2}C_2X \\ -\gamma^{-3/2}B_1^*Y & \gamma^{-1/2}B_1^*Z^* \\ 0 & -\gamma^{-1/2}B_2^* \end{pmatrix}$$

$$\check{D} := \begin{pmatrix} 0 & 0 & I & 0 \\ 0 & 0 & 0 & I \\ I & 0 & 0 & 0 \\ 0 & I & 0 & 0 \end{pmatrix}$$

Further,

$$X := Ric \begin{pmatrix} A^* & \gamma^{-2}C_1^*C_1 \\ -B_1B_1^* - B_2B_2^* & -A \end{pmatrix} \qquad (42)$$

$$Y := Ric \begin{pmatrix} A & \gamma^{-2}B_1B_1^* \\ -C_1^*C_1 - C_2^*C_2 & -A^* \end{pmatrix} \qquad (43)$$

$$Z := \gamma^{-1}XY - I \qquad (44)$$

$$\hat{A} := -A^* - \gamma^{-2}Z^{-*}YB_2B_2^* - \gamma^{-2}C_1^*C_1X. \qquad (45)$$

Applying the results of the previous section using this realization, and taking $s_0 \to \infty$ gives us the following important theorem.

Theorem 3.6. *The entropy at infinity,* $I(E; \gamma; \infty)$, *is maximized over the class of error systems* E *in the distance problem of Lemma 3.1 by the unique choice* $\Phi = 0$.

If $R(\infty) = 0$, *then the maximum entropy error system is simply*

$$E_{ME} = \gamma[R_{aa} + Q_{aa}]_{11}$$

$$= \begin{pmatrix} A & 0 & B_1 & B_2 \\ 0 & \hat{A} & 0 & \gamma^{-1}Z^{-*}YB_2 \\ C_1 & 0 & 0 & 0 \\ C_2 & -\gamma^{-1}C_2X & 0 & 0 \end{pmatrix} \qquad (46)$$

and the maximum entropy is

$$I(E_{ME}; \gamma^\cdot \infty) = Trace[B_1^*YB_1] - Trace[B_2^*Z^{-*}YB_2] \qquad (47)$$

$$= Trace[C_1XC_1^*] - Trace[C_2XZ^{-*}C_2^*]. \qquad (48)$$

Proof: From theorem 3.3 the maximum entropy error system is characterized by the unique choice $\Phi = Q_{44}^*(s_0)$. Letting $s_0 \to \infty$ along the real axis gives the maximum entropy at infinity choice as $\Phi = Q_{44}^*(\infty) = 0$, because Q_{44} is strictly proper from Lemma 3.1. For details of the limiting argument see [14]. That the maximum entropy error system has a realization (46) follows easily by setting $\Phi = 0$ in (13) and using Lemma 3.5.

To obtain the value of the maximum entropy, we take the limit as $s_0 \to \infty$ along the real axis of the result of corollary 3.4, that is,

$$I(E_{ME}; \gamma; \infty) = \lim_{s_0 \to \infty} \left(\gamma^2 s_0 \; \{ln|det(R_{31}^*(s_0))| + ln|det(Q_{42}(s_0))| \right.$$
$$\left. - (1/2)ln|det(I - Q_{44}^*(s_0)Q_{44}(s_0))|\} \right). \qquad (49)$$

Consider a typical term from (49):

$$\lim_{s_0 \to \infty} \left(s_0 \; ln \; det(I + \check{C}(s_0I - \check{A})^{-1}\check{B}) \right).$$

(We have dropped the modulus sign because s_c is real here). Now,

$$\check{C}(s_0I - \check{A})^{-1}\check{B} = \check{C}\check{B}s_0^{-1} + O(s_0^{-2})$$

so by Lemma A1 (of the appendix) we have

$$s_0 \; ln \; det(I + \check{C}(s_0I - \check{A})^{-1}\check{B}) = s_0 \left(Trace[\check{C}\check{B}s_0^{-1}] + O(s_0^{-2})\right).$$

Therefore, on taking limits as $s_0 \to \infty$,

$$\lim_{s_0 \to \infty} \left(s_0 \; ln \; det(I + \check{C}(s_0I - \check{A})^{-1}\check{B}) \right) = Trace[\check{C}\check{B}]. \qquad (50)$$

Apply this to the terms in (49) using

$$R_{31}^*(s_0) = I + \gamma^{-2}B_1^*(s_0I + A^*)^{-1}YB_1 \qquad (51)$$

and $$Q_{42}(s_0) = I - \gamma^{-2}B_2^*(s_0I - \hat{A})^{-1}Z^{-*}YB_2 \qquad (52)$$

from (41) to get

$$I(E_{ME}; \gamma; \infty) = Trace[B_1^*YB_1] - Trace[B_2^*Z^{-*}YB_2] \qquad (53)$$

as required, where the third term in (49) is zero in the limit because Q_{44} is strictly proper.

The alternative expression (48) follows in an entirely similar fashion; one notes that $I(E_{ME}; \gamma; \infty) = I(E_{ME}^*; \gamma; \infty)$ leading '

$$I(E_{ME}; \gamma; \infty) = \lim_{s_0 \to \infty} \left(\gamma^2 s_0 \; \{ln|det(R_{13}^*(s_0))| + ln|det(Q_{24}(s_0))| \right.$$
$$\left. - (1/2)ln|det(I - Q_{44}(s_0)Q_{44}^*(s_0))|\} \right) \qquad (54)$$

which gives (48) in the limit. $\triangle\triangle\triangle$

Remark 3.7. Notice that the entropy formulae (47) and (48) depend only on the state space realization of R and the solutions X and Y to the two Riccati equations (42) and (43) which are inherent in the solution to the distance problem. Calculation of the maximum entropy therefore imposes negligible computational problems. Furthermore, the maximum entropy error system (46), being the linear fractional map of $\Phi = 0$, is simply γ times the p_1 by m_1 (1,1) block of $R_{aa} + Q_{aa}$, which is also available from the solution to the distance problem with no extra computation.

Remark 3.8. Recall from Lemma 2.1 that $\{-I(G;\infty;\infty)\}^{1/2} = \|G\|_2$ for strictly proper G. Thus if we let $\gamma \to \infty$ in our maximum entropy solution we should obtain exactly the H_2 optimal solution. We show here that this is indeed the case.

By using the results of Wimmer [13] it may be shown that the positive semidefinite matrices $-X$ and $-Y$ are are monotonically decreasing as γ increases, and that $-Z$ is monotonically increasing as γ increases. Taking $\gamma \to \infty$ we obtain $Z_{\gamma \to \infty} = -I$,

$$X_{\gamma \to \infty} = Ric \begin{pmatrix} A^* & 0 \\ -B_1 B_1^* - B_2 B_2^* & -A \end{pmatrix} \quad (55)$$

and

$$Y_{\gamma \to \infty} = Ric \begin{pmatrix} A & 0 \\ -C_1^* C_1 - C_2^* C_2 & -A^* \end{pmatrix} \quad (56)$$

(with an obvious notation) which identifies the matrices $-X_{\gamma \to \infty}$ and $-Y_{\gamma \to \infty}$ as the controllability and observability gramians of $R(-s)$, respectively.

Using this fact, a simple calculation shows that

$$I(E_{ME};\infty;\infty) = Trace[B_1^* Y_{\gamma \to \infty} B_1]$$
$$- Trace[B_2^* (Z_{\gamma \to \infty})^{-*} Y_{\gamma \to \infty} B_2] \quad (57)$$
$$= -Trace[[B_1,B_2]^* [-Y_{\gamma \to \infty}][B_1,B_2]]$$
$$= -\|R\|_2^2 \quad (58)$$

and that $\dot{Q}_{ME} = 0$.

It is well-known that the $\dot{Q} \in \mathcal{R}H_\infty$ which minimizes

$$\|E\|_2 = \left\| \begin{pmatrix} R_{11} & R_{12} \\ R_{21} & R_{22} + \dot{Q} \end{pmatrix} \right\|_2 \quad (59)$$

is $\dot{Q} = Q_{H_2} = 0$ (the H_2 optimal solution) and in that case $\|E_{H_2}\|_2 = \|R\|_2$. Comparing this with (58) shows that we have $I(E_{ME};\infty;\infty) = -\|E_{H_2}\|_2^2$, illustrating the equivalence between the maximum entropy distance problem at γ, $s_0 \to \infty$ and the H_2 optimal distance problem.

Note that if $\gamma \to \gamma_{opt}$, then $E_{MF} \to E_{opt}$, the H_∞ optimal solution. It is easy to prove that $|I(E_{ME};\gamma;\infty)|$ is monotonically decreasing as γ increases from its optimal value; thus we have shown how γ can be used to move from H_∞ optimal to H_2 optimal via the maximum entropy solutions for $\gamma_{opt} < \gamma < \infty$.

Acknowledgement

We would like to thank D.J.N. Limebeer for providing an English translation of the Russian paper [2].

References

[1] D.Z. Arov and M.G. Krein, "Problem of search of the minimum entropy in indeterminate extension problems." *Functional Analysis and its Applications*, 15, 123-126, 1981.

[2] D.Z. Arov and M.G. Krein, "On the evaluation of entropy functionals and their minima in generalized extension problems." (In Russian) *Acta. Sci. Math.*, 45, 33-50, 1983.

[3] J.A. Ball and N. Cohen, "Sensitivity minimization in H_∞ norm. Parametrization of all suboptimal solutions." *Int. J. Control*, 46, No. 3, 785-816, 1987.

[4] H. Dym and I. Gohberg, "A maximum entropy principle for contractive interpolants." *J. Functional Analysis*, 65, 83-125, 1986.

[5] H. Dym and I. Gohberg, "A new class of contractive interpolants and maximum entropy principles." *Operator Theory Advances and Applications, Birkhäuser Verlag, Basel, to appear.*

[6] B.A. Francis, *A Course in H_∞ control theory* Lecture Notes in Control and Information Sciences, Vol. 88, Springer-Verlag, 1987.

[7] F.R. Gantmacher, *The theory of matrices.* Chelsea Publishing Co., New York, Vol. 1, 1959.

[8] K. Glover and J.C. Doyle, *under preparation.*

[9] D.J.N. Limebeer and Y.S. Hung, "An analysis of the pole–zero cancellations in H_∞ optimal control problems of the first kind." *SIAM Control and Optimization*, 25, No. 6, 1457-1493, 1987.

[10] R.M. Redheffer, "On a certain linear fractional transformation." *Math. and Physics*, 39, 269-286, 1960.

[11] W. Rudin, *Real and complex analysis.* Mc. Graw-Hill International edition, 3rd. edition, 1986.

[12] A.D.C. Youla, H.A. Jabr and J.J. Bongiorno, "Modern Wiener–hopf design of optimal controllers. Part II – the multivariable case." *IEEE Trans. Auto. Control*, AC-21, No. 3, 319-338, 1976.

[13] H.K. Wimmer, "Monotonicity of maximal solutions of algebraic Riccati equations." *Systems and Control Letters*, 5, 317-319, 1985.

[14] K. Glover and D. Mustafa, "Derivation of the maximum entropy H_∞-controller and a state–space formula for its entropy." *submitted, 1988.*

Appendix

The following technical lemma is needed.

Lemma A1 Let M be a square matrix and $\epsilon > 0$. Then

(i) $\ln \det(I-\epsilon M) = -\epsilon\, Trace[M] + O(\epsilon^2)$.

(ii) $-\ln \det(I - \epsilon^2 M^* M) \geq \epsilon^2\, Trace[M^* M]$.

Proof: *Part (i).* Use the Faddeev formula (Gantmacher [7], p88) to obtain

$$\det(I-\epsilon M) = 1 - \epsilon\, Trace[M] + O(\epsilon^2)$$

and expand the logarithm of this as a power series.

Part (ii). Using a well-known inequality,

$$-\ln \det(I - \epsilon^2 M^* M) = -\sum_i \ln(1 - \epsilon^2 \sigma_i^2(M))$$
$$\geq \sum_i \epsilon^2 \sigma_i^2(M)$$
$$= \epsilon^2\, Trace[M^* M]. \qquad \triangle\triangle\triangle$$

We may now proceed with the proof of Lemma 2.1

Proof of Lemma 2.1: *Part (i).* By Lemma A1 we can write

$$-I(G;\gamma;s_0) = \frac{1}{2\pi} \int_{-\infty}^{\infty} \left\{ (Trace[G^*(j\omega)G(j\omega)]) \right.$$
$$\left. \times \left[\frac{Re\, s_0}{|s_0 - j\omega|}\right]^2 \right\} d\omega + O(\gamma^{-2})$$
$$= \frac{1}{2\pi} \int_{-\infty}^{\infty} \left\{ Trace \left[\left[G(j\omega)\frac{Re\, s_0}{(s_0 + j\omega)}\right]^* \right.\right.$$
$$\left.\left. \times \left[G(j\omega)\frac{Re\, s_0}{(s_0 + j\omega)}\right]\right]\right\} d\omega + O(\gamma^{-2}).$$

Therefore,

$$-I(G;\gamma;s_0) = \|G(s)(Re\, s_0)/(s_0 + s)\|_2^2 + O(\gamma^{-2}). \quad (*)$$

Noting that the $O(\gamma^{-2})$ terms are nonnegative we have

$$-I(G;\gamma;s_0) \geq \|G(s)(Re\, s_0)/(s_0 + s)\|_2^2$$

whilst

$$-I(G;\infty;s_0) = \|G(s)(Re\, s_0)/(s_0 + s)\|_2^2$$

follows by taking $\gamma \to \infty$ in $(*)$.

Part (ii) Firstly note that the integrands in $(*)$ above are monotonically increasing with s_0 and continuous, and so by dominated convergence both sides of $(*)$ tend to a limit as $s_0 \to \infty$. Each side is finite because $\|G\|_\infty < \gamma$ and $G(\infty) = 0$ by assumption. The result then follows in a similar way to the proof of part (i). $\qquad \triangle\triangle\triangle$